COLOUR MORPHOLOGY
AND ITS APPROACHES

by

CHUN-WEI YEH

A thesis submitted to the

University of Birmingham

for the degree of

DOCTOR OF PHILOSOPHY

School of Electronic, Electrical and Computer Engineering

Faculty of Engineering

University of Birmingham

August 2014

UNIVERSITY OF BIRMINGHAM

University of Birmingham Research Archive

e-theses repository

Abstract

Mathematical morphology was first applied to binary images and readily extended to grey-level images. In extending mathematical morphology to colour it is difficult to define a suitable unambiguous ordering. We present two complete ordering schemes based on colour difference and similarity ordering for colour morphology. A novel colour difference formula is first introduced. This colour difference formula is based on colour extrema derived from a simple physical model of image formation and avoids the more arbitrary mathematical and perceptual definitions previously reported. Moreover, we define similarity criteria as the basis for mathematical morphology that can be used with flat and non-flat structuring elements. The proposed orderings meet the properties of mathematical morphology, and provide a harmonised approach for binary, grey-level and colour morphology. A comparison of ordering schemes for dilation, erosion, opening, closing and filtering operator shows the colour difference-based ordering presented here to be at least as good as other ordering schemes and better than some of the well principled, previously reported methods in not generating artefacts and reducing image noise. The value of this approach is demonstrated using the morphological operators for opening followed by closing and conditional toggle mapping to reduce "salt and pepper" noise in colour images. A considered, novel, approach to adding "salt and pepper" noise in colour images, designed to test ordering schema and provide a

proportionate and appropriate expression of "salt and pepper" noise is presented. This is a novel approach to noise addition in colour images. Additionally, the development of a similarity-based ordering to perform morphological gradient and Hit-or-Miss transforms for colour images is presented.

Acknowledgements

I would like to thank my supervisor, David Pycock, for leading me into the research area of colour morphology and spending lots of time on reviewing this thesis.

I would like to thank my examiners, Dr. Mark Fisher in University of East Anglia (UEA) and Dr. Michael Spann, for their helpful comments and discussion.

Finally, I would like to thank my girlfriend, Pei-Ling Liao, for her sacrifice and love, and thank my parents for their love and financial support.

Table of Contents

List of Figures

List of Tables

List of Symbols

I, J	binary or grey-level image
I, **J**	multichannel image
i, j	arbitrary pixels of an image
$\mathbb{R}^p$	*p*-dimensional Euclidean space
$\mathbb{Z}^p$	*p*-dimensional discrete space
$\mathbb{F}$	set of real numbers
E	set of integers
S	structure element, i.e., set of $\mathbb{R}$ or $\mathbb{Z}^p$ associated with an origin
S	structure element, i.e., set of $\mathbb{R}^p$ or $\mathbb{Z}^p$ associated with an origin
M	mask for conditional morphology, i.e., set of real numbers
c	colour vector
c^{MAX}	colour extrema
x	position of $\mathbb{R}^p$ or $\mathbb{Z}^p$ defining the coordinates of the centre of arbitrary image pixels (calculated from the image origin)
y	position of $\mathbb{R}^p$ or $\mathbb{Z}^p$ defining the coordinates of the centre of structure element pixels (calculated from the structure element origin)
b	intensity levels
$A \Leftrightarrow B$	*A* if and only if *B*
$\subseteq$	is a subset of
$\subset$	is a proper subset of
$\in$	is an element of
$\cup$	Boolean union
$\cap$	Boolean intersection
$\varnothing$	empty set
$\forall$	for all
$\vee$	point-wise maximum (supremum) operator
$\wedge$	point-wise minimum (infimum) operator
δ	dilation operator
ε	erosion operator
γ	opening
φ	closing
Δ	morphological gradient

ρ^+	white top-hat transformation (also called the residue of an opening)
ρ^-	black top-hat transformation (also called the residue of an closing)
τ	toggle mapping operator
h	h-mapping or h-ordering
h_g^d	h-mapping or h-ordering based on the proposed difference function for binary or grey-level images
h_{colour}^d	h-mapping or h-ordering based on the proposed difference function for colour images
h_g^s	h-mapping or h-ordering based on the proposed similarity for binary or grey-level images
h_{colour}^s	h-mapping or h-ordering based on the proposed similarity for colour images
Ω_g^d	a complete ordering that uses h_g^d for binary or grey-level images
Ω_{colour}^d	a complete ordering that uses h_{colour}^d for colour images
Ω_g^s	a complete ordering that uses h_g^s for binary or grey-level images
Ω_{colour}^s	a complete ordering that uses h_{colour}^s for colour images
OC	opening followed closing filter
NMSE	normalised mean squared error
PSNR	Peak signal-to-noise ratio
HMT	hit-or-miss transformation
SHMT	similarity-based hit-or-miss transformation
$SHMT_\eta$	robust similarity-based hit-or-miss transformation

Chapter 1: Introduction

1.1 Motivation

Mathematical morphology was originally developed by Georges Matheron and Jean Serra in the mid sixties [MAT75] [SER82] [SER88]. It is a mathematical theory of image processing which examines the geometric and topological structure of an image by matching it with structure elements that are scanned across the image and described by Matheron [MAT75], Serra [SER82] and Heijmans [HEI95]. There are many operations that can be defined within mathematical morphology. Commonly used operations, which are non-linear, include erosion, dilation, opening, closing, hit-and-miss and watershed transformations. It was originally developed for binary images represented using set theory. Serra [SER82] was the first to introduce a general theory of morphological image analysis and the need for complete lattices, i.e., the analyzed objects have to be a partial order set structure in which all subsets have both a supremum and an infimum. "Ordering" is the principle by which the elements of a given set may be arranged in a sequence from "low" to "high". The use of mathematical morphology for noise reduction, edge detection, segmentation, texture and shape analysis in binary and grey-level images [SER82] [SER88] [NAJ10] is widely reported.

Colour perception is important because it enriches the visual experience and contains

colourful information. Therefore, it is desirable to extend mathematical morphology from binary and grey-level images to colour. Identifying a colour ordering is problematic because colour is commonly represented as a 3 component vector rather than by the scalar quantities used for grey-level images. This objective has been pursued by others and there is a substantial body of existing research published on methods for colour ordering and colour morphology. The challenge is to define an ordering in colour that meets the requirements of mathematical morphology for complete lattices and reflects colour perception.

In this thesis methods for colour ordering are presented and evaluated for their suitability for colour mathematical morphology.

1.2 Main Contributions

This thesis contributes to the field of mathematical morphology and illustrates how the definitions of colour extrema and colour similarities can be exploited to design colour orderings and colour morphological operators. Specifically:

(1) A new definition of colour extrema, has been proposed and used to define a colour ordering based on the RGB, HSV and CIELAB colour difference. The chief contribution is the principled method that takes advantage of Angulo's method [ANG07a] in harmonising binary, grey-level and colour morphology and do not need the prior

knowledge of applications.

(2) The performance of different colour orderings is compared using a morphological filter to reduce salt-and-pepper noise. So far as the author is aware a detailed quantitative comparison of these colour orderings has been only reported in [APT07] for colour morphology but just a few colour orderings were considered.

(3) Colour similarity measures in RGB and CIELAB colour spaces are proposed and applied to define orderings for colour morphology.

(4) The potential of similarity-based ordering to extend colour mathematical morphology to the hit-or-miss transform is evaluated.

1.3 Organization of this Thesis

Chapter 2 introduces the concept of mathematical morphology based on complete lattices for scalar images.

In Chapter 3 the commonly used colour models and the concepts of the orderings commonly used for colour morphology are introduced.

Chapter 4 introduces a new definition of colour extrema and defines a colour ordering based on the RGB, HSV and CIELAB colour difference by using colour extrema. The comparison of the existing colour orderings is demonstrated using morphological noise removal filters.

In Chapter 5 two colour similarities are proposed in RGB and CIELAB colour spaces. Colour morphological operators are defined using the colour similarities. The extension of the hit-or-miss transform to colour images is presented using the complete lattice structure with colour similarities. The results of applying these operators to process synthetic and natural images are presented and discussed.

In Chapter 6, the comparison of the proposed colour orderings, difference-based ordering and similarity-based ordering, is demonstrated using morphological operations and noise removal filters.

Finally, in Chapter 7, we conclude with a summary of our findings and a discussion of directions for future work.

Chapter 2: Concepts on Scalar Morphology

The aim of this chapter is to review the basic morphological operators for scalar, binary and grey-level images. In the following subsections, the binary and grey-level morphology will be defined, and then the common morphological operators will be introduced, including dilation, erosion, opening, closing, residue operator, toggle mapping operator and the conditional morphology of dilation, erosion and toggle mapping [SOI02].

2.1 Scalar Image

Let $\mathbf{I} \subseteq \mathbb{R}^p$ be a multivariate image composed of pixel values of dimension p. Let $\mathbb{F} \subseteq \mathbb{R}^p$ be a multivariate image composed of vector values in the continuous space $\mathbb{R}^p$. Let $\mathbf{E}$ be a subset of the discrete space $\mathbb{Z}^2$; $\mathbf{E}$ is the spatial support of a 2D image, $\mathbf{I}: \mathbf{E} \rightarrow \mathbb{F}$ commonly denoted by $\mathcal{F}(\mathbf{E}, \mathbb{F})$. In this mapping pixel values are mapped from coordinates $x = (i, j) \in \mathbf{E}$ to vector values, $\mathbf{t} \in \mathbb{F} \subseteq \mathbb{R}^p$. Here p is 1 for scalar images. A binary or grey-level image is represented by the function,

$$\mathbf{I}: \begin{cases} \mathbf{E} \rightarrow \mathbb{F} \\ x \rightarrow \mathbf{t} \end{cases} \tag{2.1}$$

i.e., $\mathbf{I} \in \mathcal{F}(\mathbf{E}, \mathbb{F})$, where $\mathcal{F}(\mathbf{E}, \mathbb{F})$ denotes the functions from the discrete support $\mathbf{E}$ onto the space of values of the image $\mathbb{F}$. Thus the support $\mathbf{E}$ maps each pixel of the image $\mathbf{I}$ into a

binary or grey-level value $\mathbf{t} \in \mathbb{F}$: $\mathbf{t} = \mathbf{I}(x)$, $x \in \mathbf{E}$. Note that $\mathbb{F}$ with a partial ordering $\leq$ is a complete lattice [ROM08]. The details of the complete lattice for mathematical morphology will be described in Section 3.4. Note that if the $\mathbb{F}$ is a complete lattice, then $\mathcal{F}(\mathbf{E}, \mathbb{F})$ is a complete lattice too [SER88].

2.2 Binary Morphology

In binary morphology, the object of interest is a binary image, $\mathbf{I}$, which is mapped by the spatial support $\mathbf{E}$ onto $\mathbf{t}$, where $\mathbf{t}$ is a bi-value set $\{0, 1\}$ here.
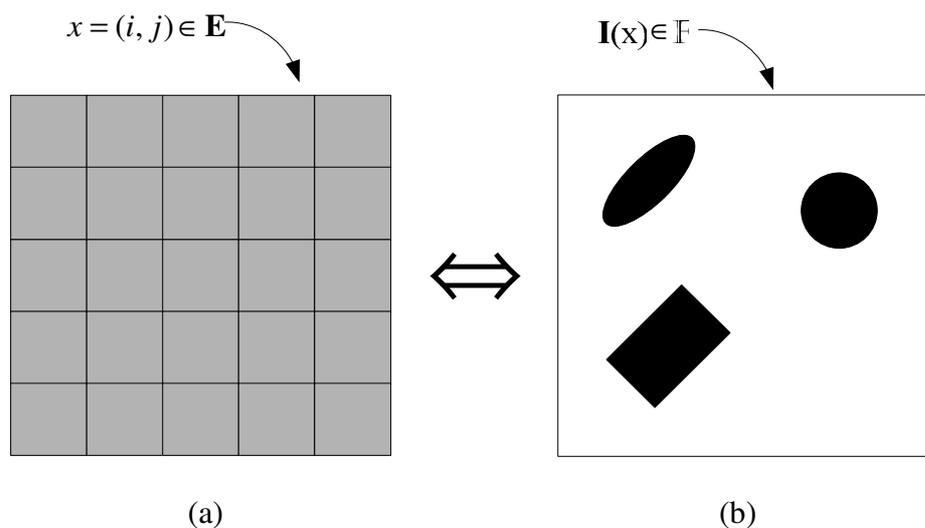
Figure 2.1. Notation for a binary image: (a) Discrete support: $\mathbf{E} = \mathbb{Z}^2$ and (b) Image range: $\mathbb{F} = \{0, 1\}$.

Morphological operators are non-linear neighbourhood operators founded in set theory. They can be affected by sliding a set of known shape, called a structure element S, through the image. Two commonly used structure elements are shown in Fig. 2.2.

(a)   (b)
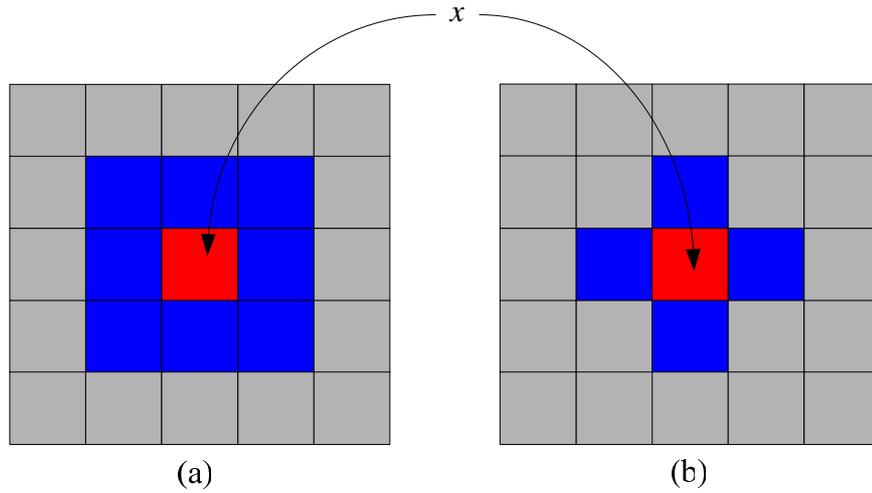
Figure 2.2. Structure element $S \subset \mathbf{E}$ is the union of the blue and red pixels forming a spatial neighbourhood. The origin is shown in red for (a) an 8 connected square structure element and (b) a 4 connected cross shaped structure element.

The two basic morphological operators are *erosion* and *dilation*. They are based on the notion of the infimum and supremum of a profile or surface. In the case of a symmetric structure element, the *erosion* and *dilation* operations $\varepsilon_S(\mathrm{I})(\mathrm{x})$ and $\delta_S(\mathrm{I})(\mathrm{x})$, on image, $\mathbf{I}$, are defined as

$$\varepsilon_S(\mathbf{I})(x) = \inf_{y \in \check{S}(x)} (\mathbf{I}(y)) \tag{2.2}$$

and

$$\delta_S(\mathbf{I})(x) = \sup_{y \in S(x)} (\mathbf{I}(y)) \tag{2.3}$$

where inf and sup denote infimum and supremum, respectively, and $S(x) \in \mathrm{E}$ denotes the spatial neighbourhood induced by the structure element S centred at x, and $\check{S}$ is the reflection of S with respect to the origin. Dilation and erosion are dual operators with respect to the image complement, i.e., $\delta_S(\mathbf{I}) = \left(\varepsilon_{\check{S}}(\mathbf{I}^c) \right)^c$. Since the structure element is symmetric, $S = \check{S}$.

For binary images erosion and dilation are simple to describe: Erosion, $\varepsilon_S(\mathbf{I})$, shrinks objects, whereas dilation, $\delta_S(\mathbf{I})$, expands objects, as shown in Fig. 2.3. The change in size and shape depends on the structure element, SE, used. Combinations of erosion and dilation can be used in image filtering, edge detection and image measurement [SOI02]. Commonly used morphological operators are described below.

(a)

(b)   (c)
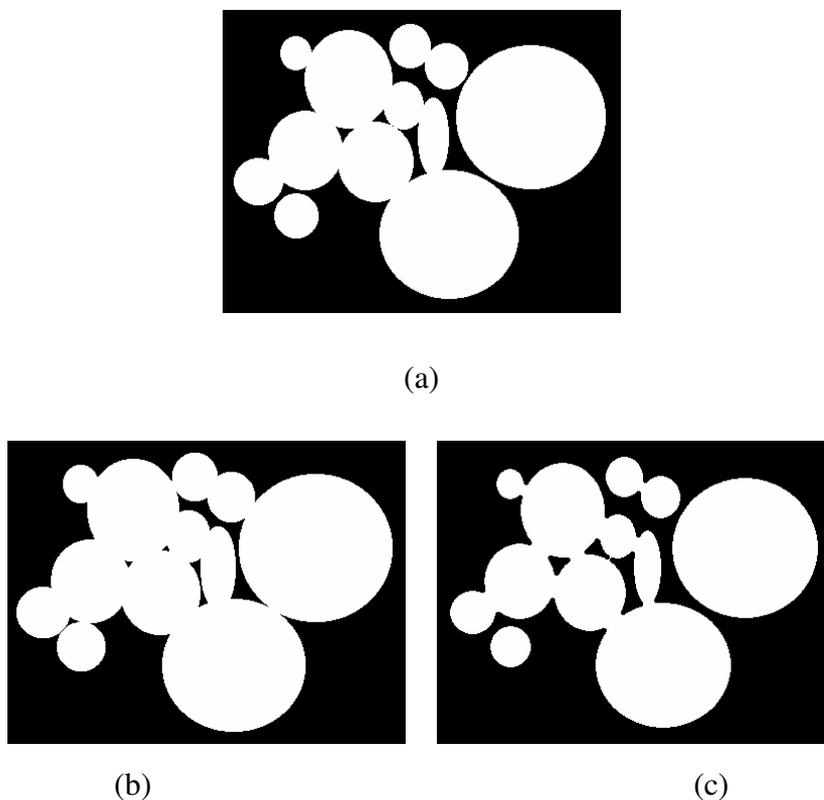
Figure 2.3. Basic morphological operators: (a) original binary image (b) dilated image and (c) eroded image.

2.3 Grey-level Morphology

For grey-level images dilation, $\delta_b(I)(x)$ and erosion, $\varepsilon_b(I)(x)$, are defined by:

$$\delta_b(\mathbf{I})(x) = \bigvee_{h \in \mathbf{E}} (\mathbf{I}(x-h) + b(h)) \tag{2.4}$$

and

$$\varepsilon_b(\mathbf{I})(x) = \bigwedge_{h \in \mathbf{E}} (\mathbf{I}(x+h) - b(h)) \tag{2.5}$$

where $\mathbf{I} \in \mathcal{F}(\mathbf{E}, \mathbb{F})$ is the original grey-level image and $b \in \mathcal{F}(\mathbf{E}, \mathbb{F})$ is the designed structure element. In the simplest case the structure element is uniform or flat topped [SOI03], defined as:

$$b(x) = \begin{cases} 0, & x \in S \\ -\infty, & x \in S^c \end{cases} \tag{2.6}$$

where S is a set which defines the shape of the structure element and S^c is the complement of S, i.e., $S \cap S^c = \varnothing$ and $S \cup S^c = \mathbf{E}$. The structure element is defined at the origin $y \in S$, and each point x of $\mathbf{E}$ corresponds to the translation mapping y to x. This translation maps S onto S_x, i.e., $S_x = \{y + x : y \in S\}$ Thus, the flat grey-level dilation $\delta_S(\mathbf{I})(x)$ with respect to the structure element S is:

$$\delta_S(\mathbf{I})(x) = \bigvee_{h \in S} (\mathbf{I}(x-h))$$
$$= \left\{ \mathbf{I}(y) : y = \arg_z \vee [\mathbf{I}(z)], z \in \check{S}_x \right\} \tag{2.7}$$

where $\check{S}_x$ is the reflection of S_x with respect to the origin, and the corresponding flat

grey-level erosion, $\varepsilon_S(\mathbf{I})(x)$, of image, $\mathbf{I}$ is:

$$\varepsilon_S(\mathbf{I})(x) = \underset{h \in S}{\wedge}(\mathbf{I}(x+h))$$
$$= \left\{ \mathbf{I}(y): y = \arg_z \wedge [\mathbf{I}(z)], z \in S_x \right\} \tag{2.8}$$

Dilation and erosion are increasing operators [SOI03]: if $\mathbf{I}(x) \le \mathbf{J}(x), \forall x \in \mathbf{E}$, then

$\delta_S(\mathbf{I})(x) \le \delta_S(\mathbf{J})(x)$ and $\varepsilon_S(\mathbf{I})(x) \le \varepsilon_S(\mathbf{J})(x), \forall x \in \mathbf{E}$. Dilation is an extensive operator, i.e.,

$\mathbf{I}(x) \le \delta_S(\mathbf{I})(x), \forall x \in \mathbf{E}$, whereas erosion is an anti-extensive operator, i.e.,

$\varepsilon_S(\mathbf{I})(x) \le \mathbf{I}(x), \forall x \in \mathbf{E}$, when the structure element S contains the origin. Additionally, the

distributive property also holds:

$$\delta_S(\mathbf{I} \vee \mathbf{J})(x) = \delta_S(\mathbf{I})(x) \vee \delta_S(\mathbf{J})(x)$$
$$\varepsilon_S(\mathbf{I} \wedge \mathbf{J})(x) = \varepsilon_S(\mathbf{I})(x) \wedge \varepsilon_S(\mathbf{J})(x) \tag{2.9}$$

Fig. 2.4 shows the effect of these operators for an industrial image. These two basic operators

can be used together as building blocks of advanced morphological operators. Note the

changes in the highlighted regions, shown enlarged in each case. The dark area on the pad in

the bottom right of the highlighted image patch is removed by dilation, as shown in Fig.

2.4(b). The light track in the middle of the highlighted image patch is removed by erosion, as

shown in Fig. 2.4(c).

(a)   (b)   (c)
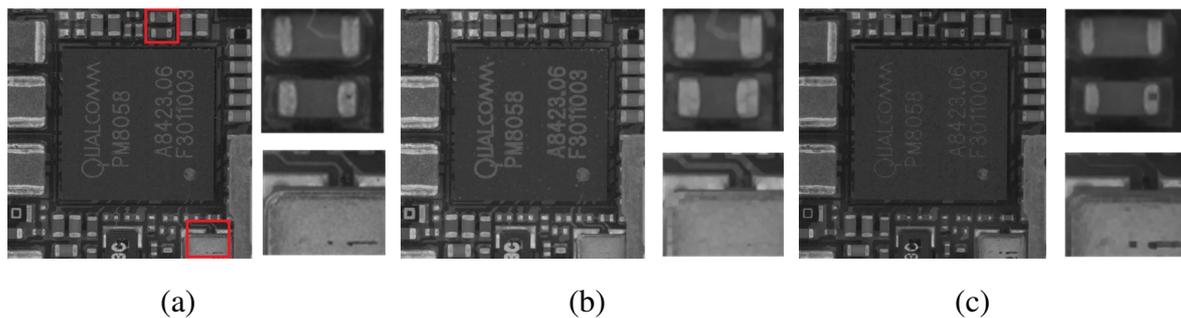
Figure 2.4. Basic morphological operators: (a) original grey-level image (b) dilated image and (c) eroded image. The Structure element SE is a square of 3 x 3-pixels (8-connected).

2.4 Morphological Operators

The two elementary operators of scalar erosion and dilation can be concatenated to yield a new set of morphological operators, described in the following section. Here, only the flat structure element is considered so that scalar morphological operators can be described for both binary and grey-level images together.

2.4.1 Opening and Closing

The flat opening and closing are obtained by using the flat erosion and flat dilation by the structure element SE, given respectively by:

$$\gamma_S(\mathbf{I})(x) = \delta_S(\varepsilon_S(\mathbf{I}))(x) \tag{2.10}$$

and

$$\varphi_S(\mathbf{I})(x) = \varepsilon_S(\delta_S(\mathbf{I}))(x) \tag{2.11}$$

Opening removes bright structures according to the predefined size and shape of the structure element S, whereas closing removes dark structures. These are nonlinear smoothing filters, commonly used to remove noise from images.

The opening $\gamma_S(\cdot)$ and closing $\varphi_S(\cdot)$ have the following properties [SOI03].

■ Increasing (ordering preservation): $\gamma_S(\cdot)$ and $\varphi_S(\cdot)$ are increasing operators, i.e.,

$$\mathbf{I}(x) \leq \mathbf{J}(x) \Rightarrow \gamma_S(\mathbf{I})(x) \leq \gamma_S(\mathbf{J})(x), \quad \varphi_S(\mathbf{I})(x) \leq \varphi_S(\mathbf{J})(x), \forall x \in \mathbf{E}.$$

■ Idempotence (invariance to operator itself) i.e., $\gamma_S(\gamma_S(\mathbf{I})) = \gamma_S(\mathbf{I})$,

$$\varphi_S(\varphi_S(\mathbf{I})) = \varphi_S(\mathbf{I}).$$

■ Extensive and anti-extensive: $\gamma_S(\cdot)$ is anti-extensive, i.e., $\gamma_S(\mathbf{I}(x)) \leq \mathbf{I}(x), \forall x \in \mathbf{E}$,

whereas $\varphi_S(\cdot)$ is extensive, i.e., $\mathbf{I}(x) \leq \varphi_S(\mathbf{I}(x)), \forall x \in \mathbf{E}$.

Examples of opening and closing in an industrial image are illustrated in Fig. 2.5. The light track in the middle of the highlighted image patch is largely removed by opening and the dark area on the pad in the bottom right of the highlighted image patch is largely removed by closing.

(a)

(b)   (c)
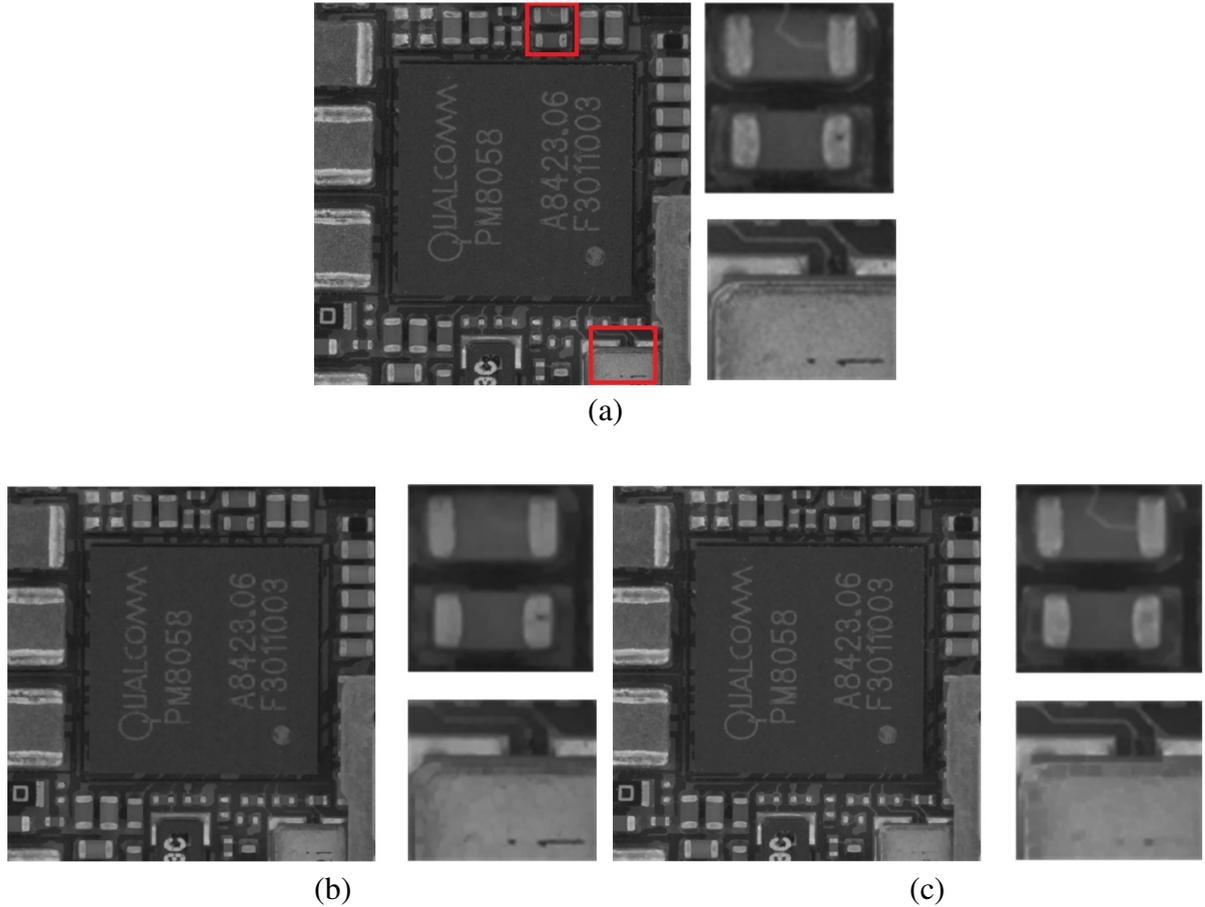
Figure 2.5. Morphological operators: (a) original image (b) opening image and (c) closing image. The Structure element, SE, is an 8-connected square of 3x3 pixels.

2.4.2 Residue-based Operators

The morphological gradient can be defined in terms of erosion and dilation, i.e.,

$$\Delta_S(\mathbf{I})(x) \coloneqq \delta_S(\mathbf{I})(x) - \varepsilon_S(\mathbf{I})(x) \tag{2.12}$$

The structure element, S, for the gradient is usually a unit of flat square. This operator gives

the contours of the image. An internal gradient is defined by $\mathbf{I}(x) - \varepsilon_S(\mathbf{I})(x)$ and an external

gradient is defined by $\delta_S(\mathbf{I})(x) - \mathbf{I}(x)$. The internal gradient is obtained by the difference

between a given image and its eroded image and the external gradient is obtained by the

difference between the dilation of the given image and the given image. They are images

where each pixel value indicates the contrast intensity in the close neighbourhood of that pixel.

Therefore, they are useful for edge detection and segmentation applications.

Similarly, the white top-hat transformation is the residue of an opening, i.e.:

$$\rho_S^+(\mathbf{I})(x) = \mathbf{I}(\mathrm{x}) - \gamma_S(\mathbf{I})(x) \tag{2.13}$$

The complementary operator is the black top-hat transformation given by:

$$\rho_S^-(\mathbf{I})(x) = \varphi_S(\mathbf{I})(x) - \mathbf{I}(\mathrm{x}) \tag{2.14}$$

The top-hat transformation yields grey-level images, and it is an operation that extracts small

elements and details from given images. The white top-hat transformation returns an image

that contains those elements which are smaller than the structure element and are brighter than

their surroundings. Oppositely, the dark top-hat transformation returns an image, containing

the elements which are smaller than the structure element and are darker than their

surroundings.

The original results of top-hat transformation were difficult to be observed. Therefore, an

equalisation was applied after the two top-hat transforms, as shown in Fig. 2.6 (b) and Fig. 2.6

(c).

(a)

(b)   (c)
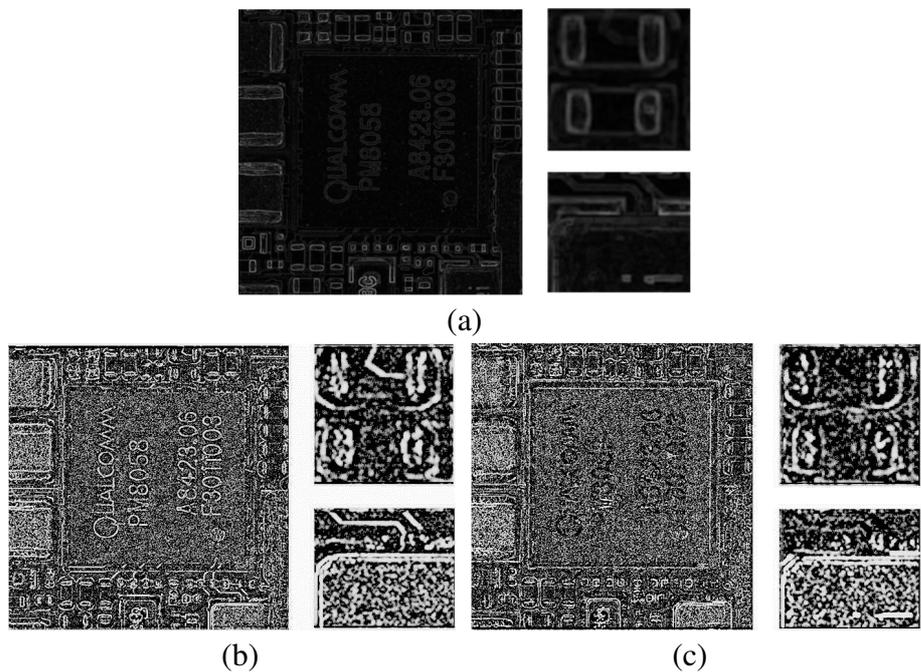
Figure 2.6. Morphological gradients: (a) morphological gradient (b) white top-hat transformation after equalisation and (c) black top-hat transformation after equalisation. The Structure element, SE, is an 8-connected square of 3 x 3 pixels.

2.4.3 Toggle mapping operator

The toggle mapping operator [KRA75] is a non-linear operator that uses a combination of erosion and dilation to enhance the edges of an image. Meyer and Serra [MEY89] formalised and generalised this approach and named it toggle mapping [MEY89] [SER92]. The toggle contrast mapping uses a dilation near a local maxima and an erosion around local minima. The equivalent situation was not considered in the original two-state toggle contrast mapping. Here a three-state toggle contrast mapping, based on the grey-level erosion, dilation and identity transformations [SCH00] [VEL13], is defined as:

$$\tau_S(\mathbf{I})(x) = \begin{cases} \varepsilon_S(\mathbf{I})(x) & \text{if } \rho_S^\delta(\mathbf{I})(x) > \rho_S^\varepsilon(\mathbf{I})(x) \\ \delta_S(\mathbf{I})(x) & \text{if } \rho_S^\delta(\mathbf{I})(x) < \rho_S^\varepsilon(\mathbf{I})(x) \\ \mathbf{I}(x) & \text{otherwise} \end{cases} \qquad (2.15)$$

Where $\rho_S^\delta(\mathbf{I})(x) = (\delta_S(\mathbf{I})(x) - \mathbf{I}(x))$ and $\rho_S^\varepsilon(\mathbf{I})(x) = (\mathbf{I}(x) - \varepsilon_S(\mathbf{I})(x))$ [RIV93]. The local maxima and minima are identified using the morphological Laplacian. The morphological Laplacian of the original image $\mathbf{I}$ was defined in [VAN89]:

$\Delta_S(\mathbf{I}) = \rho_S^\delta(\mathbf{I}) - \rho_S^\varepsilon(\mathbf{I}) = (\delta_S(\mathbf{I}) - \mathbf{I}) - (\mathbf{I} - \varepsilon_S(\mathbf{I}))$ where δ_S and ε_S are dilation and erosion by using a structure element S. A pixel is considered as a maximum if the morphological Laplacian is negative, i.e., $\rho_S^\delta(\mathbf{I})(x) < \rho_S^\varepsilon(\mathbf{I})(x)$. Conversely, a pixel is considered a minima if the Laplacian is positive, i.e., $\rho_S^\delta(\mathbf{I})(x) > \rho_S^\varepsilon(\mathbf{I})(x)$. The three-state toggle mapping is more

robust than the two-state mapping because it includes the "otherwise" case to preserve the

original pixel when there is one pixel alone on the slope between two levels

by $\rho_S^\delta(\mathbf{I})(x) = \rho_S^\varepsilon(\mathbf{I})(x)$.

An example of the three-state toggle contrast mapping demonstrated the edge enhancement

with one-dimensional (1D) signal case, as shown in Fig. 2.7.
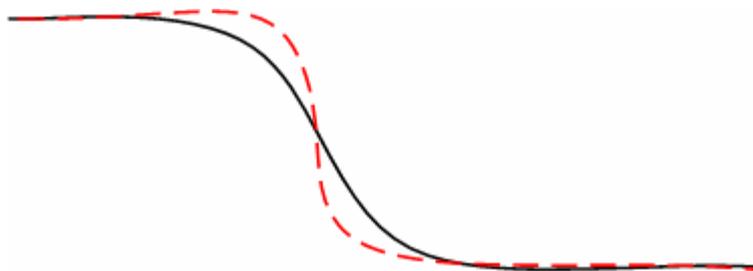
Figure 2.7. Three-state toggle contrast mapping operator: solid line represents the original 1D signals and dashed line shows the 1D signals after doing the toggle mapping operator.

In the uniform parts of the 1D signals, their external gradients, $\rho_S^\delta(\mathbf{I})(x)$, equal to the internal

gradients, $\rho_S^\varepsilon(\mathbf{I})(x)$; hence, the original signals are preserved. In the upper slop, their internal

gradients are greater than the external gradients, and the dilation operator was then applied in

the original signals. Oppositely, in the lower slop, the internal gradients are less than the

external gradients, and the erosion operator was applied. The result signals are shown in the

dashed line of Fig. 2.7. This caused the contrasted signals for edge enhancement that clearly

expresses Eq. (2.15).

Iteration is normally continued until idempotence, i.e.,

$$\tau_S^{\infty}(\mathbf{I})(x) = \lim_{m \to \infty} \tau_S^m(\mathbf{I})(x) \tag{2.16}$$

Where $\tau_S^m(\mathbf{I}) = \tau_S(\tau_S^{m-1}(\mathbf{I}))$, $\tau_S^0(\mathbf{I})(x) = \mathbf{I}(x)$ and $\tau_S(\mathbf{I})(x)$ is given by Eq. (2.15). The

iterations of the toggle operator converge to a fixed point [KRA75] after a finite number of

iterations. The examples of results obtained with the toggle mapping operator in the different

iterations are shown in Fig. 2.8. The edges were enhanced after 1-10 iteration as shown in Fig.

2.8 (b). After 10 iterations noise is progressively emphasised producing a ringing effect, as

shown in Fig. 2.8 (c)-(f) but a large number of iterations are needed to converge to a stable

result, as shown in Fig. 2.8 (d).

(a)

(b)

(c)

(d)

(e)

(f)
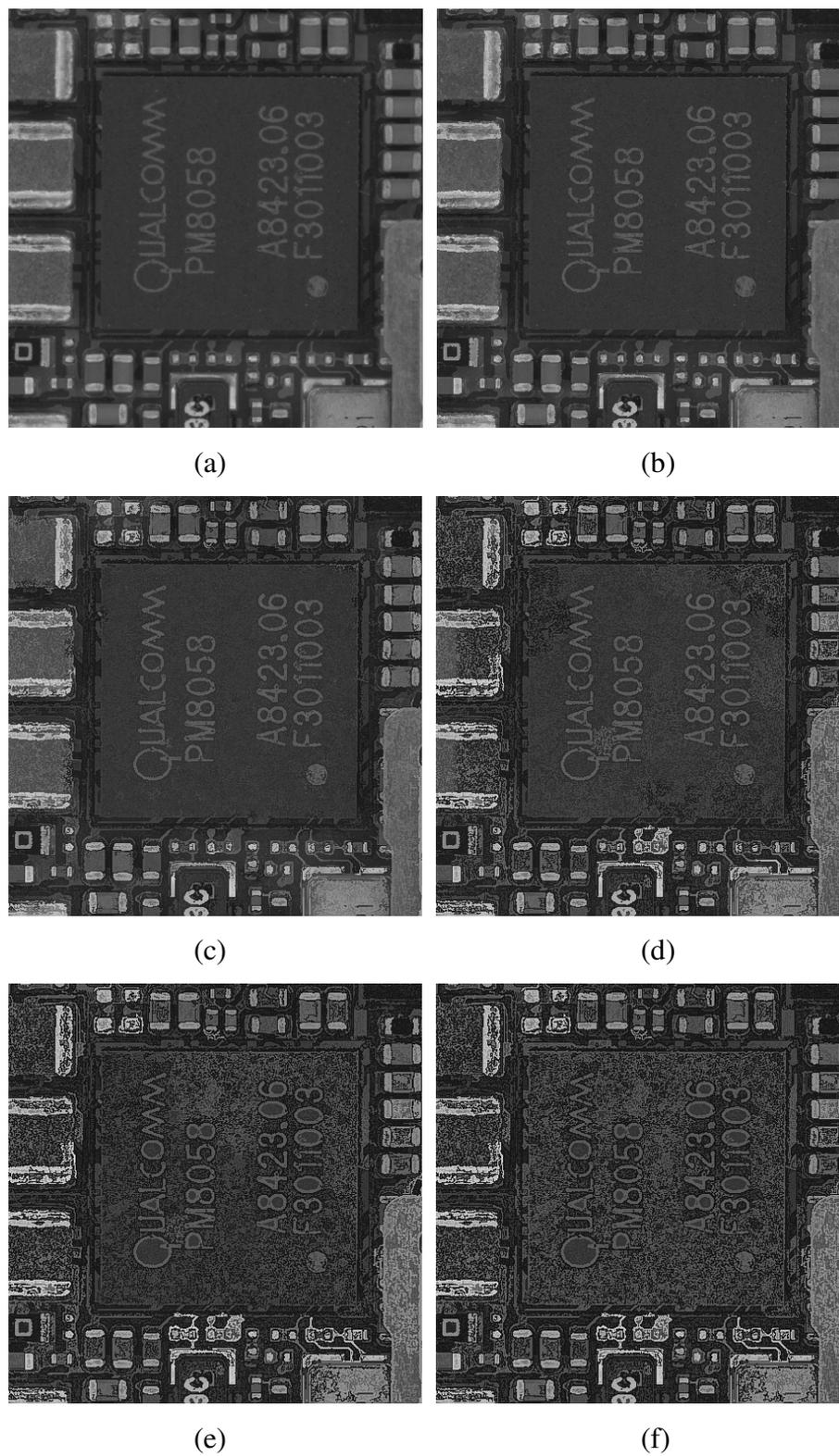
Figure 2.8. Toggle mapping operator: (a) original image, (b) first iteration, (c) 10th iteration, (d) 50th iteration, (e) 200th iteration and (f) convergence in 659th iteration. The Structure element SE is an 8-connected square of 3 x 3 pixels.

2.4.4 Binary Hit-or-Miss transform

Mathematical morphology is a family of nonlinear image processing operations based on the application of lattice theory to spatial structures. The traditional binary HMT (Hit-or-miss Transform) uses a pair of structure elements (S_1, S_2) to detect positions where S_1 has to match the foreground and S_2 the background of an image. The process is to find all positions where, S_1, will fit within an image, $\mathbf{I}$, and S_2^c within the background $\mathbf{I}^c$. This is defined as:

$$
\begin{aligned}
HMT\ (\mathbf{I}; S_1, S_2) &= \varepsilon_{S_1}(I) \bigcap \varepsilon_{S_2^c}(\mathbf{I}^c) \\
&= \left\{ \varepsilon_{S_1}(\mathbf{I}(x)) = \varepsilon_{S_2^c}(\mathbf{I}^c(x)) = 1,\ x \in \mathbf{E} \right\}
\end{aligned}
\tag{2.17}
$$

Where $S = S_1 \cup S_2$, $S_1 \cap S_2 = \varnothing$ and $S_1, S_2 \in \mathbf{E}$; $\mathbf{E}$ is the support region of the image, and S_1 and S_2 are the foreground and background structure elements, respectively. The traditional binary HMT is illustrated in Fig. 2.9. Fig. 2.9 describes the combination of structure elements S_1 and S_2 into a single structure element with specific foreground and background elements. The HMT is applied to locate the two corner shaped regions in the "image". The small bar at the top right is not detected. Note that the definition of the background structure element results in the lower corner region being detected despite having an extended horizontal bar.
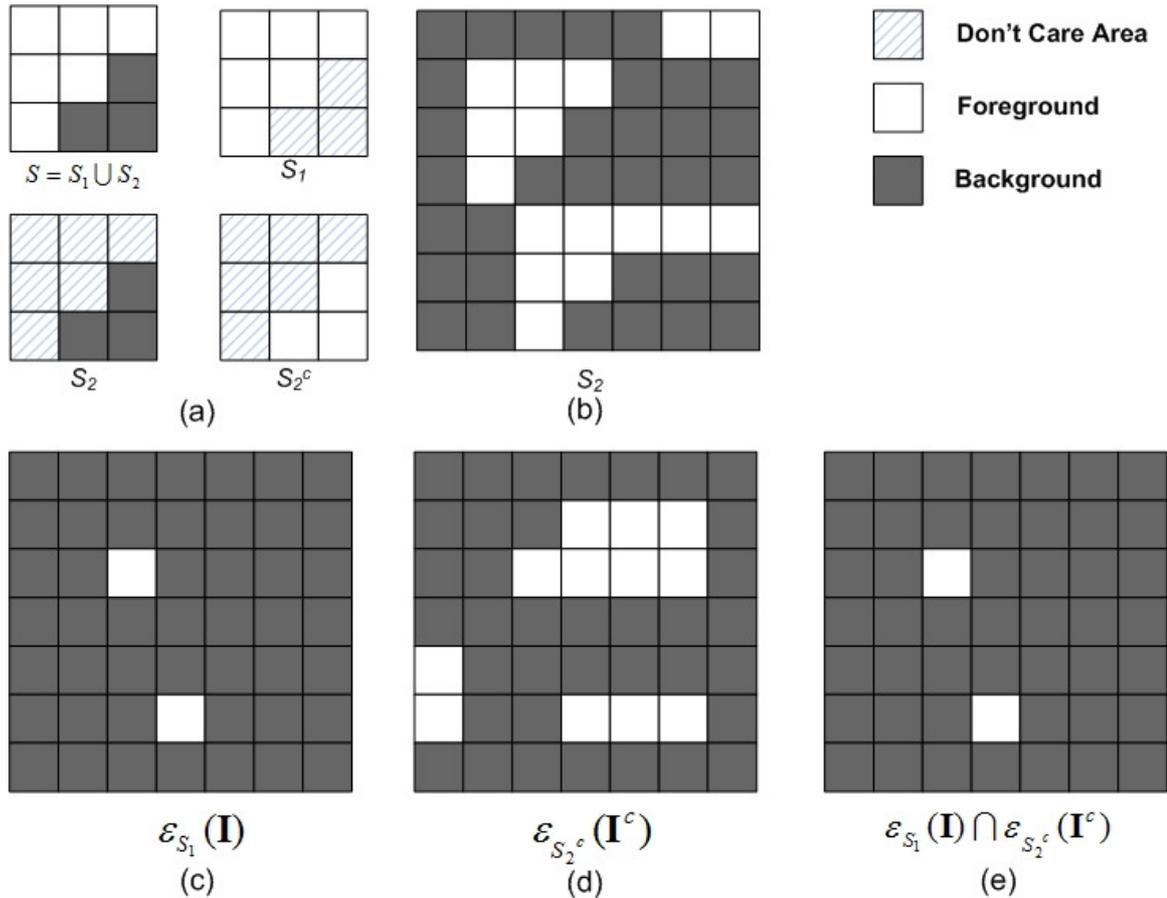
Figure 2.9. Traditional Hit-or-Miss Transform in binary images: (a) structure elements S, S_1 and S_2^c, (b) original image, (c) the erosion of image $\mathbf{I}$ using S_1, (d) the erosion of image $\mathbf{I}^c$ using S_2^c and (e) the result of Hit-or-Miss transform using S.

2.5 Principles of Conditional Toggle Mapping

In this section, we review the principles of conditional toggle mapping [VEL13]. The

conditionality relates to a set of pixels in a binary mask determining if any change is to be

considered. This provides a generic framework for edge enhancement and image noise

reduction. The key definitions for conditional erosion and dilation are introduced in Section

2.5.1. These definitions leading to the concept of conditional toggle mapping as described in

Section 2.5.2. How this is used for edge enhancement and noise reduction is described in

Section 2.5.3.

2.5.1 Conditional dilation and erosion

Let $\mathbf{M}$ be the characteristic function of a mask, such that, $\mathbf{M} \in \mathcal{F}(\mathbf{E},\{0, 1\})$ maps each position $x \in \mathbf{E}$ into $\{0, 1\}$. In this approach a structure element, SE, is modified by a mask, $\mathbf{M}$, using an association, N, defined as:

$$N_{(S,\mathbf{M})}(x) = \left\{ y \in S(x) \text{ and } \mathbf{M}(y) = 1 \right\} \tag{2.18}$$

The definitions of the conditional erosion and dilation with a mask, $\mathbf{M}$, and structure element, S, of an image, I, are then given, using Eq. (2.18), as:

$$\varepsilon_S(\mathbf{I}, \mathbf{M})(x) = \begin{cases} \wedge_{y \in N_{(S,\mathbf{M})}(x)} \mathbf{I}(y) & \text{if } \mathbf{M}(x) = 0 \text{ and } N_{(S,\mathbf{M})}(x) \neq \varnothing \\ \mathbf{I}(x) & \text{otherwise} \end{cases} \tag{2.19}$$

and

$$\delta_S(\mathbf{I}, \mathbf{M})(x) = \begin{cases} \vee_{y \in N_{(S,\mathbf{M})}(x)} \mathbf{I}(y) & \text{if } \mathbf{M}(x) = 0 \text{ and } N_{(S,\mathbf{M})}(x) \neq \varnothing \\ \mathbf{I}(x) & \text{otherwise} \end{cases} \tag{2.20}$$

The idea of the conditional morphology was firstly presented by Jochems [JOC97] for binary images. Eqs. (2.19) and (2.20) are equivalent to the ones introduced in [JOC97] for binary images but differs in grey-level images due to the "otherwise" case. The motivation of this idea is that pixels in the mask are considered as sources in the morphological operations.

2.5.2 Conditional toggle mapping

Similarly to conditional morphology, once the mask **M** is given, the conditional toggle

criterion can be defined as follows:

$$\tau_S(\mathbf{I}, \mathbf{M}) = \begin{cases} \varepsilon_S(\mathbf{I}, \mathbf{M}) & \text{if } \rho_S^\delta(\mathbf{I}, \mathbf{M}) > \rho_S^\varepsilon(\mathbf{I}, \mathbf{M}) \\ \delta_S(\mathbf{I}, \mathbf{M}) & \text{if } \rho_S^\delta(\mathbf{I}, \mathbf{M}) < \rho_S^\varepsilon(\mathbf{I}, \mathbf{M}) \\ \mathbf{I} & \text{otherwise} \end{cases} \qquad (2.21)$$

Where $\rho_S^\delta(\mathbf{I}, \mathbf{M}) = (\delta_S(\mathbf{I}, \mathbf{M}) - \mathbf{I}(x))$ and $\rho_S^\varepsilon(\mathbf{I}, \mathbf{M}) = (\mathbf{I}(x) - \varepsilon_S(\mathbf{I}, \mathbf{M}))$. The mask **M** plays

the role of a seed indicator when the dilation operator iteratively works on the mask **M**,

identifying the spread of pixel values through image **I,** according to the toggle criterion. The

toggle mapping is iterated spreading the values of **M** through the image until no pixel changed

in the mapping. Hence, a mapping $\tilde{\tau}_{SE}(\cdot, \cdot)$ is defined from and onto the image **I** and mask **M**,

using Eq. (2.21) and dilation operator on **M**, i.e.,

$$\tilde{\tau}_S(\mathbf{I}, \mathbf{M}) = (\tau_S(\mathbf{I}, \mathbf{M}), \delta_S(\mathbf{M})) \qquad (2.22)$$

The next iteration can be calculated as follows.

$$\begin{aligned} \tilde{\tau}_S^2(\mathbf{I}, \mathbf{M}) &= \tilde{\tau}_S(\tilde{\tau}_S(\mathbf{I}, \mathbf{M})) \\ &= \tilde{\tau}_S(\tau_S(\mathbf{I}, \mathbf{M}), \delta_S(\mathbf{M})) \\ &= \tau_S(\tau_S(\mathbf{I}, \mathbf{M}), \delta_S(\mathbf{M}), \delta_S(\delta_S(\mathbf{M}))) \\ &= \tau_S(\tilde{\tau}_S(\mathbf{I}, \mathbf{M}), \delta_S^2(\mathbf{M})) \end{aligned} \qquad (2.23)$$

As in Eq. (2.16), the conditional toggle mapping is then defined by iteration until convergence

$\widetilde{\tau}_S^\infty$ as follows:

$$\widetilde{\tau}_S^\infty(\mathbf{I}, \mathbf{M}) = \lim_{m \to \infty} \widetilde{\tau}_S^m(\mathbf{I}, \mathbf{M}) \tag{2.24}$$

Where $\widetilde{\tau}_S^m(\mathbf{I}, \mathbf{M}) = \tau_S(\widetilde{\tau}_S^{m-1}(\mathbf{I}, \mathbf{M}), \delta_S^m(\mathbf{M}))$, $\widetilde{\tau}_S^0(\mathbf{I}, \mathbf{M}) = (\mathbf{I}, \mathbf{M})$.

A proof of the convergence of the conditional toggle mapping with the mask $\mathbf{M}$ was presented in [VEL13].

2.5.3 Edge enhancement and image denoising

After defining the conditional toggle mapping, we can apply it in edge enhancement and image noise reduction as determined by the mask $\mathbf{M}$. In edge enhancement, the mask is defined in terms of local extrema as:

$$\mathbf{M}_E(x) = \begin{cases} 1 & \text{if } \min(\rho_S^\delta(\mathbf{I})(x), \rho_S^\varepsilon(\mathbf{I})(x)) = 0 \\ 0 & \text{otherwise} \end{cases} \tag{2.25}$$

The pixels in the mask, where $\mathbf{M}_E(x) = 1$, are considered as sources in the conditional toggle mapping when they contain the local maximum/minimum pixel value. Therefore, this will retain the contrasted pixels of the image.

In the case of impulse noise removal, mask $\mathbf{M}$ is defined by the pixels which are not corrupted

by impulse noise as:

$$\mathbf{M}_N(x) = \begin{cases} 1 & \text{if } \min(\rho_S^{\delta}(\mathbf{I})(x), \rho_S^{\varepsilon}(\mathbf{I})(x)) > 0 \\ 0 & \text{otherwise} \end{cases} \qquad (2.26)$$

Here, the pixels in the mask, where $\mathbf{M}_N(x) = 1$, are considered as sources in the conditional toggle mapping when they do not contain the local maximum/minimum pixel value. It should be noted that salt-and-pepper noises are always defined as the maximum/minimum pixel value. Therefore, this will remove the local extrema of the image.

Figure 2.10 demonstrates the performance of edge enhancement using the conditional toggle mapping operator with the mask $\mathbf{M}_E$ after 1st iteration and convergence after 7th iteration without showing ringing effects, and Fig. 2.11 demonstrates ability to suppress the salt-and-pepper noise using iteratively conditional toggle mapping with mask $\mathbf{M}_N$ after 8th iteration (convergence).

In the case of grey-level images an uncorrelated salt and pepper impulse noise was simulated according to the following rule: the added noise was distributed so that 50% of the noise level in salt impulse noise and 50% of the noise level in pepper impulse noise was randomly added to grey-level images, respectively.

A simple model is the following [BON00]: Let $I(i, j)$ be the original image and $J(i, j)$ be the image after it has been altered by salt and pepper noise.

$$J(i, j) = \begin{cases} \text{MAX,} & \text{with probability } \alpha/2 \\ \text{MIN,} & \text{with probability } \alpha/2 \\ I(i, j), & \text{with probability } 1 - \alpha \end{cases} \qquad (2.26)$$

where MAX and MIN are the maximum and minimum image values, respectively. For 8 bit images, MIN = 0 and MAX = 255. The idea is that with probability $1 - \alpha$ the pixels are unaltered; with probability α the pixels are changed to the largest or smallest values. The altered pixels look like black and white dots sprinkled over the image. Here, Fig. 2.10(b) shows the overall 40% noise level of salt and pepper noise was added to the original image for evaluation. Approximately 40% of the pixels have been set to black or white (60% are unchanged).

This chapter only focused on binary and grey-level morphology, and the extension to colour morphology will be reviewed in the next chapter.
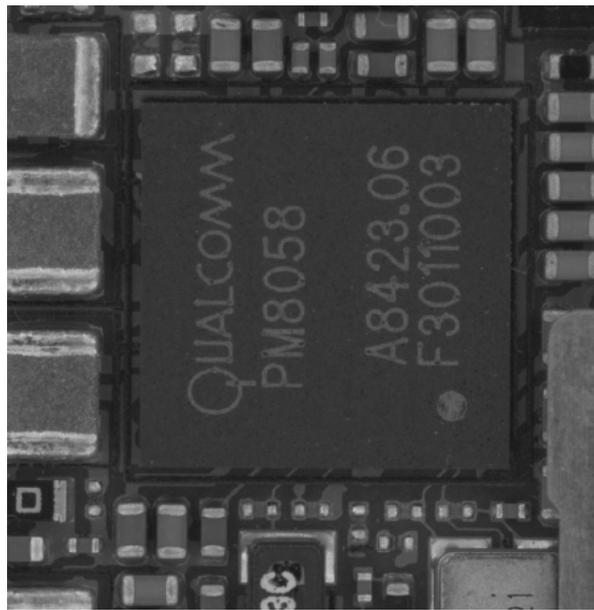
(a)
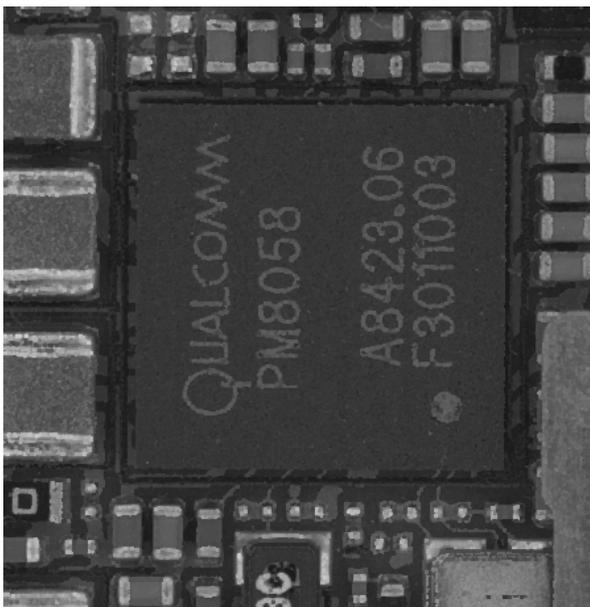
(b)
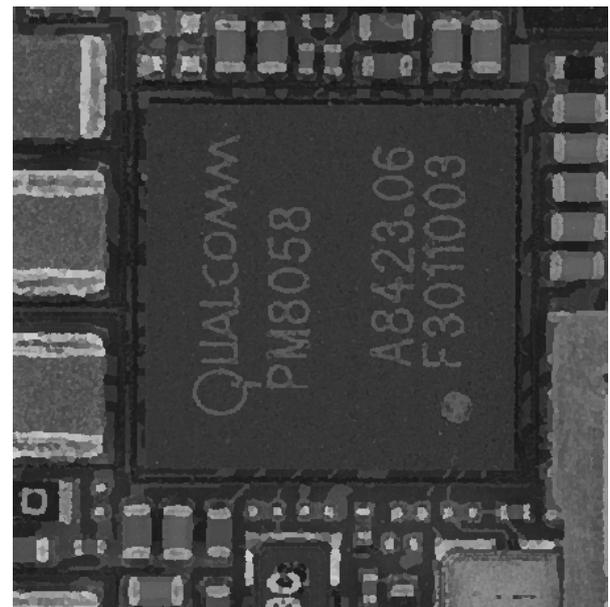
(c)

Figure 2. 10. Edge enhancement using the conditional toggle mapping operator: (a) original grey-level image, (b) first iteration and (c) convergence after the 7th iteration of conditional toggle mapping. The Structure element SE is a 8-connected square of 3 x 3 pixels.

(a)

(b)

(c)

(d)
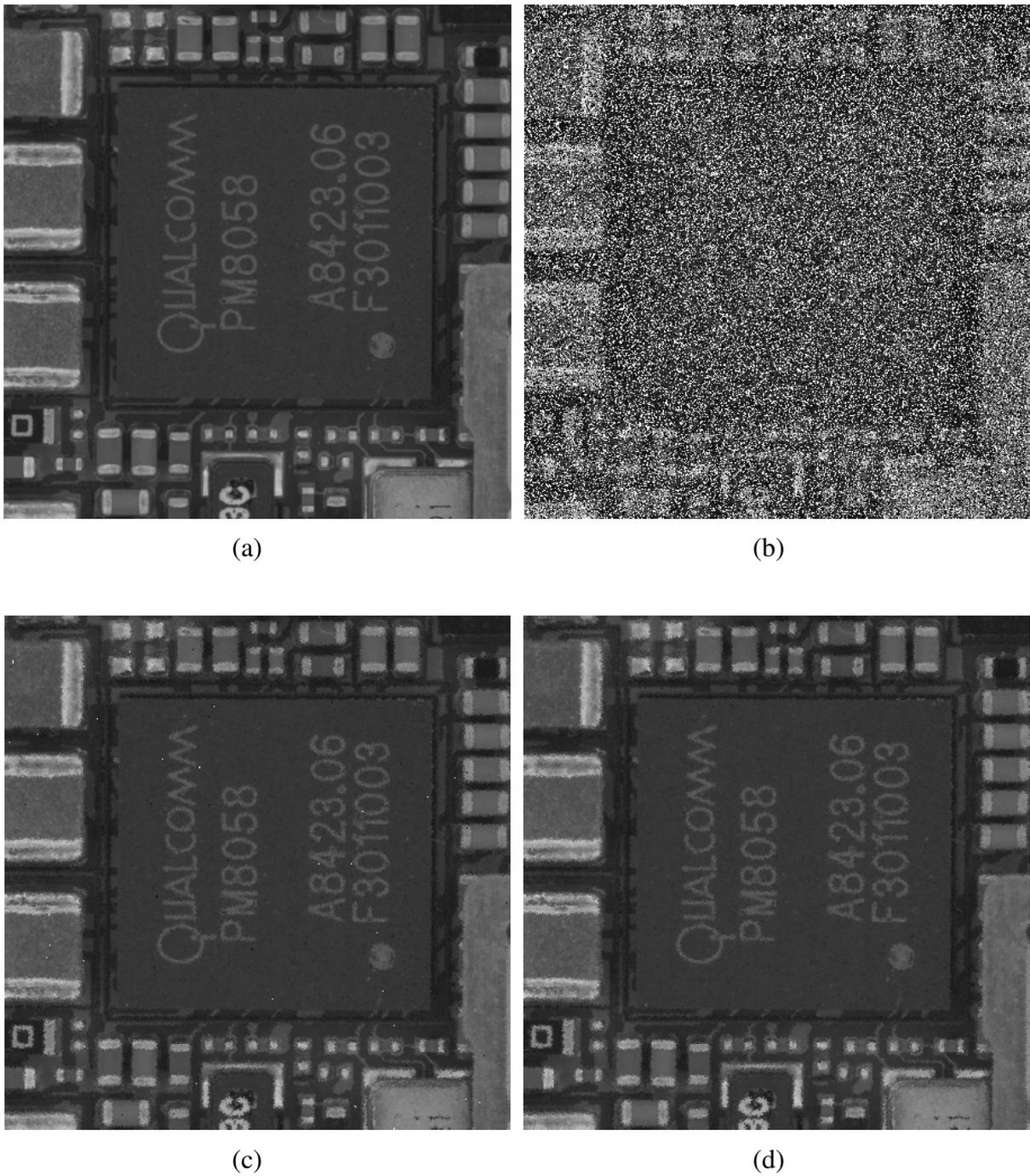
Figure 2.11. Salt-and-pepper noise removal using the conditional toggle mapping operator: (a) original grey-level image, (b) image with 40% salt-and-pepper noise added, (c) first iteration and (d) convergence after 8th iterations of conditional toggle mapping.

Chapter 3: Review of Colour Morphology

As discussed in Chapter 2, the use of mathematical morphology for noise reduction, edge detection, segmentation, texture and shape analysis in binary and grey-level images is well established [NAJ10]. Here we review the commonly used colour models and the previous approaches to colour morphology that seek to address the need for an ordering or criteria for a maxima and minima in vector or multi-dimensional spaces. Moreover, the complete lattices will be introduced for mathematical morphology.

3.1 Colour Image Notation

Following Chapter 2 Let $\mathbf{I} \subseteq \mathbb{R}^p$ be a multivariate images composed of pixel values of dimension p. Let $\mathbb{F} \subseteq \mathbb{R}^p$ be a multivariate image composed of vector values in the continuous space $\mathbb{R}^p$. Let $\mathbf{E}$ be a subset of the discrete space $\mathbb{Z}^2$; $\mathbf{E}$ is the spatial support of a 2D image, $\mathbf{I}:\mathbf{E} \rightarrow \mathbb{F}$ commonly denoted by $\mathcal{F}(\mathbf{E}, \mathbb{F})$. In this mapping pixel values are mapped from coordinates $x =(i, j) \in \mathbf{E}$ to vector values, $\mathbf{t} \in \mathbb{F} \subseteq \mathbb{R}^p$. Here, p is 3 for colour images. Let us introduce the notation for a colour image, as shown in Fig. 3.1, where the object of interest is a region in a *3*-channel image which is mapped from the spatial support $\mathbf{E}$ to the vector support $\mathbb{F}$, i.e.,

$$\mathbf{I} : \begin{cases} \mathbf{E} \to \mathbb{F} \\ x \to \mathbf{t} \end{cases} \qquad (3.1)$$

Where image $\mathbf{I}$ is mapped by the spatial support $\mathbf{E}$ at each position $x \in \mathbf{E}$ into a colour vector

$\mathbf{t} \in \mathbb{F}$: $\mathbf{t} = \mathbf{I}(x)$.

$x = (i, j) \in \mathbf{E}$ $\mathbf{I}(x) \in \mathbb{F}$

(a)   (b)
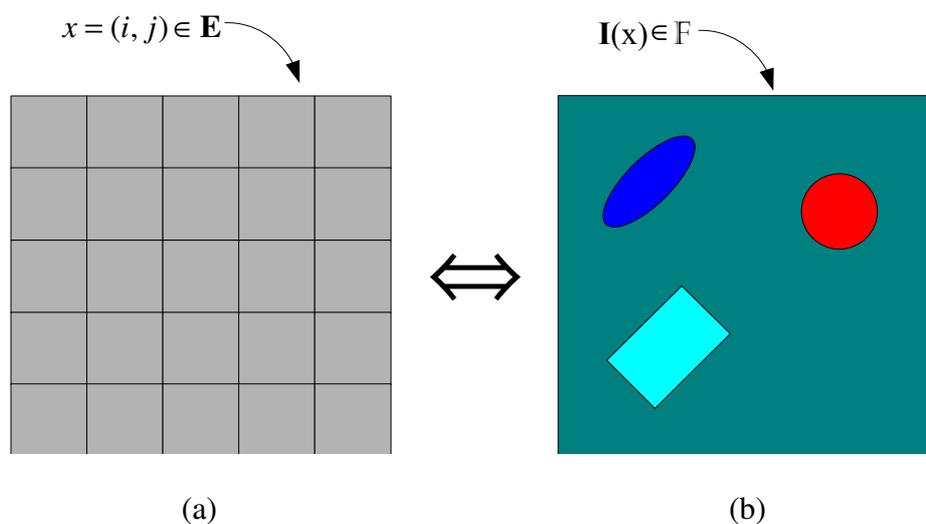
Figure 3.1. Notation for a colour image: (a) Discrete support: $\mathbf{E} = \mathbb{Z}^2$ and (b) Image range: $\mathbb{F} = \mathbb{R}^3$.

3.2 Colour Models

A colour model is an abstract mathematical model that describes the representation of colour.

Coordinates in the colour space specify a colour. The coordinates represent the location of

each colour.

The set of all colours that can be generated on a device is called the colour gamut. Different

colour models have been developed to meet the requirements of applications, display and

image acquisition devices. The limited gamut of a display device is why some colours cannot

be represented and in acquisition why some colours cannot be distinguished.

Colour models are also distinguished by the scale that they represent, by their representation of additive or subtractive colour representation and by the perceptual uniformity, or not, of unit changes in each axis of the colour space. In the following review of commonly used colour models we draw on the description given by [SHA03].

3.2.1 RGB colour model

Colours in the RGB colour model are represented by the three primary colours, red, green and blue. Thus, a colour in the RGB colour model can be defined as a vector in a three-dimensional (3D) space that can be also represented as a unit cube using a Cartesian coordinate scheme. The grey-level spectrum lies on the line between black and white that consists of colours with a constant proportion of red, green and blue present. The disadvantage of the RGB colour model is that not all colours visible to the human eye can be expressed because the RGB primary colours are the additive combinations in this model. The RGB representation has been mostly used in digital cameras and computer displays because it provides a natural representation for the hardware implementation of acquisition devices.

3.2.2 CMY and CMYK colour model

The CMY colour model provides a subtractive representation based on channels for cyan,

magenta and yellow as the primary colours. The subtractive CMY and additive RGB colour models provide complementary colours. The CMYK colour model is an extension of the CMY colour model with black added to the representation because it is difficult to produce black by combining cyan, magenta and yellow. The CMY and CMYK colour models are well suited to printing where colours combine subtractively.

3.2.3 YUV, YIQ and YCbCr colour model

These colour models are commonly used in television (TV) transmission. They are a recoding of the RGB colour model to provide channels for brightness, hue and saturation that are used for colour television broadcasting in Europe and in the USA, respectively. Having a brightness channel means that more bits can be allocated to encode this information, which is critical to visual perception and provides comparability with monochrome TV systems. The YCbCr colour model is independent of transmission coding systems and is commonly used for representing TV images in digital systems.

3.2.4 HSV and HSL colour model

The HSV colour model also represents a colour using three components for hue, saturation and value; in the HSL representation value is replaced by luminance.

The hue component ranges from 0 to 2π, which begins and ends by red, and the colour wheel

is along two axes, red-green and blue-yellow. Saturation indicates the colour purity that ranges from 0% if the colour is not saturated, but is a grey-level, to 100% if the colour is a saturated pure colour. The intensity component of a colour in both the HSV and HSL colour models shows the brightness of the colour. Maximum intensity is defined as pure white and minimum intensity as pure black. The value component in the HSV colour model ranges from 0 to 1, where the colours become brighter. The HSV colour model is represented as a cone whilst the RGB colour model as a cube.

3.2.5 CIE colour models

All the colour models reviewed above express colours in a device dependent manner. To define a colour in a device independent way, the CIE (Commission Internationale de l'Eclairage) provides a standard method for specifying a colour under the controller capturing conditions, including light, object and eye [SHA03].

The details of the CIE XYZ colour model can be found in [SHA03]. It is based on the direct measurements of the human eye. The CIE introduced three values X, Y and Z that can produce all human perceptions. The X, Y and Z values are also called the standard colour coordinates, but it is difficult to be used directly because they do not correspond to real colours. The following CIE colour models are transferred from the CIE XYZ model.

The L*a*b* and the L*u*v* colour models are a linear representation providing a uniform correspondence between geometric distances and perceptual distances between colours with the same conditions of illumination.

In these two models, the colour difference can be quantified by the Noticeable Colour Difference or Just-Noticeable Difference (JND). The common light source is daylight, defined as illuminant D65, introduced for the colour industries [SHA03]. Both the L*a*b* and L*u*v* colour models represent colours with a reference white point and, therefore are not completely device independent.

Both L*a*b* and L*u*v* colour models use a common lightness scale L*, which ranges from 0 (black) to 100 (white). The axis a* represents red-green colours that positive a* is close to red and negative a* green. In the same way, the axes b* and u* represent yellow-blue and red-green colours, respectively. At every colour axis values range from positive to negative. On the a* and u* axis the positive values give the amount of red and negative values the amount of green whilst at the b* and v* axis yellow is positive and blue negative. The L*a*b* colour model is always used in colour imaging and printing industries whilst the L*u*v* colour model is useful in the display industry. For more information we refer to [SHA03].

3.2.6 Comparison of colour models

In practice, only a finite number of colours can be represented in any one colour model. Each

colour component is usually stored as 8 bits so that a colour in a 3D colour model is stored as

a 24-bit value. The value of each colour component ranges in the interval [0, 255], and we can

scale them to the interval [0, 1] in the colour models for ease of representation. The

representation of a colour component in 8bits is used because this fits the digital

implementation. Not all axes need the same detail for colour models. For example in YCbCr

the NTSC system will transmit colour on alternate lines. This can use far fewer bits for colour

than luminance.

Although the RGB representation is commonly employed for colour morphology the RGB

channels are strongly correlated [ANG07a] [LOU02] [HAN01a]. The hue-saturation-value

(HSV) and hue-luminance-saturation (HLS) colour spaces show less correlation between

channels and have been used for colour morphology [LOU02] [HAN01a][[VAR02]] but they

lack perceptual uniformity as also does RGB [ANG07b]. The correlation between the

channels in CIE L*a*b* colour space is low and the perceptual linearity is good.

As described above, the RGB, HSV and CIE L*a*b* colour models have been commonly

considered in previous research because these colour models are well defined and widely

accepted for colour image processing. Therefore, these colour spaces will be reviewed with a view to their suitability for colour morphology in the following subsection.

3.3 Colour Orderings for Mathematical Morphology

In mathematical morphology, we need the concept of a supremum and infimum to define morphological operators. Hence, an ordering between colour vectors has to be developed for colour morphology. There is no unambiguous way to order colours. Two common approaches to colour morphology are: to use component-wise (marginal) and vector ordering. Barnett identified four families of ordering for vectors [BAR76]: marginal ordering (M-ordering), reduced or aggregate ordering (R-ordering), partial ordering (P-ordering), and conditional ordering (C-ordering).

In M-ordering, each colour component is ordered independently and the morphological operations are applied to each colour component of the colour image. A major disadvantage of this ordering is the well-known problem of false colours [SER09]. In this case a false colour is a colour, produced as the result of a morphological operation that was not present in the original image.

In R-ordering, each vector is reduced to a scalar value according to distance or projection criteria. For each colour, $\mathbf{c}_i$, there is a scalar value $d_i = d(\mathbf{c}_i)$ such that $d : \mathbb{R}^3 \rightarrow \mathbb{R}$. After d_i has been obtained for each i, the colours $\mathbf{c}_1, \dots, \mathbf{c}_n$ can be ordered using $d_1, \dots, d_n$ as follows.

$$\mathbf{c}_{(1)} \leq \mathbf{c}_{(2)} \leq \dots \leq \mathbf{c}_{(n)} \tag{3.2}$$

Where $\mathbf{c}_{(1)}, \mathbf{c}_{(2)} \dots, \mathbf{c}_{(n)}$ are the colour vectors corresponding to the scalar values $d_1, d_2 \dots, d_n$. The output colour vector using this ordering is one of the original colour vectors. Hence, no false colour can be introduced. The output is influenced by the choice of the scalar-valued function. Functions that have been used are the Mahalanobis distance measure [ALO03], projection using principal component analysis (PCA) [LI04] and other non-linear transformations [LEZ09]. These methods led to results that were unstable depending, in an erratic manner, on the set of colours present in the neighbourhood.

In P-ordering, the colour vectors were first clustered and then ordered. Recently, combinational techniques and median filters have been used to construct colour orderings [LEZ07] [PLA04]. However, these orderings were depended on the local values of the spatial window so that dilation (erosion) cannot commute with the supremum (infimum) nor distribute.

In C-ordering, also known as lexicographical ordering, the colours are ordered using one each colour component in turn. When all the components are used, the C-ordering is a total ordering [APT08]. Let $\mathbf{c} = \{ c_1, c_2, c_3 \}$ and $\mathbf{t} = \{ t_1, t_2, t_3 \}$ be the two colour vectors in the selected colour model then conditional ordering is defined as:

$$\mathbf{c} < \mathbf{t} \Leftrightarrow \begin{cases} c_1 < t_1 \ \text{ or} \\ c_1 = t_1 \ \text{ and } \ c_2 < t_2 \ \text{ or} \\ c_1 = t_1 \ \text{ and } \ c_2 = t_2 \ \text{ and } \ c_3 < t_3 \end{cases} \tag{3.3}$$

The magnitude of each component of the vector is processed in sequence, with the disadvantage that the outcome may be arbitrarily decided by the first one or two image channel(s) considered. This makes sense when a priority can be placed on particular components, but can lead to arbitrary results and is especially inappropriate when the RGB colour space is used. It is difficult to decide the first and second important channels in the RGB colour space.

3.3.1 Colour morphology in the RGB model

Several approaches to using RGB for colour morphology [COM99] [CHE03] [SAR01] have been presented. In [COM99] a reduced ordering was proposed using linear combinations of RGB values, i.e., the luminance function and the Euclidean norm. A PCA-like transformation was used to order RGB colour vectors, and the fundamental colour morphological operators, erosion and dilation, were defined on the basis of this reduced ordering [CHE03]. Sartor and Weeks [SAR01] proposed a combination of reduced ordering and conditional ordering to form a set of morphological operators for RGB colour images. The RGB colours were transformed to the $C - Y$ colour space. A reduced ordering was defined using a measure of distance to a reference colour vector determined by its hue. This provides the primary ordering criterion. The reference colour should have maximum luminance and maximum saturation to obtain a total ordering for colour vectors. White and black cannot be used as the reference colour under these conditions because they provide no concept of saturation.

3.3.2 Colour morphology in the HSV model

The uses of the HSV and related colour models are attractive for colour morphology [ANG05][LOU02] because the information of hue, saturation and luminance can be easily separated. Angulo [ANG05] introduced a unified framework that considers different ways to define colour morphological operators with the colour representation of luminance, saturation

and hue by using conditional orderings on the HSL colour model. In [LOU02], a colour

ordering in the HSV colour model was presented. This ordering was defined, for two colours

$\mathbf{c}_1$ (h_1, s_1, v_1) and $\mathbf{c}_2$ (h_2, s_2, v_2), as:

$$\mathbf{c}_1 \leq \mathbf{c}_2 \Leftrightarrow \begin{cases} v_1 < v_2 & \text{or} \\ v_1 = v_2 & \text{and } s_1 \geq s_2 \end{cases}$$
$$\mathbf{c}_1 = \mathbf{c}_2 \Leftrightarrow v_1 = v_2 \text{ and } s_1 = s_2$$

(3.4)

The subtraction of two colours was defined as:

$$\mathbf{c}_1 - \mathbf{c}_2 \Leftrightarrow c(h_1, s_1 - s_2, v_1 - v_2)$$

(3.5)

Where $s_1 - s_2 = 0$ if $s_1 - s_2 < 0$ and $v_1 - v_2 = 0$ if $v_1 - v_2 < 0$. Addition was defined as

$$\mathbf{c}_1 + \mathbf{c}_2 \Leftrightarrow c(h_1, s_1 + s_2, v_1 + v_2)$$

(3.6)

Where $s_1 + s_2 = 1$ if $s_1 + s_2 > 1$ and $v_1 + v_2 = 1$ if $v_1 + v_2 > 1$. This is hue preserving and the

infimum and supremum operators are defined to form the corresponding colour

morphological operators.

In the HSV colour model, it is difficult to order by hue because it is distributed on the unit

circle and is a continuous scale (360 is close to 0) and no-value has a dominant position.

Research into the colour morphology based on hue includes that by [HAN01a] [HAN01b]

[PET97] [APT09]. However, these hue orderings are ambiguous because their definitions of hue origin are context dependent and arbitrary.

3.3.3 Colour morphology in the CIE L*a*b* model

The CIE L*a*b* colour model has been used with complex weighting functions and including a C-ordering based on the adoption of an "electrostatic potential" analogy to define colour morphology [HAN02]. A lower weight is assigned to colour vectors that are close to colours of maximum chroma, and higher weights to colour vectors that are close to the lightness axis. The complexity of the weighting function used reflects the difficulty of defining extrema in the irregularly shaped gamut of the CIE L*a*b* colour model.

3.3.4 The state-of-the-art overview for colour morphology

To generalise the above colour orderings for mathematical morphology an algorithmic framework has been developed using distance and conditional approaches. This framework supports the extension of morphological operations to colour images for different colour models (e.g. RGB, HSL and L*a*b*) and the definition of metric distances to a reference colour [ANG07a]. It is important that it should be possible to specialise colour morphology operators to form binary and grey-level operators. Most previously reported schemes do not permit this because the colour orderings are developed independently without considering the

properties of morphological operators, such as increasing (ordering preservation), idempotence (invariant to the operator itself), extensivity and anti-extensivity. Therefore, Angulo [ANG07a] proposed a reference-based ordering to consider the above properties but the defined maximum distance is associated with the "farthest" vector to the reference colour that needs the prior knowledge of applications.

There is no universal and widely accepted method for colour morphology because each method introduced to date has limitations. The key issue is the need to define a total ordering for colour vectors. In comprehensive reviews of colour morphology [ANG07a] [APT07], the challenge has been identified as being to define a colour ordering that meets the requirements of mathematical morphology using complete lattices, that reflects colour perception and avoids the need for context dependence.

Recent research into mathematical morphology was undertaken by Velasco-Forero and Angulo [VEL11] [VEL12], by Caliman et al. [CAL13] and Burgeth and Kleefeld [BUR13]. Velasco-Forero and Angulo introduced the notion of supervised ordering based on a learning algorithm, and evaluated their work using hyperspectral images [VEL11]. With this approach the reference colours in the foreground and background must be given to define a vector ordering for multivariate mathematical morphology. Velasco-Forero and Angulo [VEL12]

further proposed an unsupervised ordering based on a statistical depth criterion computed using random projections. This ordering and the associated morphological operators can be interpreted in a similar way for grey-level images, without using reference colours. In [CAL13] PCA was used to find an axis, and the distance to the extrema to generate an ordering. The main disadvantage of this method is that the estimated extrema depends on the colour vectors of the spatial window. The selection of extremas is therefore not stable. As a result dilation (erosion) can neither commute nor distribute with the supremum (infimum). In a more complex approach [BUR13], matrices and cones are used to find a colour that can be considered to be larger than all colours under the spatial window. This was done by embedding the colour vector into a symmetric, positive definite matrix so that the Loewner ordering may be used. This produces a local ordering. A large body of diverse mathematical concepts has been used to form colour morphological operators. However, it is difficult to identify a colour ordering that meets the requirements of mathematical morphology using complete lattices. Also the operations of these methods are often not compatible with binary and grey-level morphology. The use of matrices and cones has been shown to be effective in the analysis of complex data such as that produced by the diffusion tensor MRI, where each pixel is a positive definite matrix.

Grundland and Dodgson [GRU07] presented a new contrast enhancing colour to grey-level

conversion algorithm that takes advantage of continuous mapping, global consistency, and grey-level preservation. This method has the predictable luminance, saturation, and hue ordering properties that imposes an image dependent colour ordering relation in extending mathematical morphology in colour. However, the contrast calculation of this method depends on the colour vectors of neighbourhood, so that it is difficult to identify this colour ordering that meets the requirements of mathematical morphology using complete lattices.

To extend the idea of morphological scale-spaces for colour images, Gibson et al. [GIB03] presented a natural extension of graph-based morphology in colour that uses the max or min tree [SAL95] [SAL98] to form the extrema. This introduced a new colour scale-space processor that is devised by introducing colour equivalents of the extrema-identification step and the merging step. For more details about graph-based morphology, please refer to [NAJ14]. The difficulty of extending graph-based morphology to colour images is to define the connectivity in colour. There is a need to ensure the colour connectivity for advanced mathematical morphology but not included in this thesis.

3.4 Complete Lattices in Mathematical Morphology

In [RON90], the authors show that the generalisation of morphological operations to complete

lattices is necessary for mathematical morphology on grey-level images. In this section, we

first briefly recall the theoretical concepts of colour morphology [HEI90] [GOU95] and

describe the proposed ordering schemes.

3.4.1 Definitions

Complete lattice theory is widely regarded as the most appropriate framework for

mathematical morphology. For a detail exposition on complete lattice theory, we refer to

Chapter 2 in [NAJ10]. The importance of lattice theory for mathematical morphology is also

explained in [NAJ10].

Definition 1. A space $\mathcal{L}$ endowed with a partial order $\leq$ is called a *complete lattice*,

denoted $(\mathcal{L}, \leq)$ if every subset $\mathcal{H} \subseteq \mathcal{L}$ has both supremum (join) $\vee \mathcal{H}$ and infimum (meet) $\wedge \mathcal{H}$.

A minimum (smallest) n is contained in the lattice $\mathcal{H}$ if $l \in \mathcal{H} \Rightarrow n \leq l, \forall l$. We denote the

minimum element of $\mathcal{L}$ by $\text{Inf}_{\mathcal{L}}$. Equivalently, the maximum element of $\mathcal{L}$ is denoted by $\text{Sup}_{\mathcal{L}}$.

Definition 2. A mapping $h : \mathcal{L}_1 \rightarrow \mathcal{L}_2$ of a complete lattice $\mathcal{L}_1$ into a complete lattice $\mathcal{L}_2$ is

said to be a dilation if $h(\vee_{i \in \mathbf{I}} c_i) = \vee_{i \in \mathbf{I}} h(c_i)$ for all families $(c_i)_{i \in \mathbf{I}}$ of elements in $\mathcal{L}_1$. A

mapping is said to be erosion if $h(\wedge_{i \in \mathbf{I}} c_i) = \wedge_{i \in \mathbf{I}} h(c_i)$ for all families $(c_i)_{i \in \mathbf{I}}$ of elements in

$\mathcal{L}_1$.

Dilation and erosion are each a dual of the other from the lattice point of view [SER88].

3.4.2 *h*-mapping in pre-ordering

Let $\mathbb{F}$ be a nonempty set of image pixels values with the support space **E** and $\mathcal{L}$ a complete

lattice. In [GOU95] the basis for a surjective mapping h: $\mathbb{F} \rightarrow \mathcal{L}$ was defined. An equivalence

relation $=_h$ on $\mathbb{F}$ was also defined as follows:

$$r =_h r' \Leftrightarrow h(r) = h(r'), \quad \forall r, r' \in \mathbb{F} \tag{3.7}$$

We refer by $\leq_h$ to the *h*-ordering given by the following relation on $\mathbb{F}$:

$$r \leq_h r' \Leftrightarrow h(r) \leq h(r'), \quad \forall r, r' \in \mathbb{F} \tag{3.8}$$

Note that $\leq_h$ preserves reflexivity ($r \leq_h r$) and transitivity ($r_1 \leq_h r_2$ and $r_2 \leq_h r_3 \Rightarrow r_1 \leq_h r_3$).

However, $\leq_h$ is not a partial ordering because $r \leq_h r'$ and $r' \leq_h r$ implies only that $r =_h r'$ but

not $r = r'$. This means that an *h*-ordering for a set of colours only compares the *h*-mapping. It

should be noted that *h*-ordering is a pre-order in $\mathbb{F}$. Here, the partial ordering means a

complete ordering, which is injective. On the contrary, the pre-ordering is a surjective

ordering.

An operator $\varphi: \mathbb{F} \rightarrow \mathbb{F}$ is *h*-increasing if $r \leq_h r'$ implies that $\varphi(r) \leq_h \varphi(r')$. Additionally, since *h* is surjective, an equivalence class can be defined by $\mathcal{L}[z] = \{r \in \mathbb{F} \, | h(r) = z\}$. Most importantly, the *h*-ordering has to be completed in each equivalence class to lead to a *h*-injective for a complete total ordering.

This chapter reviewed the colour models and the previous reported colour orderings for mathematical morphology. Next chapter will deal with the idea of analyse colour images taking advantage of the lattice representation via *h*-orderings that harmonises binary, grey-level and colour morphology.

Chapter 4: Importance of Extrema in Colour Morphology

In binary and grey-level images, the nature of erosion (minima) and dilation (maxima) is determined by the choice of foreground and background colours. It is commonly presumed that grey-level erosion is achieved by taking the minimum when the foreground is white (a high value). This is valid but it is a major simplification that is not open to generalisation. Angulo [ANG07a] proposed a generic framework for morphology based on extrema that are "reference colours". It is difficult to naturally define a foreground colour, which is an extrema in colour spaces, such as RGB, HSV and L*a*b*. Here, a colour correction model [HEO11] inspired us to arrive at a more generic sense of extrema in colour, with colour difference formula that include the Euclidean and the CIE-94 colour difference E^*_{94} in RGB and CIE L*a*b* colour spaces, respectively. The CIE-94 colour difference formula was used because it has a more uniform chromaticity scale than the basic Euclidean distance and the CIE-2000 colour difference in the CIE L*a*b* space, for which it was designed [SHA03].

In this chapter, we develop a total ordering based on complete lattices for colour erosion, dilation and filtering operations that only combines R- and C-ordering. This is because M-ordering always produces false colours and P-ordering does not meet the requirements of

mathematical morphology for complete lattices, as reviewed in Chapter 3. The R-ordering was based on the colour difference formulae and the C-ordering on a lexicographical cascade by colour difference and colour channel. C-ordering was used to resolve any remaining ambiguity of colour difference. The definition of colour extrema inspired by the colour correction model [HEO11] and the use of extrema as a basis for colour mathematical morphology are novel and permit the creation of a complete lattice that can be used in a traditional definition of mathematical morphology operators for colour that can be specialised to grey-level and binary morphology.

4.1 The Definition of Colour Extrema

One of the challenges for colour morphology is to define the foreground in colour images. Angulo [ANG07a] defined "reference colours" as the foreground, and Velasco-Forero and Angulo [VEL11] proposed a supervised ordering using the pre-defined foreground and background. This is only appropriate with prior knowledge of an application. Here, a generic definition of colour extrema that facilitates the definition of a foreground colour is presented and discussed with reference to various colour models.

Image formation by a linear imaging device was mostly used in [FIN98] [FIN01] that can be described by:

$$p_k^x = \int_w E(\lambda)S^x(\lambda)R_k(\lambda)d\lambda, \tag{4.1}$$

where p_k^x represents the response of the kth sensor at position x. For a colour channel it is

common to refer the triplet of sensor responses (p_1^x, p_2^x, p_3^x) as R, G and B (red, green and

blue), respectively at point x in the scene. $E(\lambda)$ represents the spectral power distribution of

the incident illumination, $S^x(\lambda)$ the surface reflectance at a point x in the scene and $R_k(\lambda)$ the

spectral response of the kth sensor, where λ is the wavelength. Changing either the spectral

power distribution or the surface reflection function will change the values detected by the

imaging device.

The image formation model of Eq. (4.1) is simplified by ignoring any non-Lambertian

reflectance as this work is based on the assumption of the Lambertian surface. The

radiometric variations induced by non-Lambertian reflectance effects are not considered

because they are difficult to be formulated, such as specular highlights [FIN03]. Hence the

colour image formation is expressed at p as [HEO11]:

$$\begin{pmatrix} R(p) \\ G(p) \\ B(p) \end{pmatrix} \rightarrow \begin{pmatrix} \tilde{R}(p) \\ \tilde{G}(p) \\ \tilde{B}(p) \end{pmatrix} = \begin{pmatrix} \rho(p)aR(p)^\gamma \\ \rho(p)bG(p)^\gamma \\ \rho(p)cB(p)^\gamma \end{pmatrix} \tag{4.2}$$

where each pixel, p, has its own individual brightness factor $\rho(p)$ which depends on the angle

between the direction of the light and the direction of the surface normal at that point in the

scene. The exponent γ is the gamma correction of the imaging device; a non-linear scaling of

image intensity. It is assumed that the camera responds in a linear fashion to light intensity

(i.e. has $\gamma = 1$). This is commonly the case for cameras used for image interpretation.

Changing the illumination colour with a fixed lighting geometry will result in a change of

response from each of the three colour channels, expressed by the global scale factors a, b,

and c, on the right hand side of Eq. (4.2).

In this model, if the illumination colour is not known then the CIE D_{65}, daylight illuminant is

assumed [HAN02]. Letting the global scale factors, a, b, and c, be approximately equal to 1

provides illumination colour independence, and the chromaticity of colour appearance is,

therefore, rendered invariant to changes in illumination intensity. To adjust the illumination

intensity, the brightness factor (p) will increase or decrease. Here, the chromaticity of a colour

can be interpreted as a unit vector in the RGB colour space. The extrema of each colour in

RGB colour space can be determined by the brightness factor (p) whilst retaining the

chromaticity. Given the colour image formation model of Eq. (4.2), each chromaticity has its

own extrema colour vector, $\mathbf{c}^{MAX}$, defined as:

$$\mathbf{c}^{MAX} = \begin{cases} (\rho^{Max}R, \ \rho^{Max}G, \ \rho^{Max}B), & \text{if } \max(R, G, B) > 0 \\ (255, \ 255, \ 255), & \text{if } \max(R, G, B) = 0 \end{cases} \qquad (4.3)$$

where (R_i, G_i, B_i) is the colour representation of **c**, p^{Max} is the maximum brightness factor in each chromaticity, calculated using:

$$\rho^{Max} = \frac{MAX}{\max(R,G,B)} \tag{4.4}$$

where *MAX* is 255 for a device such as a digital camera giving 8-bit integer responses. When the maximum value of the colour representation of **c** is 0 in RGB, $\mathbf{c}^{MAX}$ is set to white. The minimum value of **c** is always set to black. Fig. 4.1 shows an example of the appearances in the increased colours that a RGB colour (R: 51, G: 25, B: 10) is linearly increased or decreased until reaching its colour extrema.
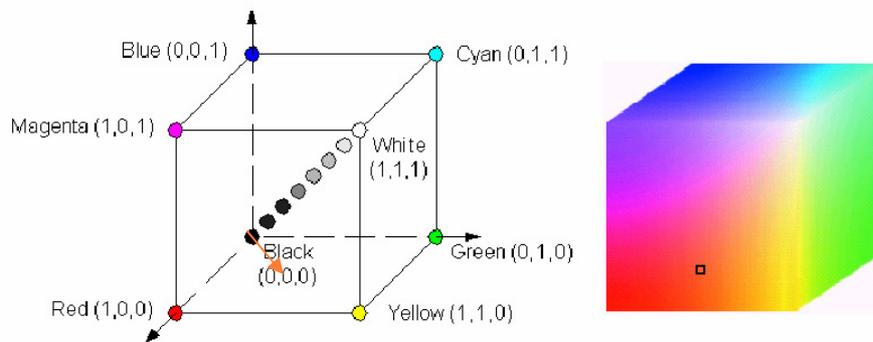
(a)

(b)

Figure 4.1. The linear increasing colours which share the colour extrema from the minimum colour vector (0, 0, 0) to maximum colour vector (255, 125, 50): (a) its colour vector in the RGB colour space and (b) the profile of this colour vector.

4.2 The Definition of Colour Difference

Given a definition for colour extrema that can be used as the foreground for colour morphology, a method is needed to measure the difference between a colour and its extrema in the RGB, HSV and L*a*b colour spaces, respectively. In the latter case, the distance relates to the perception of colour difference. Thus, the notion of distance between the values of the different colour pixels is critical in comparing these colour pixels.

As discussed in Section 4.2.2, the V component can be used directly as a measure of colour difference in the HSV colour space. Alternative distance functions for measuring colour difference are needed in the RGB and L*a*b* colour spaces. Let $\mathbf{c}_k = (c_k^U, c_k^V, c_k^W)$ be the kth colour pixel in a generic UVW colour space. The notion of colour distance between two colour pixels in this space is denoted by ΔCD^{UVW}. The definitions of the colour distance functions are given in the following subsections.

4.2.1 RGB colour space

Although the RGB colour space is highly correlated, the Euclidean distance is still commonly used as a perceptual difference between two colour vectors, $\mathbf{c}_i$ and $\mathbf{c}_j$, i.e.,

$$\Delta\text{CD}^{RGB}(\mathbf{c}_i, \mathbf{c}_j) = \sqrt{\sum_{n=R,G,B}(c_i^n - c_j^n)^2} \qquad (4.5)$$

4.2.2 HSV colour space

Table 4.1 indicates the influence of the colour components in the HSV colour space when an RGB colour is linearly increased until reaching its colour extrema, using Eq. (4.3). Only the V value changed between the colour and its extrema in the HSV colour space. This is because the S component is calculated by $(\max(R,G,B) - \min(R,G,B))/\max(R,G,B)$, and the S value will be the same between the colour and its extrema. The H component behaves similarly as shown in Table 4.1. Hence, the V component of the HSV model can be regarded as equivalent to the intensity in Eq. (4.2), described in Section 4.1, for our purposes and the difference between a colour $\mathbf{c}_j$ and its extrema $\mathbf{c}_i$ can be regarded as the difference in the Value component in the HSV space, i.e.,

$$\Delta\text{CD}^{HSV}(\mathbf{c}_i, \mathbf{c}_j) = \left| c_i^V - c_j^V \right| \times 100 \qquad (4.6)$$

Table 4.1 The relationship between the RGB and HSV colour models using the presented definition of colour extrema.

RGB colours (**R**, **G**, **B**)	HSV model		
	H	S	V
(51, 25, 10)	22°	80%	20%
(255, 125, 50)	22°	80%	100%

4.2.3 CIE L*a*b* colour space

In the L*a*b* colour space, $L*$ represents the lightness (0=black and 100 white), $a*$ encodes red-green colouration and $b*$ yellow-blue coloration. CIE L*C*h is a similar colour space based on chrominance $(C*)$ and hue (h). The CIE-94 colour difference formula E_{94}^* between two colour vectors $\mathbf{c}_i$ and $\mathbf{c}_j$ in the CIE L*C*h space [SHA03], denoted ΔCD^{L*a*b*} is given by:

$$\Delta CD^{L*a*b*}(\mathbf{c}_i, \mathbf{c}_j) = \Delta E_{94}^* = \sqrt{\left(\frac{\Delta L^*}{k_L S_L}\right)^2 + \left(\frac{\Delta C^*}{k_C S_C}\right)^2 + \left(\frac{\Delta H^*}{k_H S_H}\right)^2} \qquad (4.7)$$

where k_L, k_C and k_H are real-valued, application-dependent scaling parameters with default values of 1. S_L, S_C, and S_H are the lightness-, chroma- and hue-dependent scaling functions, respectively, defined as:

$$S_L = 1 \qquad S_C = 1 + 0.045\sqrt{C_1^* C_2^*} \qquad S_H = 1 + 0.015\sqrt{C_1^* C_2^*}, \qquad (4.8)$$

The terms $\Delta L*$, $\Delta C*$ and $\Delta H*$ are referred to as the lightness, chroma and hue differences, respectively. These are defined in terms of the standard CIE L*a*b* values as:

$$\Delta L^* = c_i^{L*} - c_j^{L*}, \qquad \Delta C^* = C_1^* - C_2^*, \qquad \Delta H^* = \sqrt{(\Delta a^*)^2 + (\Delta b^*)^2 - (\Delta C^*)^2}$$
$$C_1^* = \sqrt{(c_i^{a*})^2 + (c_i^{b*})^2}, \quad C_2^* = \sqrt{(c_j^{a*})^2 + (c_j^{b*})^2}, \quad \Delta a^* = c_i^{a*} - c_j^{a*}, \quad \Delta b^* = c_i^{b*} - c_j^{b*} \qquad (4.9)$$

4.3 Complete Lattices in Mathematical Morphology

Let $\mathbf{I} \subseteq \mathbb{R}^p$ be a multivariate images composed of pixel values of dimension p. Let $\mathbb{F} \subseteq \mathbb{R}^p$ be a multivariate image composed of vector values in the continuous space $\mathbb{R}^p$. Let $\mathbf{E}$ be a subset of the discrete space $\mathbb{Z}^2$; $\mathbf{E}$ is the spatial support of a 2D image, $\mathbf{I}: \mathbf{E} \to \mathbb{F}$ commonly denoted by $\mathcal{F}(\mathbf{E},\ \mathbb{F})$. Following Section 3.4 the concept of complete lattices for $\mathbb{R}^p$ was proposed by [HEI91] [ROM08] [VEL11]. The fundamental concept that is the basis for this is reviewed in this section. The basic definition of the h-mapping was described in Section 3.4.2.

4.3.1 h-differnece mapping

In the case of a h-mapping on colour difference the challenge in building complete lattice structures is to define a mapping, $h: \mathbb{F} \subseteq \mathbb{R}^P \to \mathcal{L}$, where $\mathcal{L}$ can be the lattice of the binary, grey-level and colour images using a pre-ordering $\leq_h$. Two main cases of mappings, h, for a given $\mathbf{c} \in \mathbb{F}$ can be defined as follows.

- Based on binary and grey-level images ($p = 1$), i.e. the mapping:

$$h_g^d(c) = \frac{1}{1 + \Delta\mathrm{CD}(c^{MAX}, c)} \tag{4.10}$$

where $\Delta\mathrm{CD}$ is the colour difference and represents the lightness differences between c^{MAX} and c, using Eq. (4.5), Eq. (4.6) and Eq. (4.7); Here c^{MAX} is the maximum luminance for

grey-level = 255 and V = 100% in the RGB and HSV colour spaces, respectively. In CIE

L*a*b* colour space, the terms for ΔC^* and ΔH^* are null and the lightness difference ΔL^*

is as defined in Eq (4.7), leading to $h_g^d(c) = \dfrac{1}{1 + \Delta L^* / kS_L}$. This lightness difference, ΔL^*,

is equivalent to the difference between c^{MAX} and c with c^{MAX} expressed as the maximum

luminance, $L^* = 100$.

When c is close to c^{MAX}, then c is close to the foreground value, and h_g is close to 1.

Moreover, h_g is set to 0 directly when c is pure black. This mapping $h_g \in [0, 1]$, is

equivalent to the conventional definition for an image in a complete lattice for binary and

grey-level morphology. The *h*-mapping for colour or grey-level reduces down to the one

for binary as a special case.

■ Based on colour images ($p = 3$), i.e. the colour mapping:

$$h_{colour}^d(\mathbf{c}) = \frac{1}{1 + \Delta CD(\mathbf{c}^{MAX}, \mathbf{c})} \tag{4.11}$$

where ΔCD is the colour difference with the colour extrema defined as in Eq. (4.5), Eq.

(4.6) and Eq. (4.7) in the RGB, HSV, L*a*b* colour spaces, respectively, and $\mathbf{c}^{MAX}$, as in

Eq. (4.3). Here, $\mathbf{c}$ and $\mathbf{c}^{MAX}$ are colour vectors. This is a simple extension from binary and

grey-level to colour morphology. In the same way, h_{colour} is set to 0 directly when $\mathbf{c}$ is

pure black.

The motivation for defining a colour difference ordering scheme is to develop mathematical

morphology in a complete lattice, $\mathcal{L}$, that can be interpreted in terms of defined colour extrema.

Under the mapping $h^{d}_{colour} \in [0, 1]$, both supremum and infimum are present in a complete

lattice. The foreground colour, C_F, is defined by the colour extrema of Eq. (4.3). The

background colour, C_B can be naturally defined as the grey-level or colour most dissimilar to

the colour extrema within the structure element. Note that $\text{Inf}_{\mathcal{L}}$ and $\text{Sup}_{\mathcal{L}}$ are the smallest and

largest elements in the lattice $\mathcal{L}$, respectively. This ordering satisfies the conditions $h^{d}_{colour}(c)$

$= \text{Sup}_{\mathcal{L}}$ if $c \in C_F$ because the colour difference, ΔCD, is 0 and $h^{d}_{colour}(c) = 1$. Alternatively

$h^{d}_{colour}(c) = \text{Inf}_{\mathcal{L}}$ if $c \in C_B$ and $h^{d}_{colour}(c) = 0$.

4.4 Colour Difference-based Mathematical Morphology

The importance of complete lattices for colour ordering was described in Section 4.3. The

infimum and and supremun are used here to define erosion and dilation.

4.4.1 Binary and grey-level morphology

For a single channel binary or grey-level image $p = 1$. Let S represent a structure element of a

finite size, N. Also let $I_x = \{c_i \subseteq \mathbb{R}; i=1, 2, \ldots, N\}$ represent a set of image pixels within the

region of the structure element S, where $c_1,\ c_2,\ \dots,\ c_N$ is the set of image pixel values in that

neighbourhood, centred at position x of an image.

Using the colour difference formula in binary and grey-level morphology, an ordering Ω_g is

defined as:

$$c_i \leq_{\Omega_g^d} c_j \Leftrightarrow h_g^d(c_i) \leq h_g^d(c_j) \tag{4.12}$$

where h_g^d represents the mapping in binary and grey-level images defined by Eq. (4.11). Here

the mapping is calculated between c and its corresponding extrema value, c^{MAX}. It has been

shown, Eq. (4.12), that this leads to a conventional definition of binary and grey-level

morphology.

Operators $\wedge_{\Omega_g^d}$ and $\vee_{\Omega_g^d}$ are defined to identify the infimum and supremum pixels with the

ordering Ω_g^d, respectively, within the flat structure element, S. Let the matrix of mapping, $I \in$

$\mathcal{F}(\mathbf{E},\ \mathcal{L})$ at position $x \in \mathbf{E}$ by the structure element S, *binary (Grey-level) erosion* $\varepsilon_{\Omega_g^d,S}$ be

given by:

$$\varepsilon_{\Omega_g^d,S} I(x) = \left\{ I(y) : y = \arg_z \wedge_{\Omega_g^d} [I(z)], z \in S_x \right\} \tag{4.13}$$

The corresponding *dilation* $\delta_{\Omega_g^d,S}$ is given by:

$$\delta_{\Omega_g^d, S} I(x) = \left\{ I(y) : y = \arg_z \vee_{\Omega_g} [I(z)], z \in S_x \right\} \qquad (4.14)$$

4.4.2 Colour morphology

For a colour image, where $p = 3$, let $\mathbf{S}$ represent a set of reference colour pixels within a structure element of a finite size, N. Also let $\mathbf{I}_x = \{\mathbf{c}_i \subseteq \mathbb{R}^3; i = 1, 2, \ldots, N\}$ represent a set of image colour pixels within the region of the structure element $\mathbf{S}$, where $\mathbf{c}_1, \mathbf{c}_2, \ldots, \mathbf{c}_N$ is a set of image colour pixel vectors in a neighbourhood centred at position x of the image. To extend mathematical morphology to colour images the ordering, Ω_{colour}^d, must be modified to resolve any remaining ambiguity. The total ordering, Ω_{colour}^d, with a lexicographical cascade by the colour difference and colour channels with the RGB representation is defined as:

$$\mathbf{c}_i <_{\Omega_{colour}^d} \mathbf{c}_j \Leftrightarrow \begin{cases} h_{colour}^d(\mathbf{c}_i) < h_{colour}^d(\mathbf{c}_j) \text{ or} \\ h_{colour}^d(\mathbf{c}_i) = h_{colour}^d(\mathbf{c}_j) \\ \text{and} \\ \begin{cases} c_i^G < c_j^G \text{ or} \\ c_i^G = c_j^G \text{ and } c_i^R < c_j^R \text{ or} \\ c_i^G = c_j^G \text{ and } c_i^R = c_j^R \text{ and } c_i^B < c_j^B \end{cases} \end{cases} \qquad (4.15)$$

where $h_{colour}^d(\mathbf{c}_i)$ and $h_{colour}^d(\mathbf{c}_j)$ represent the mappings of $\mathbf{c}_i$ and $\mathbf{c}_j$ using Eq. (4.11), respectively, and c^R, c^G and c^B are the red, green and blue channels of $\mathbf{c}$, respectively. The colour components of the L*a*b* colour model are not considered because the order of the channels is difficult to be selected from their significance. In the HSV colour space the

ordering of hue is ambiguous because it has an arbitrary origin. To avoid ordering the hue

information, the colour components in the RGB colour space are only considered in the

conditional ordering. For human perception the order of importance for sensitivity of the

colour channels is Green, Red and Blue [SHA03]. If $\mathbf{c}_i$ is similar to $\mathbf{c}_i^{MAX}$, then the mapping

h_{colour}^d will be close to 1, and this also means that $\boldsymbol{c}_i$ is close to the foreground. Here $\mathbf{c}^{MAX}$ is

defined using Eq. (4.3) as a colour extrema.

Operators $\wedge_{\Omega_{colour}^d}$ and $\vee_{\Omega_{colour}^d}$ are defined to identify the infimum and supremum colour

pixel vectors, respectively, using the total ordering Ω_{colour}^d. Let $\mathbf{I} \in \mathcal{F}(\mathbf{E}, \mathcal{L})$ at position $\mathrm{x} \in \mathbf{E}$ by

the structure element S. *Colour erosion* $\varepsilon_{\Omega_{colour}^d, \mathbf{S}}$ is given by:

$$\varepsilon_{\Omega_{colour}^d, \mathbf{S}}(\mathbf{I})(x) = \left\{ \mathbf{I}(y) : y = \arg_z \wedge_{\Omega_{colour}^d} [\mathbf{I}(z)], z \in \mathbf{S}_x \right\} \qquad (4.16)$$

The Corresponding *Colour dilation,* $\delta_{\Omega_{colour}^d, \mathbf{S}}$, is given by:

$$\delta_{\Omega_{colour}^d, \mathbf{S}}(\mathbf{I})(x) = \left\{ \mathbf{I}(y) : y = \arg_z \vee_{\Omega_{colour}^d} [\mathbf{I}(z)], z \in \mathbf{S}_x \right\} \qquad (4.17)$$

In this process the output of erosion or dilation is one of the input colour pixel vectors. This

avoids the introduction of false colours, and provides a harmonised approach for binary,

grey-level and colour morphology.

4.5 Approaches to Salt & Pepper Noise Reduction and Edge Enhancement

Many morphological filters for noise reduction can be defined as combinations of operators, such as, erosion and dilation. This includes opening, closing [SER82] and conditional toggle mapping [VEL13] which are effective in suppressing impulse noise in grey-level [STE87] and colour images [COM99] [LOU02] [ZHO08] as judged using the normalised mean squared error (NMSE) [APT07] and peak signal-to-noise ratio (PSNR) [VEL13].

4.5.1 Opening followed by closing filtering

A common nonlinear filter for impulse noise removal using morphological operators is an opening followed by a closing (OC) filter, i.e.,

$$\text{OC}_{\Omega_{colour}^d, \mathbf{s}}(\mathbf{I})(x) = \varphi_{\Omega_{colour}^d, S}(\gamma_{\Omega_{colour}^d, S}(\mathbf{I})(x)) \tag{4.18}$$

where $\gamma_{\Omega_{colour}^d}$ and $\varphi_{\Omega_{colour}^d}$ are the colour opening and colour closing, respectively. The colour opening is a colour dilation of a colour erosion, i.e.,

$$\gamma_{\Omega_{colour}^d, \mathbf{s}}(\mathbf{I})(x) = \delta_{\Omega_{colour}^d, S}(\varepsilon_{\Omega_{colour}^d, \mathbf{s}}(\mathbf{I})(x)) \tag{4.19}$$

and the colour closing is a colour erosion of a colour dilation, i.e.,

$$\varphi_{\Omega_{colour}^d, \mathbf{s}}(\mathbf{I})(x) = \varepsilon_{\Omega_{colour}^d, \mathbf{s}}(\delta_{\Omega_{colour}^d, \mathbf{s}}(\mathbf{I})(x)) \tag{4.20}$$

4.5.2 Conditional toggle mapping in colour

The grey-level version of the conditional toggle mapping was reviewed in Section 2.5. In this section the extension of the conditional toggle mapping to colour was introduced by using the proposed colour ordering Ω^d_{colour}. Definitions for colour conditional erosion and dilation were introduced in Section 4.5.2.1. Conditional toggle mapping in colour was described in Section 4.5.2.2 and. colour edge enhancement and image denoising in Section 4.5.2.3.

4.5.2.1 Conditional dilation and erosion in colour

Let $\mathbf{M}$ be the characteristic function of a mask, i.e., $\mathbf{M} \in \mathcal{F}(\mathbb{F}, \{0, 1\})$ maps each pixel $x \in \mathbf{E}$ into $\{0, 1\}$. In this approach, a neighbourhood association, N, which is used to count the pixels satisfying $\mathbf{M}(y) = 1$ within the structure element, $\mathbf{S}$ and the mask, $\mathbf{M}$, and is defined as:

$$N_{(\mathbf{S},\mathbf{M})}(x) = \left\{ y \in \mathbf{S}_x \text{ and } \mathbf{M}(y) = 1 \right\} \qquad (4.21)$$

Using Eq (4.21) the definitions for conditional erosion and dilation in colour are as described below.

The conditional erosion of a colour image, $\mathbf{I}$, with respect to binary mask, $\mathbf{M}$, is defined as:

$$\varepsilon_{\Omega_{colour}^{d},\mathbf{s}}(\mathbf{I},\mathbf{M})(x) = \begin{cases} \wedge_{\Omega_{Colour},\mathbf{s}} \mathbf{I}(y) & \text{if } \mathbf{M}(x) = 0 \text{ and } N_{(\mathbf{S},\mathbf{M})}(x) \neq \varnothing, \ y \in N_{(\mathbf{S},\mathbf{M})}(x) \\ \mathbf{I}(x) & \text{otherwise} \end{cases}$$

(4.22)

and similarly the conditional dilation in colour is defined by:

$$\delta_{\Omega_{colour}^{d},\mathbf{s}}(\mathbf{I},\mathbf{M})(x) = \begin{cases} \vee_{\Omega_{Colour},\mathbf{s}} \mathbf{I}(y) & \text{if } \mathbf{M}(x) = 0 \text{ and } N_{(\mathbf{S},\mathbf{M})}(x) \neq \varnothing, \ y \in N_{(\mathbf{S},\mathbf{M})}(x) \\ \mathbf{I}(x) & \text{otherwise} \end{cases}$$

(4.23)

The mask determines which pixels are used in the colour morphology operation.

4.5.2.2 Conditional toggle mapping in colour

Adopting a similar description to that given above for toggle mapping criteria, conditional toggle criterion in colour can be defined as:

$$\tau_{\Omega_{colour}^{d},\mathbf{s}}(\mathbf{I},\mathbf{M}) = \begin{cases} \varepsilon_{\Omega_{colour}^{d},\mathbf{s}}(\mathbf{I},\mathbf{M}) & \text{if } \rho_{\Omega_{colour}^{d},\mathbf{s}}^{\delta}(\mathbf{I},\mathbf{M}) > \rho_{\Omega_{colour}^{d},\mathbf{s}}^{\varepsilon}(\mathbf{I},\mathbf{M}) \\ \delta_{\Omega_{colour}^{d},\mathbf{s}}(\mathbf{I},\mathbf{M}) & \text{if } \rho_{\Omega_{colour}^{d},\mathbf{s}}^{\delta}(\mathbf{I},\mathbf{M}) < \rho_{\Omega_{colour}^{d},\mathbf{s}}^{\varepsilon}(\mathbf{I},\mathbf{M}) \\ \mathbf{I} & \text{otherwise} \end{cases}$$

(4.24)

where $\rho_{\Omega_{colour}^{d},\mathbf{s}}^{\delta}(\mathbf{I},\mathbf{M}) = \Delta CD(\delta_{\Omega_{colour}^{d},\mathbf{s}}(\mathbf{I},\mathbf{M}),\mathbf{I}(x))$ and

$\rho_{\Omega_{colour}^{d},\mathbf{s}}^{\varepsilon}(\mathbf{I},\mathbf{M}) = \Delta CD(\mathbf{I}(x), \varepsilon_{\Omega_{colour}^{d},\mathbf{s}}(\mathbf{I},\mathbf{M}))$. The distance function ΔCD is defined using Eq.

(4.5), Eq. (4.6) and Eq. (4.7) for the RGB, HSV and L*a*b* colour spaces, respectively. The

mask $\mathbf{M}$ plays the role of a seed indicator that locates the local maximum and local minimum

in colour images. The **M** should spread their values through the image during the dilation operators. Based on the principles of the conditional toggle mapping described in Section 2.5, we now present conditional toggle mapping for colour images. In this case a mapping $\widetilde{\tau}_{\Omega^d_{colour}, \mathbf{S}}(\cdot, \cdot)$ is defined from and onto the pair formed by the colour image, **I,** and the mask, **M,** using Eq. (4.24) on **I** and Eq. (2.3) on **M**, i.e.:

$$\widetilde{\tau}_{\Omega^d_{colour}, \mathbf{S}}(\mathbf{I}, \mathbf{M}) = (\tau_{\Omega^d_{colour}, \mathbf{S}}(\mathbf{I}, \mathbf{M}), \delta_{\mathbf{S}}(\mathbf{M})) \tag{4.25}$$

The next iteration is calculated using:

$$\begin{aligned}
\widetilde{\tau}^2_{\Omega^d_{colour}, \mathbf{S}}(\mathbf{I}, \mathbf{M}) &= \widetilde{\tau}_{\Omega^d_{colour}, \mathbf{S}}(\widetilde{\tau}_{\Omega^d_{colour}, \mathbf{S}}(\mathbf{I}, \mathbf{M})) \\
&= \widetilde{\tau}_{\Omega^d_{colour}, \mathbf{S}}(\tau_{\Omega^d_{colour}, \mathbf{S}}(\mathbf{I}, \mathbf{M}), \delta_{\mathbf{S}}(\mathbf{M})) \\
&= \tau_{\Omega^d_{colour}, \mathbf{S}}(\tau_{\Omega^d_{colour}, \mathbf{S}}(\mathbf{I}, \mathbf{M}), \delta_{\mathbf{S}}(\mathbf{M}), \delta_{\mathbf{S}}(\delta_{\mathbf{S}}(\mathbf{M}))) \\
&= \tau_{\Omega^d_{colour}, \mathbf{S}}(\widetilde{\tau}_{\Omega^d_{colour}, \mathbf{S}}(\mathbf{I}, \mathbf{M}), \delta^2_{\mathbf{S}}(\mathbf{M}))
\end{aligned}$$

$$\tag{4.26}$$

The conditional toggle mapping in colour is then defined by iteration until convergence $\widetilde{\tau}^\infty_{\Omega^d_{colour}, S}$ as follows:

$$\widetilde{\tau}^\infty_{\Omega^d_{colour}, \mathbf{S}}(\mathbf{I}, \mathbf{M}) = \lim_{m \to \infty} \widetilde{\tau}^m_{\Omega^d_{colour}, \mathbf{S}}(\mathbf{I}, \mathbf{M}) \tag{4.27}$$

where $\widetilde{\tau}^m_{\Omega^d_{colour}, \mathbf{S}}(\mathbf{I}, \mathbf{M}) = \tau_{\Omega^d_{colour}, \mathbf{S}}(\widetilde{\tau}^{m-1}_{\Omega^d_{colour}, \mathbf{S}}(\mathbf{I}, \mathbf{M}), \delta^{\mathrm{m}}_{\mathbf{S}}(\mathbf{M}))$, $\widetilde{\tau}^0_{\Omega^d_{colour}, \mathbf{S}}(\mathbf{I}, \mathbf{M}) = (\mathbf{I}, \mathbf{M})$.

The convergence criterion of the conditional toggle mapping is iterated spreading the values of **M** through the image until no pixel changed in the mapping. A proof of the convergence of the conditional toggle mapping with the mask **M** was presented in [VEL13].

4.5.2.3 Edge enhancement and image denoising for colour images

Having defined conditional toggle mapping in colour edge enhancement and image denoising for colour images can be defined using the mask **M**. For edge enhancement, the mask is defined in terms of local extrema as:

$$\mathbf{M}_E(x) = \begin{cases} 1 & \text{if } \min(\rho_{\Omega_{colour}^d, \mathbf{s}}^{\delta}(\mathbf{I})(x), \rho_{\Omega_{colour}^d, \mathbf{s}}^{\varepsilon}(\mathbf{I})(x)) = 0 \\ 0 & \text{otherwise} \end{cases} \quad (4.28)$$

Where the removal of impulse noise in colour images is concerned the mask, **M,** is defined in terms of the pixels that are not corrupted by the impulse noise as:

$$\mathbf{M}_N(x) = \begin{cases} 1 & \text{if } \min(\rho_{\Omega_{colour}^d, \mathbf{s}}^{\delta}(\mathbf{I})(x), \rho_{\Omega_{colour}^d, \mathbf{s}}^{\varepsilon}(\mathbf{I})(x)) > 0 \\ 0 & \text{otherwise} \end{cases} \quad (4.29)$$

4.6 Experimental Method

In these experiments, the performance of the morphological operations defined under marginal ordering [COM99], conditional ordering with a lexicographical cascade of G→R→B, Angulo's ordering with a reference colour, $\mathbf{c}_0$ = (255, 255, 255) using Euclidean

distance [ANG07a], and Cheng's PCA-like ordering [CHE03] were compared for their significance and ease of implementation. These experiments qualitatively compare the results of basic morphological operations and edge enhancement, and quantitatively made a comparison in salt-and-pepper impulse noise reduction.

4.6.1 Noise model and image design

Synthetic and natural images were used to evaluate colour erosion, dilation and other filters using a 3 x 3 structure element. When a transformation from RGB to L*a*b* colour space is performed the maximum, in *RGB* for the image is used as a white reference.

The synthetic test image of Fig. 4.2 (a) has regions coloured green (R: 0, G: 80, B: 0), light blue (R: 126, G: 179, B: 231) and maroon (R: 145, G: 0, B: 0). This set of colours was chosen to observe the behaviour of colour morphological operations when one colour component is the largest or the smallest. The natural test images of Fig. 4.2 (b), Fig. 4.2 (c) and Fig. 4.2 (d) were chosen because they contain contrasting colours and any errors will therefore show up clearly.

A range of salt-and-pepper impulse noise levels ranging from 0 to 95% of pixels was used. In the case of colour images a channel-independent salt and pepper impulse noise was simulated according to the following rule [BON00]: a channel is selected at random and the impulse

noise is then added to the channel. The added noise was distributed so that 50% of the noise was salt impulse noise with pixel values set to 255 and 50% of the noise was pepper impulse noise with pixel values set to zero in each RGB channel, selected at random. A simple model is the following [BON00]: Let $\mathbf{I}(i, j)$ be the original colour image and $\mathbf{J}(i, j)$ be the image after it has been altered by salt and pepper noise.

$$\mathbf{J}(i, j) = \begin{cases} \text{MAX,} & \text{with probability } \alpha/2 \\ \text{MIN,} & \text{with probability } \alpha/2 \\ \mathbf{I}(i, j), & \text{with probability } 1 - \alpha \end{cases} \tag{4.30}$$

where MAX and MIN are the maximum and minimum image values, respectively. For colour images, MIN = 0 and MAX = 255 selected randomly in each RGB channel or full RGB channel. The idea is that with probability $1 - \alpha$ the pixels are unaltered; with probability α the pixels are changed to the largest or smallest values in each RGB channel or full RGB channel.

This is an extension of a widely adopted noise model used to evaluate morphological image processing in binary, grey-level and colour images [VEL13]. Salt-and-pepper impulse noise was similarly added to the natural test images. Here noise was added as a maximum or minimal value to each colour channel in the RGB colour space, in a manner that reflects the behaviour of common image capture devices. This provides a clear basis for the addition of

impulse noise. It is not appropriate to set pepper pixel values to (0, 0, 0) in RGB colour space

because this gives greater emphasis to the pepper noise, than the other changes do to colour

impulse noise.

(a)   (b)

(c)   (d)
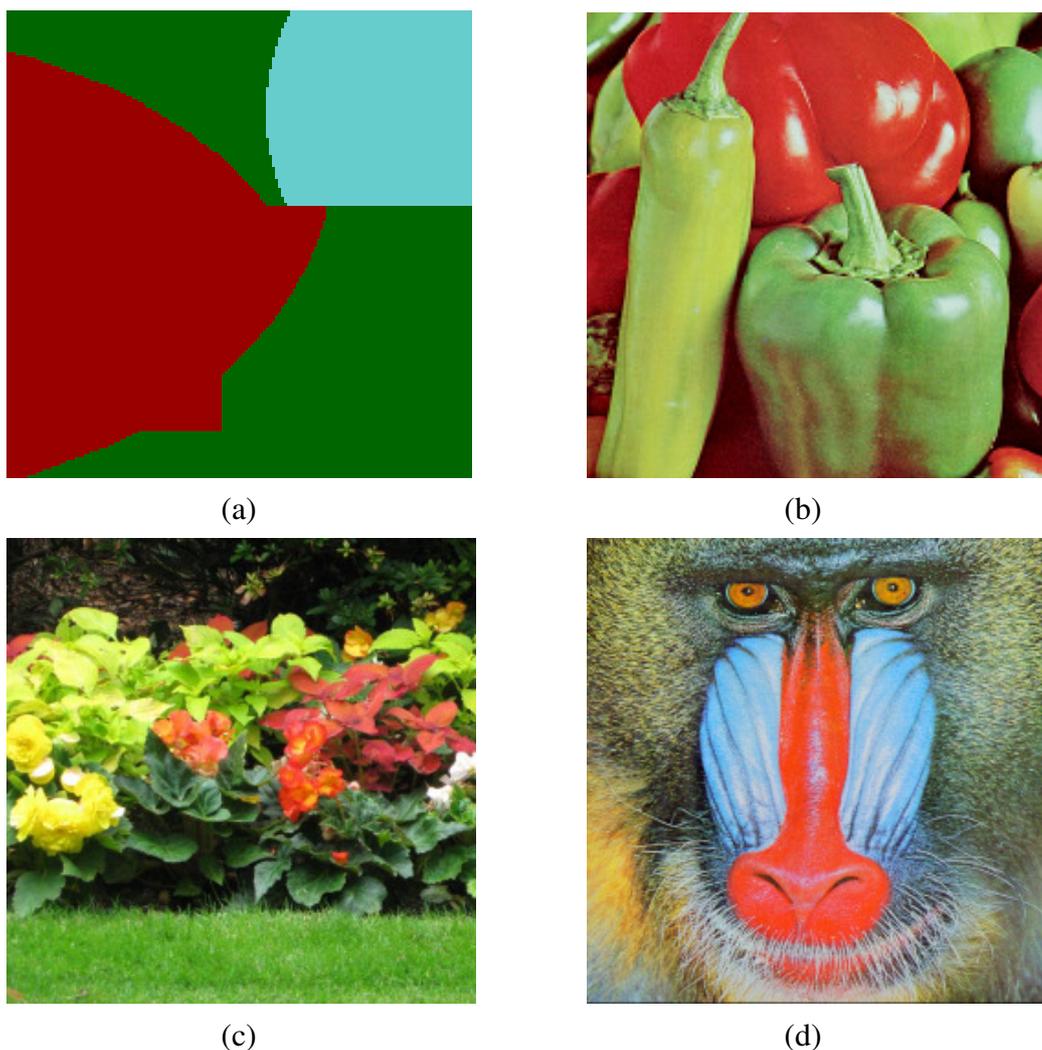
Figure 4.2. Original test images: (a) synthetic image, and natural images of (b) peppers, (c) flowers and (d) Mandrill [UMB10].

4.6.2 Comparison of basic morphological operations

The results for the synthetic colour image are shown in Fig. 4.3 and Fig. 4.4 for colour dilation and for colour erosion, respectively, using marginal ordering, conditional ordering, Angulo's ordering, Cheng's PCA-like ordering and the proposed ordering in the RGB and L*a*b* colour spaces. Our proposed orderings had similar results for the synthetic image in

the HSV colour space. This experiment clarifies the main difference between the marginal approach and vector approach in colour morphology. Marginal ordering produces colour artefacts, manifest as a yellow line and a black line around the maroon region after dilation and erosion, respectively, and shown in Fig. 4.3 (a) and Fig. 4.4 (a). The method presented here does not suffer from any such artefact, as illustrated in Fig. 4.3 (e), Fig 4.3 (f), Fig. 4.4 (e) and Fig. 4.4 (f). The increase in the size of the maroon region after dilation is shown in Fig. 4.3 (e) and Fig. 4.3 (f) whilst in erosion the size is decreased is shown in Fig. 4.4 (e) and Fig. 4.4 (e). In particular, Angulo's ordering produced the equivalent results to the proposed orderings as shown in Fig. 4.3 (c) and Fig. 4.4 (c).
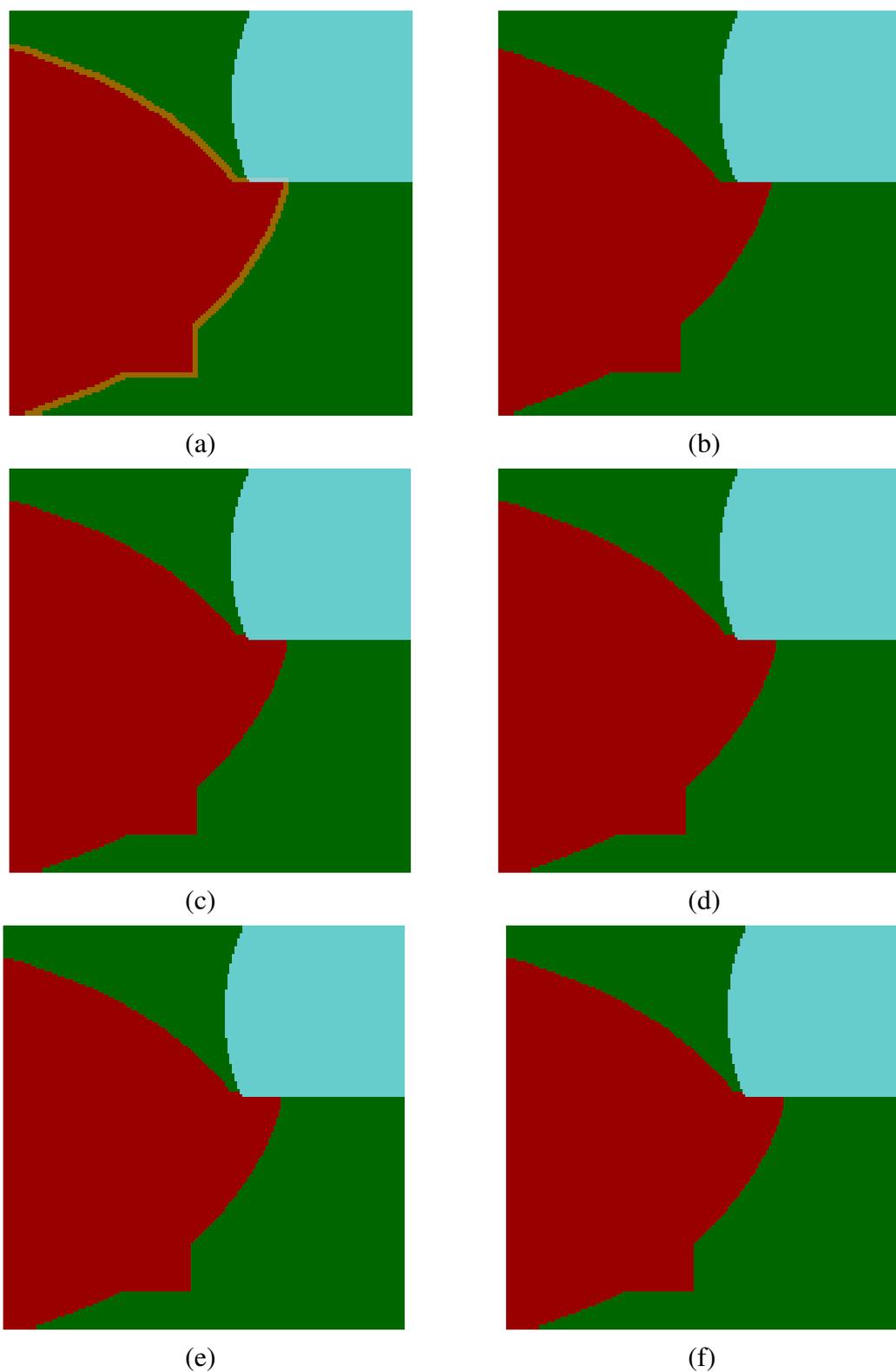
Figure 4.3. Colour dilation of the original synthetic image shown in Fig. 4.2 (a) by using (a) marginal ordering, (b) conditional ordering, (c) Angulo's ordering, (d) Cheng's PCA-like ordering and the proposed ordering in (e) RGB and (f) L*a*b* colour spaces.
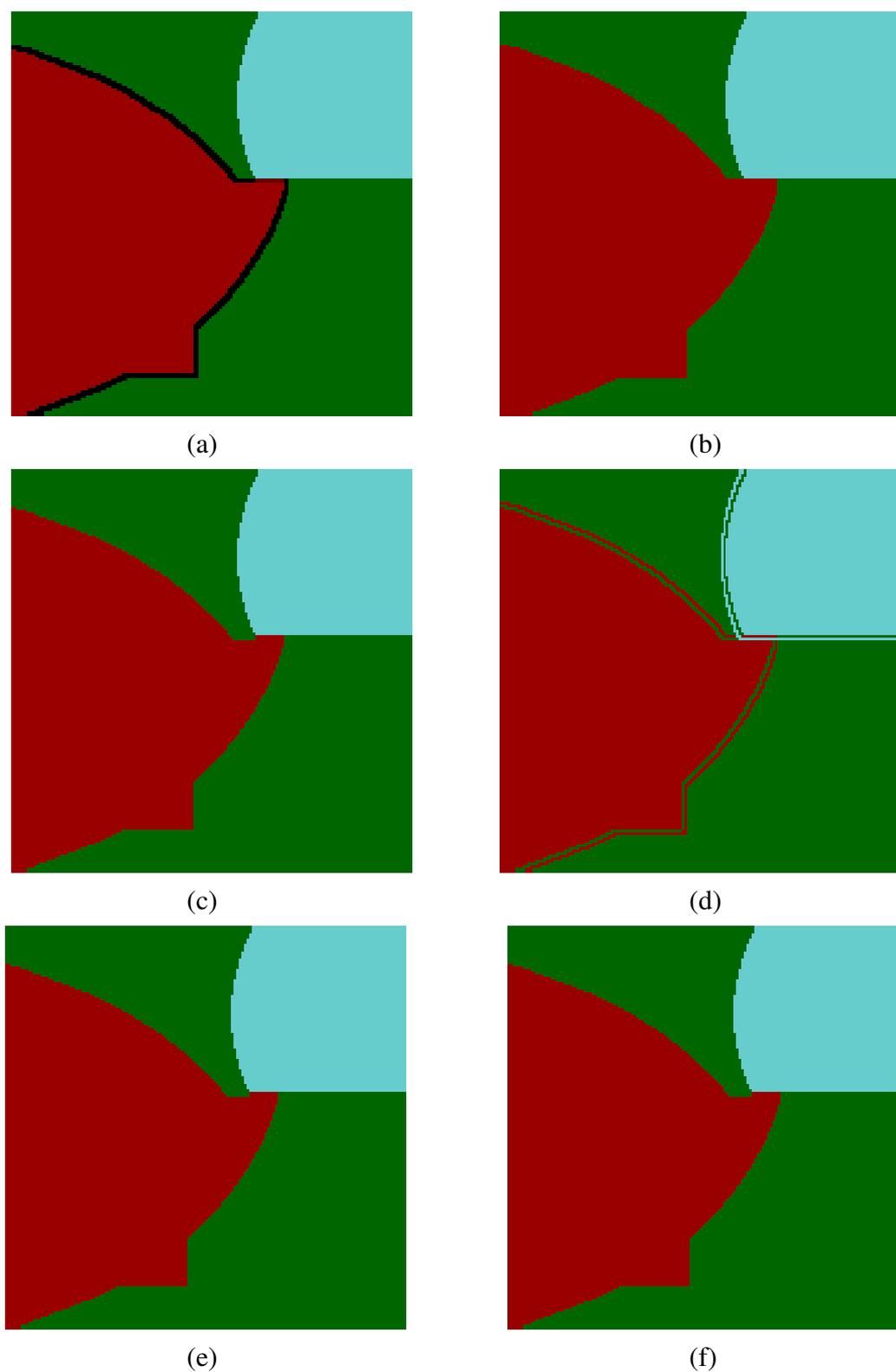
Figure 4.4. Colour erosion of the original synthetic image shown in Fig. 4.2 (a) by using (a) marginal ordering, (b) conditional ordering, (c) Angulo's ordering, (d) Cheng's PCA-like ordering and the proposed ordering in (e) RGB and (f) L*a*b* colour spaces.

Fig. 4.5 and Fig. 4.6 show the results of dilation and erosion for a natural image. The results for dilation in Fig. 4.5 (e) and (f) show that the red region increased in size compared to the original image whilst Fig. 4.6 (e) and (f) show that in erosion the dark and green regions are enlarged in size. In particular, the white highlight surrounded by the red region is increased in size and the green region surrounding a white highlight shrinks after dilation. Under erosion, when a white region is surrounded by a red region it grows and when surrounded by a green region it shrinks. The colour that grows or shrinks is determined by the colour difference to the colour extrema. The pixels in the red region are closer to the red extrema than the green values in the surrounding region are to the green extrema (and the white pixels to white extrema in the test image). Fig. 4.5 and Fig 4.6 also show the absence of colour artefacts for erosion and dilation using the proposed ordering, respectively. A closer inspection of the pepper images of Fig. 4.6 reveals that after erosion the edges of the long yellow pepper take on a serrated appearance in Fig 4.6 (e) and smooth in Fig. 4.6 (f). In Fig. 4.5 (a) and Fig. 4.6 (a), with marginal ordering, the edges of the long yellow pepper have artefacts around the boundaries. This is analogous to the effect observed in the synthetic test image. In particular, Angulo's ordering demonstrated the best results in this qualitative evaluation that produced no false colour and had smooth boundaries after colour dilation and colour erosion. In Fig. 4.7 and Fig. 4.8, the morphological operations of opening and closing are demonstrated using

marginal ordering, conditional ordering, Angulo's ordering, Cheng's PCA-like ordering and our proposed orderings. The ability of each ordering to avoid or generate colour artefacts is shown. As can be seen, the proposed orderings demonstrated that the edges of the long yellow pepper take on a strong serrated appearance in Fig 4.7 (e), Fig 4.8 (e) and Fig 4.8 (f). Moreover, Angulo's ordering still demonstrated the best results in this qualitative evaluation of colour opening and colour closing. The results of dilation, erosion, opening and closing for natural images of the Flowers and the Mandrill, are shown in Appendix A.1.

(a)

(b)

(c)

(d)

(e)

(f)

Figure 4.5. Colour dilation for "Pepper" image using (a) marginal ordering, (b) conditional ordering, (c) Angulo's ordering, (d) Cheng's PCA-like ordering and the proposed ordering in the (e) RGB and (f) L*a*b* colour spaces.

Figure 4.6. Colour erosion for "Pepper" image using (a) marginal ordering, (b) conditional ordering, (c) Angulo's ordering, (d) Cheng's PCA-like ordering and the proposed ordering in the (e) RGB and (f) L*a*b* colour spaces.
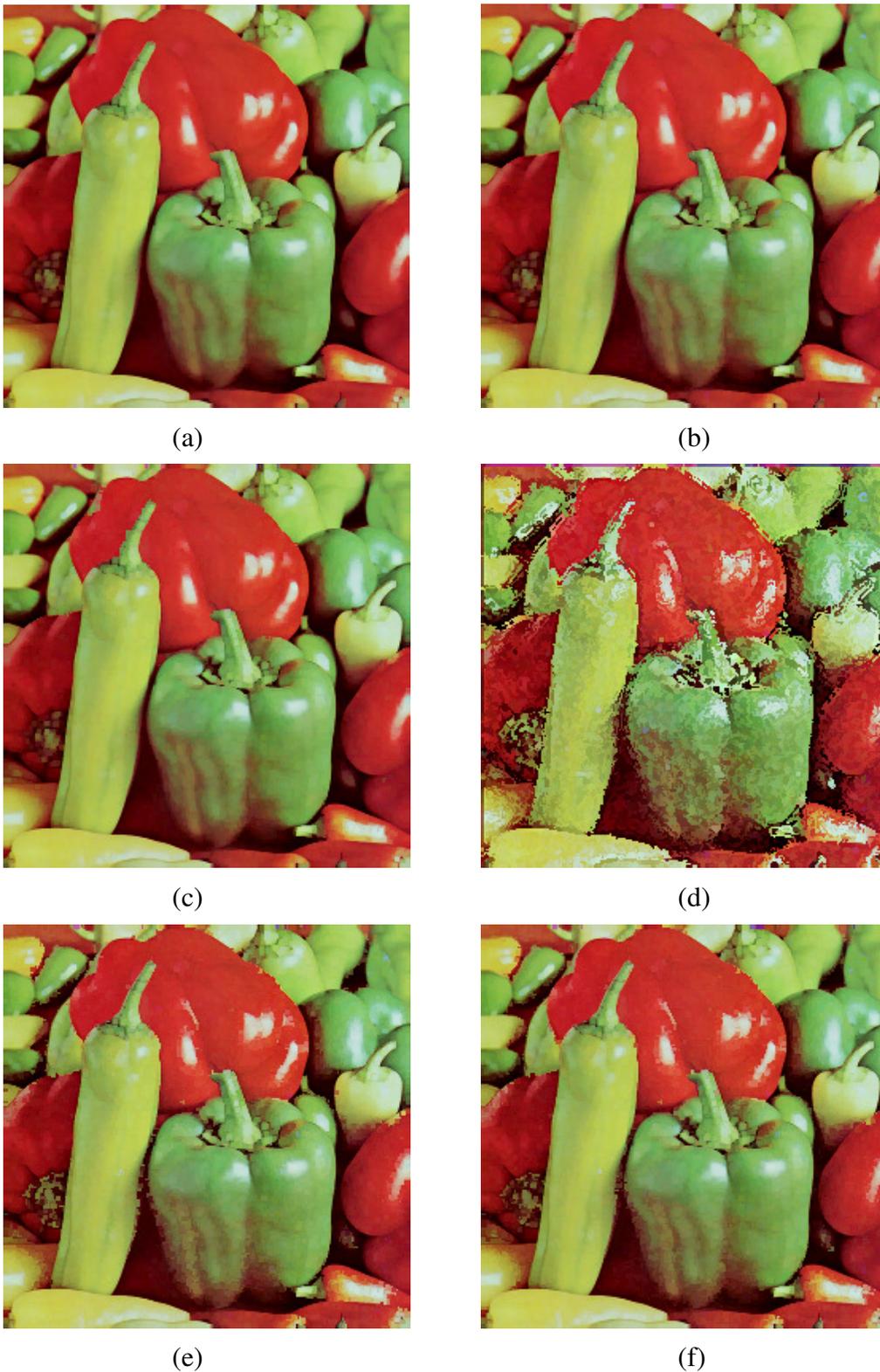
Figure 4.7. Colour opening of "Pepper" image using (a) marginal ordering, (b) conditional ordering, (c) Angulo's ordering, (d) Cheng's PCA-like ordering and the proposed ordering in the (e) RGB and (f) L*a*b* colour spaces.
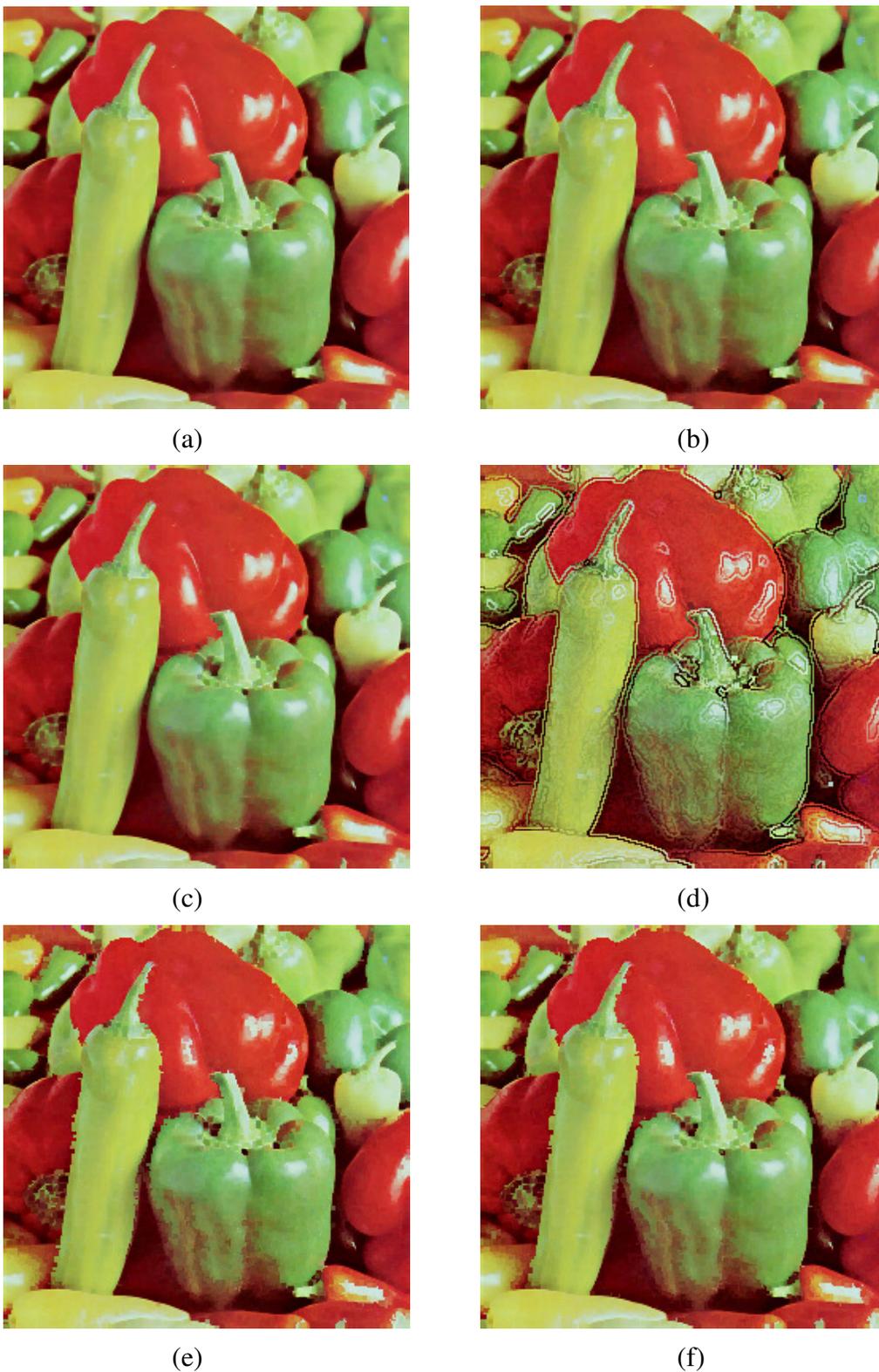
Figure 4.8. Colour closing of "Pepper" image using (a) marginal ordering, (b) conditional ordering, (c) Angulo's ordering, (d) Cheng's PCA-like ordering and our proposed ordering in the (e) RGB and (f) L*a*b* colour spaces.

4.6.3 Comparison of salt and pepper noise reduction

In this section we report on the performance of morphological operators designed with colour

vector ordering for noise reduction using the normalised mean squared error (NMSE) and the

peak signal-to-noise ratio (PSNR) as measures of image distortion by residual noise, i.e.:

$$\text{NMSE} = \frac{\sum_{i=1}^{N}\sum_{j=1}^{M}\left\|\mathbf{I}(i,j)-\mathbf{I}'(i,j)\right\|^2}{\sum_{i=1}^{N}\sum_{j=1}^{M}\left\|\mathbf{I}(i,j)\right\|^2} \tag{4.31}$$

and

$$\text{PSNR} = 10\log_{10}\frac{255^2}{\dfrac{1}{3NM}\sum_{i=1}^{N}\sum_{j=1}^{M}\left\|\mathbf{I}(i,j)-\mathbf{I}'(i,j)\right\|^2} \tag{4.32}$$

where N and M represent the image dimensions; $\mathbf{I}(i,j)$ and $\mathbf{I}`(i,j)$ are the values of the colour

pixels at positions (i, j) for the original and filtered noisy image, respectively.

4.6.3.1 OC filter

The ordering schemes compared in the previous subsection were adopted for these tests, for consistency. The NMSE value of Cheng's method was very poor, being 49 for 5% overall added impulse noise. NMSE values above 45 are not shown in Fig. 4.9 because they represent very high levels of residual noise or distortion and, therefore, are not of interest.

In Fig. 4.9 a lower NMSE value represents better noise removal. The proposed ordering in both the RGB and CIE L*a*b* colour spaces outperforms the other ordering schemes at high levels of added noise (from 30% to 70% of overall impulse noise). Additionally, for noise suppression the result obtained using the CIE L*a*b* colour space is slightly and significantly better than that that obtained using the RGB and HSV colour spaces, respectively.
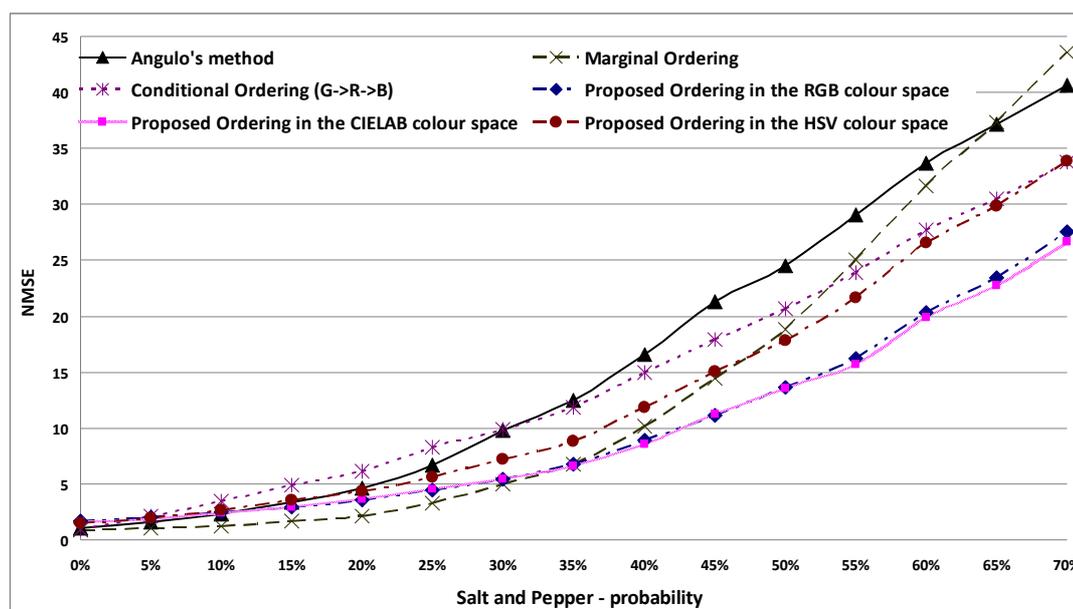
Figure 4.9. Impulse noise reduction using OC filter and selected ordering schemes.

Only marginal ordering is slightly better than the ordering scheme presented here and this is at relatively low overall impulse noise levels of 5% to 25%.

Fig. 4.10 shows a natural image with 40% of overall impulse noise and the result after opening followed by closing (OC) under the selected ordering schemes. With conditional ordering and Angulo's ordering large areas of image corruption remain and the impact of the added noise is extended. Marginal ordering performs a little better. The scheme proposed here reduces the number of corrupted pixels and is more effective at limiting the spatial spread of this corruption in the RGB and CIE L*a*b* colour spaces. The image results for various levels of added noise using OC filter under the selected orderings of Fig. 4.10 are shown in Appendix A.2.

4.6.3.2 Conditional toggle mapping

Using Eq. (4.27), the conditional toggle mapping can be applied with the mask $\mathbf{M}_N$, including an additional condition that $\mathbf{M}_N(x) = 0$ if the value of any RGB channel at the position, x, is 0, to remove pepper impulse noises. Here we present results for conditional toggle mapping extended to colour using the ordering schemes presented for the OC filter as reported in the previous section. We also present results for the vector median filter [GON08] as a comparison for salt-and-pepper noise removal. The vector median (VM) of colour vectors $\mathbf{c}_1$,

$\mathbf{c}_2, \ldots, \mathbf{c}_N$ is the vector $\mathbf{c}_{vm}$ such that

$$\mathbf{c}_{vm} \in \left\{ \mathbf{c}_i \,\middle|\, i = 1, 2, \ldots, N \right\} \tag{4.33}$$

and for all $j = 1, 2, \ldots, N$

$$\sum_{i=1}^{N} \left\| \mathbf{c}_{vm} - \mathbf{c}_i \right\|^2 \le \sum_{i=1}^{N} \left\| \mathbf{c}_j - \mathbf{c}_i \right\|^2 \tag{4.34}$$

The three natural images of the Pepper, the Flowers and the Mandrill have been tested in this section. A lower NMSE or higher PSNR value represents better noise removal.

In Fig. 4.11, the performance of different noise removal methods was evaluated using the NMSE and PSNR measures for the "Pepper" image with added noise. Only those methods with a low NMSE measure were evaluated using the PSNR measure because methods that do not perform well according to the NMSE do not perform well by the PSNR measure.

(a) Noisy image

(b) NMSE = 10.197
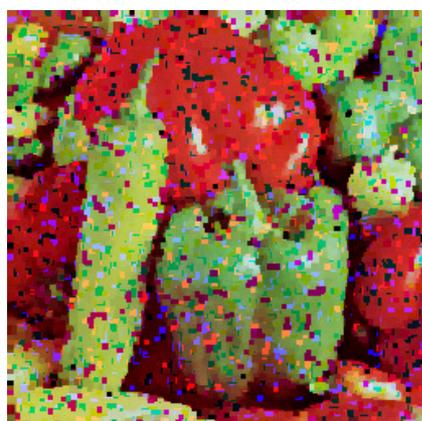
(c) NMSE = 14.954
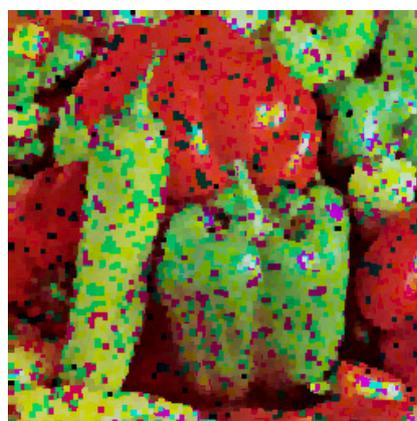
(d) NMSE = 16.612

(e) NMSE = 8.947
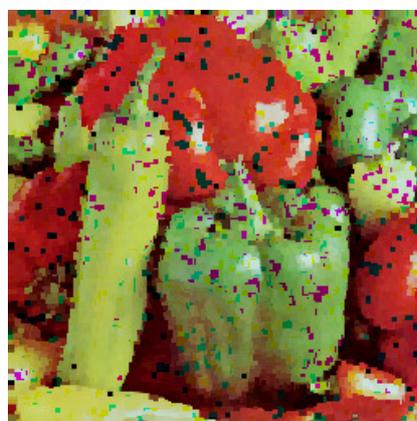
(f) NMSE = 8.581

Figure 4.10. (a) Original image with 40% salt and pepper noise added. The result of noise reduction using, an OC filter with (b) marginal ordering, (c) conditional ordering, (d) Angulo's ordering, (e) the proposed ordering in RGB and (f) the proposed ordering in L*a*b* colour space.
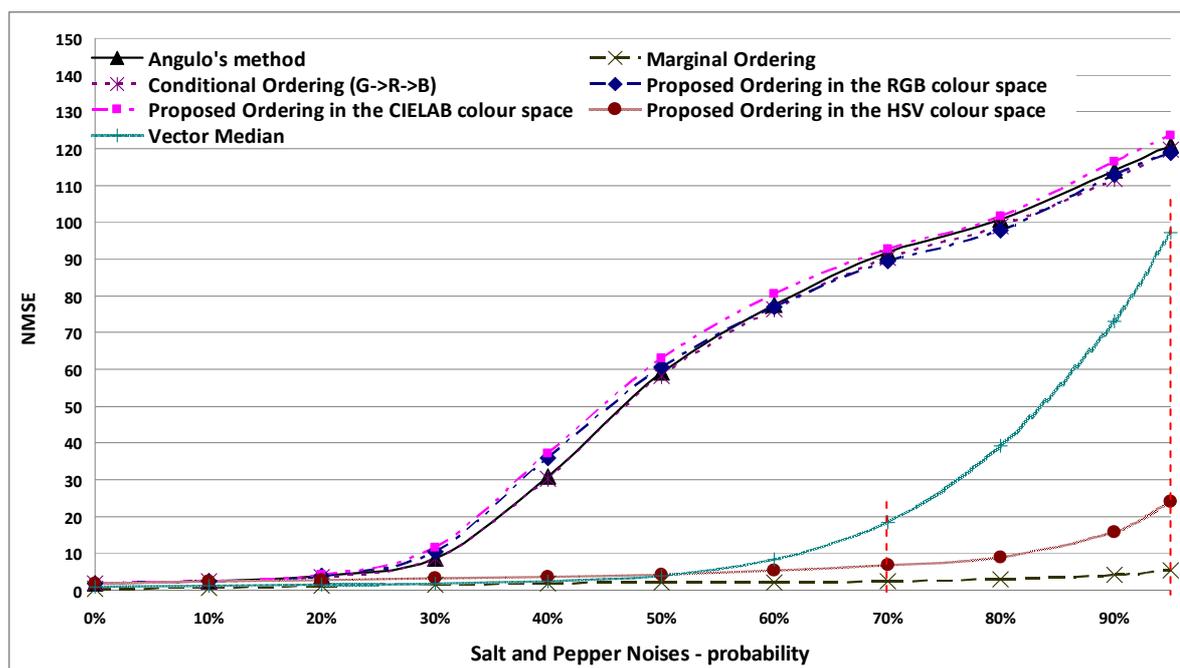
(a)
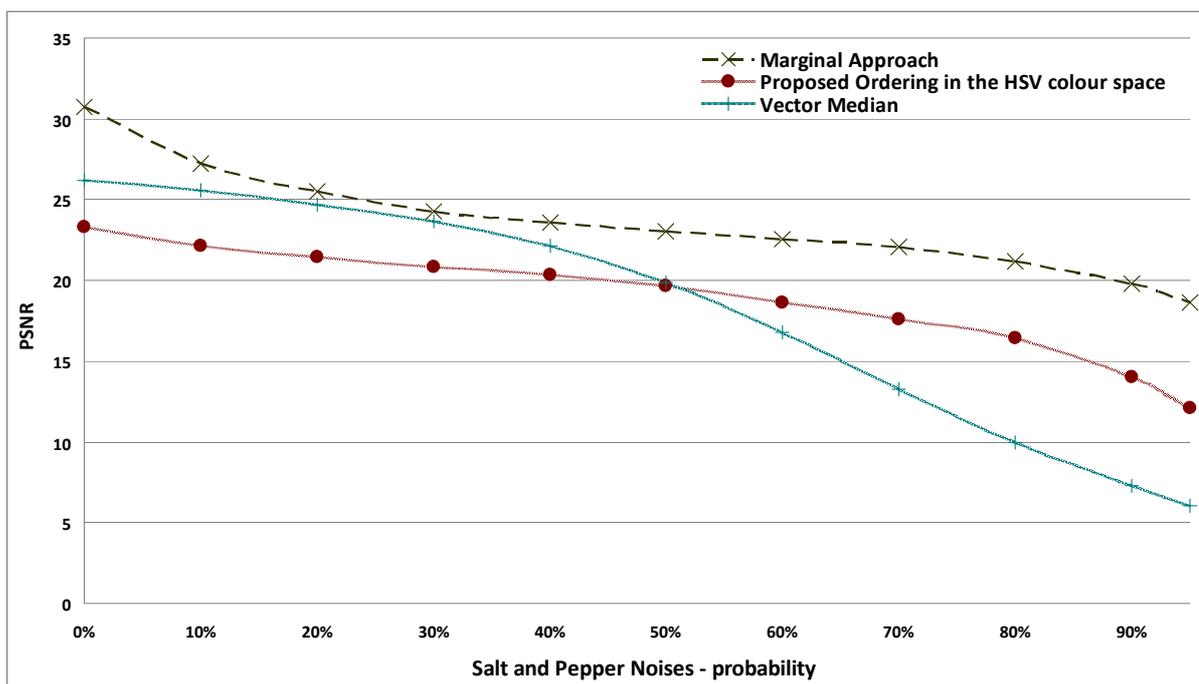
(b)

Figure 4.11. Performance of impulse noise reduction using the conditional toggle mapping, vector median filter and various ordering schemes, evaluated by (a) NMSE, and (b) PSNR for the "pepper" image.

The marginal ordering outperformed all other methods at all levels of added noise. Additionally, the conditional toggle mapping using the proposed ordering in the HSV colour space outperformed the other vector ordering schemes, except the marginal ordering method at all levels of added noise. The vector median filter performed significantly worse than the proposed ordering in the HSV colour space at noise levels of 70% to 95%. The NMSE values of the other orderings are very poor at relatively high noise levels of 40% to 95%. The results shown in Fig. 4.12 and Fig. 4.13 are for noise reduction using the "Mandrill" and "Flowers" images with the vector median and the conditional toggle mapping using marginal ordering and the proposed HSV ordering. The other orderings were not further evaluated because their performance was very poor in the evaluation using the "Peppers" image and therefore were not considered to be of interest. The evaluations of Fig 4.12 and 4.13 were similar to those for noise removal with the "Peppers" image. Fig. 4.14 to Fig. 4.17 show the "Pepper" image with 20%, 40%, 70% and 95% of impulse noise and the results after noise removal using the vector median filter, the toggle condition mapping, the marginal ordering method and the proposed ordering in HSV colour space.
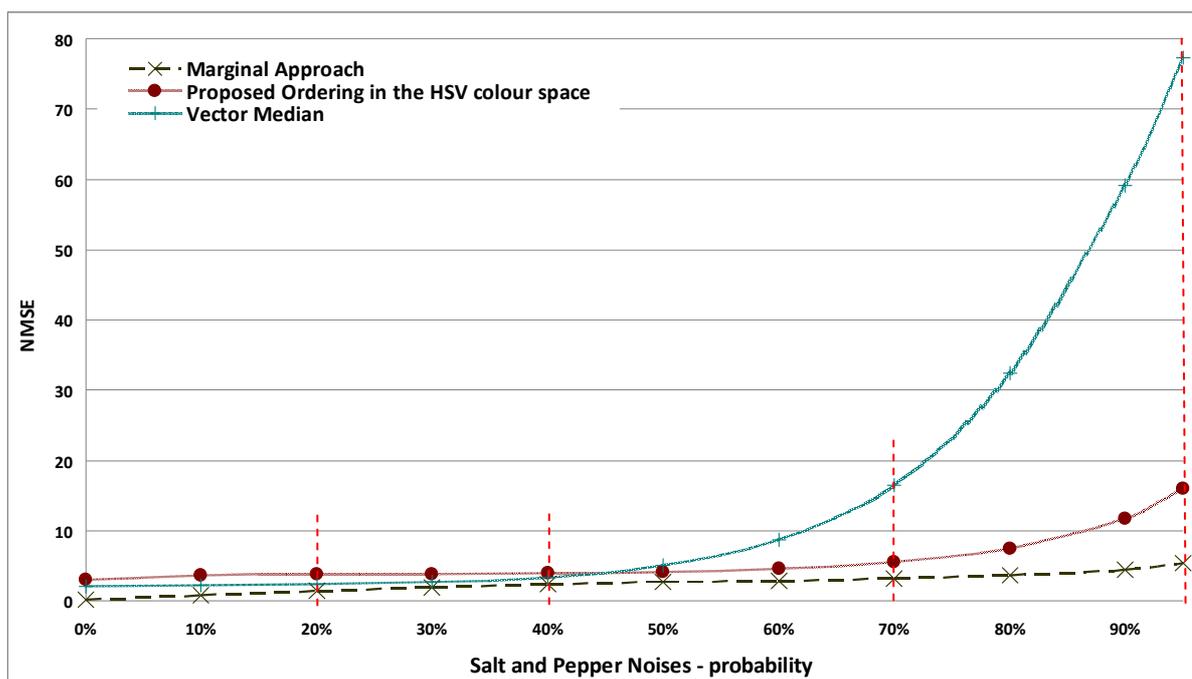
(a)
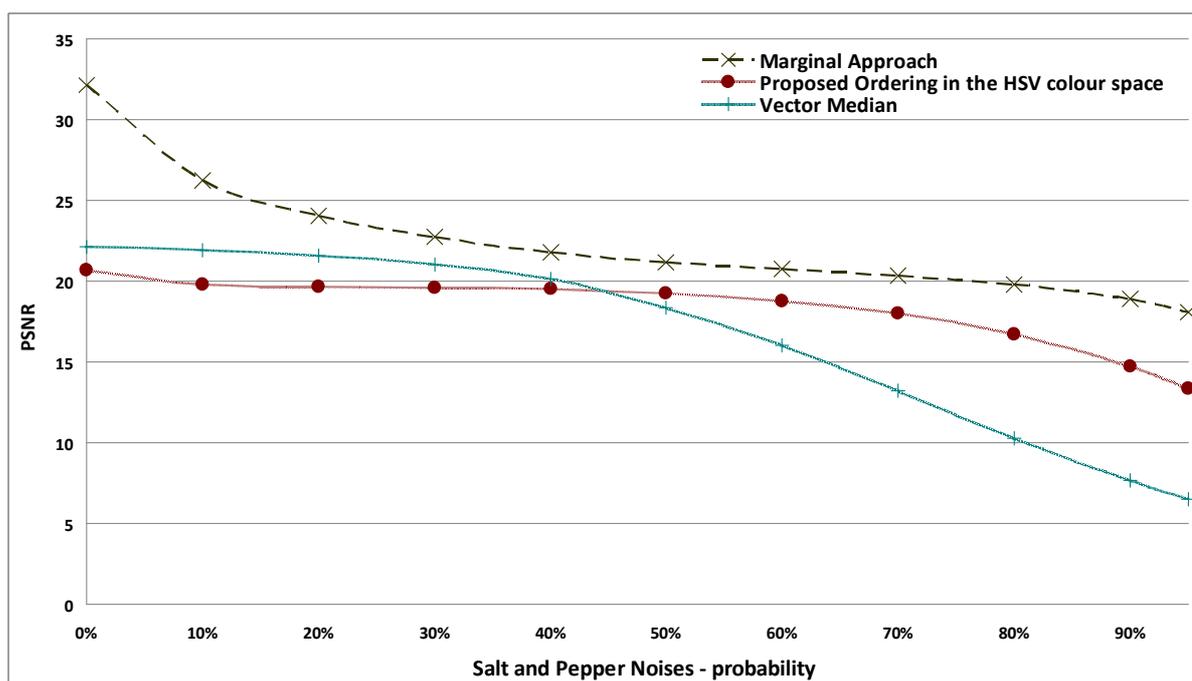
(b)

Figure 4.12. Impulse noise reduction in "Mandrill" image using the conditional toggle mapping with selected ordering schemes and the vector median filter, evaluated by (a) NMSE, and (b) PSNR.
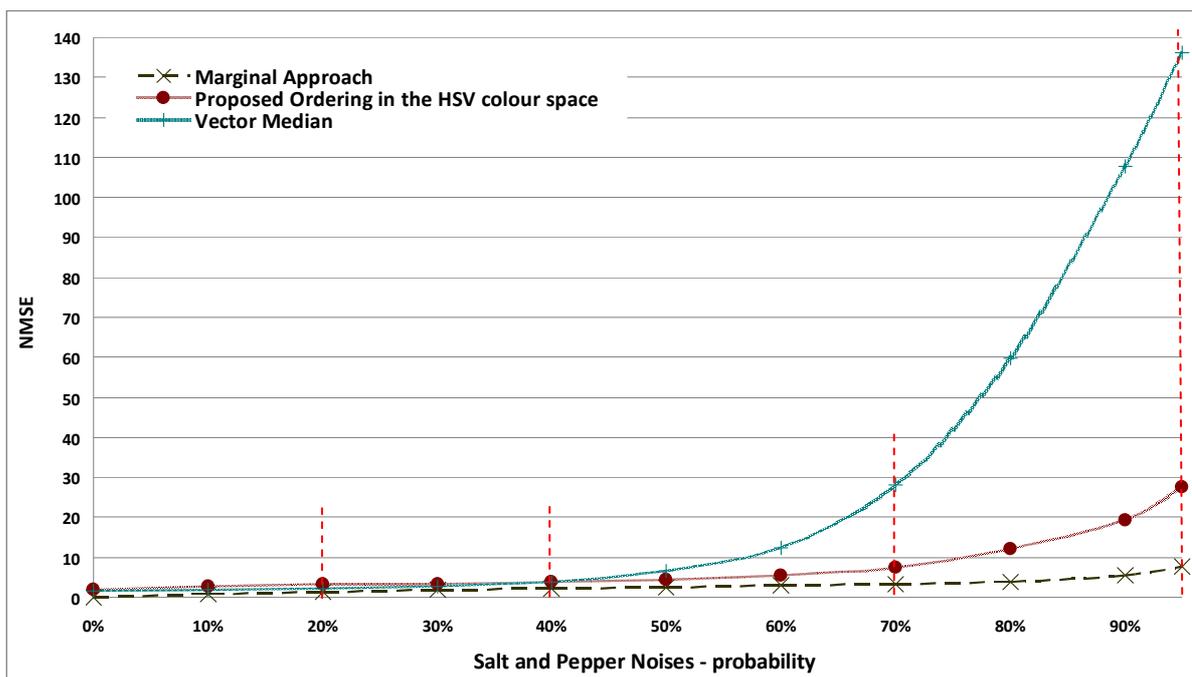
(a)
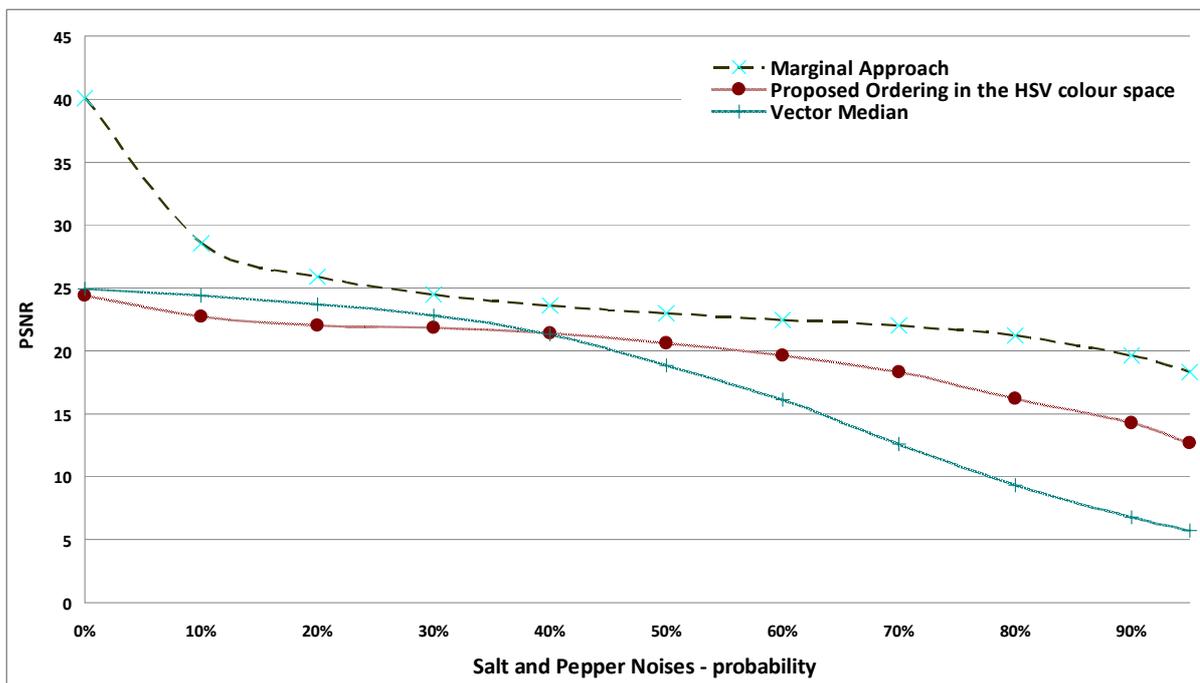
(b)

Figure 4.13. Impulse noise reduction in "Flowers" image using the conditional toggle mapping with selected ordering schemes and the vector median filter, evaluated by (a) NMSE, and (b) PSNR.

(a)   (b) NMSE = 1.338

(c) NMSE = 1.11   (d) NMSE = 2.782
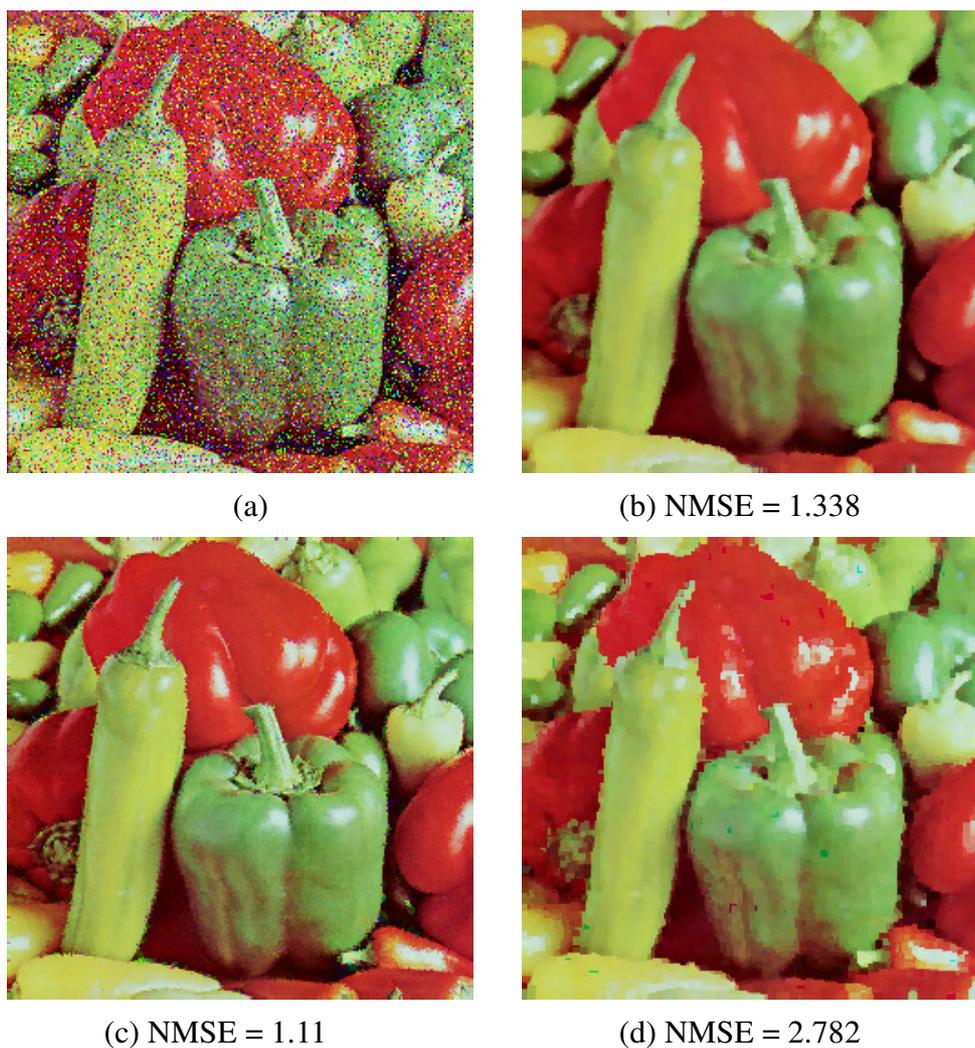
Figure 4.14. Results of noise reduction (a) pepper image with 20% salt and pepper noise added, (b) vector median filter; and conditional toggle mapping by using (c) marginal ordering and (d) the proposed HSV ordering.

Fig. 4.17 to Fig. 4.20 and Fig. 4.21 to Fig. 4.24 show the "Mandrill" image and the "Flowers" image with 20%, 40%, 70% and 95% of impulse noise and the results after noise removal using the vector median filter with marginal ordering and conditional toggle mapping with the proposed HSV ordering, respectively.

(a)

(b) NMSE = 2.394

(c) NMSE = 1.709

(d) NMSE = 3.612
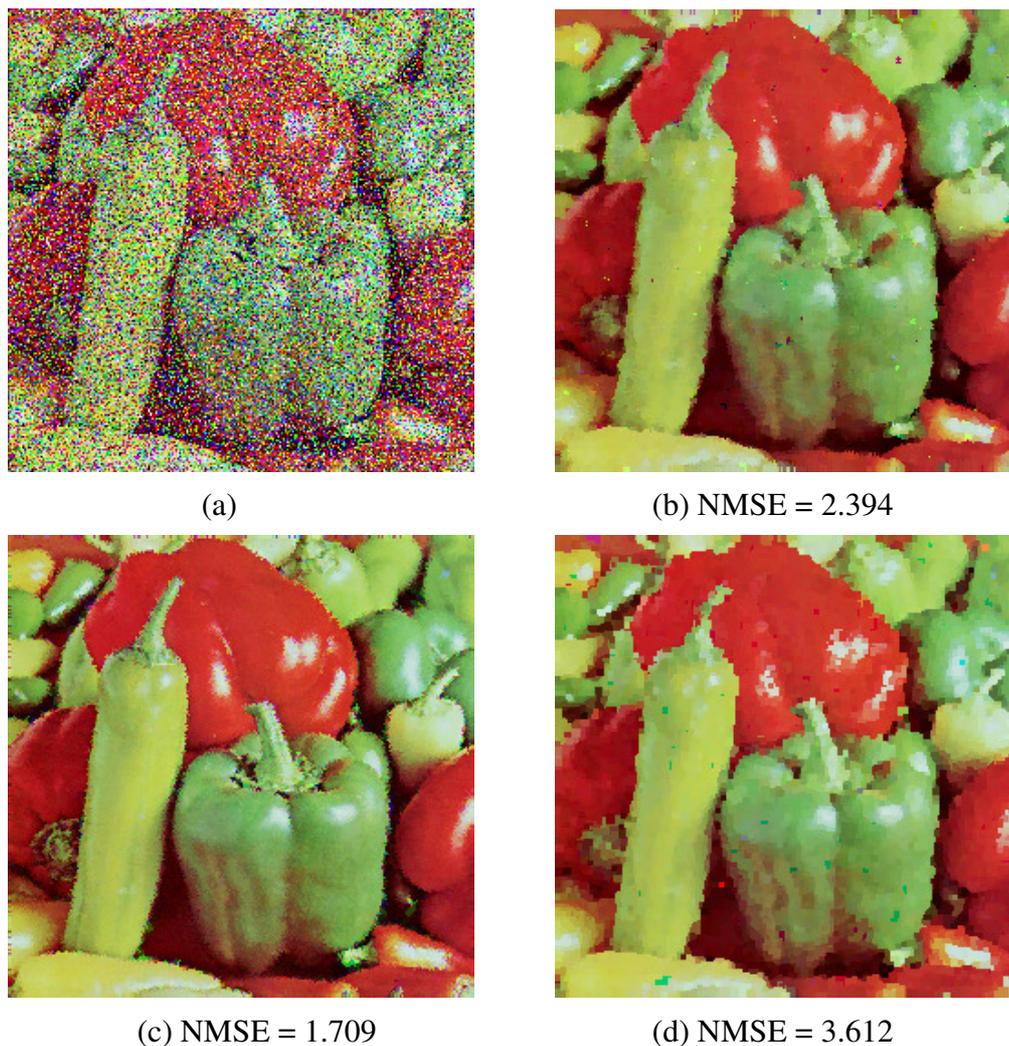
Figure 4.15. Results of noise reduction (a) pepper image with 40% salt and pepper noise added, (b) vector median filter; and conditional toggle mapping by using (c) marginal approach and (d) the proposed HSV ordering.

Subjectively, the marginal ordering is the best at noise removal but it also introduced artefacts around the boundary of the peppers, as shown in Fig. 4.14 (c) to Fig. 4.17 (c) where the false colours are clearly visible, especially for the flowers in Fig. 4.22 (c) to Fig. 4.25 (c). In these images, the vector median filter provided an appropriate response in noise removal when the noise level is less than 50% but the edges were blurred. The proposed method does not generate false colours at edges in images but a modest level of noise remained. As can be seen,

the conditional toggle mapping performs well at noise removal for colour images at noise

level above 50%.

(a) (b) NMSE = 18.385

(c) NMSE = 2.438 (d) NMSE = 6.795
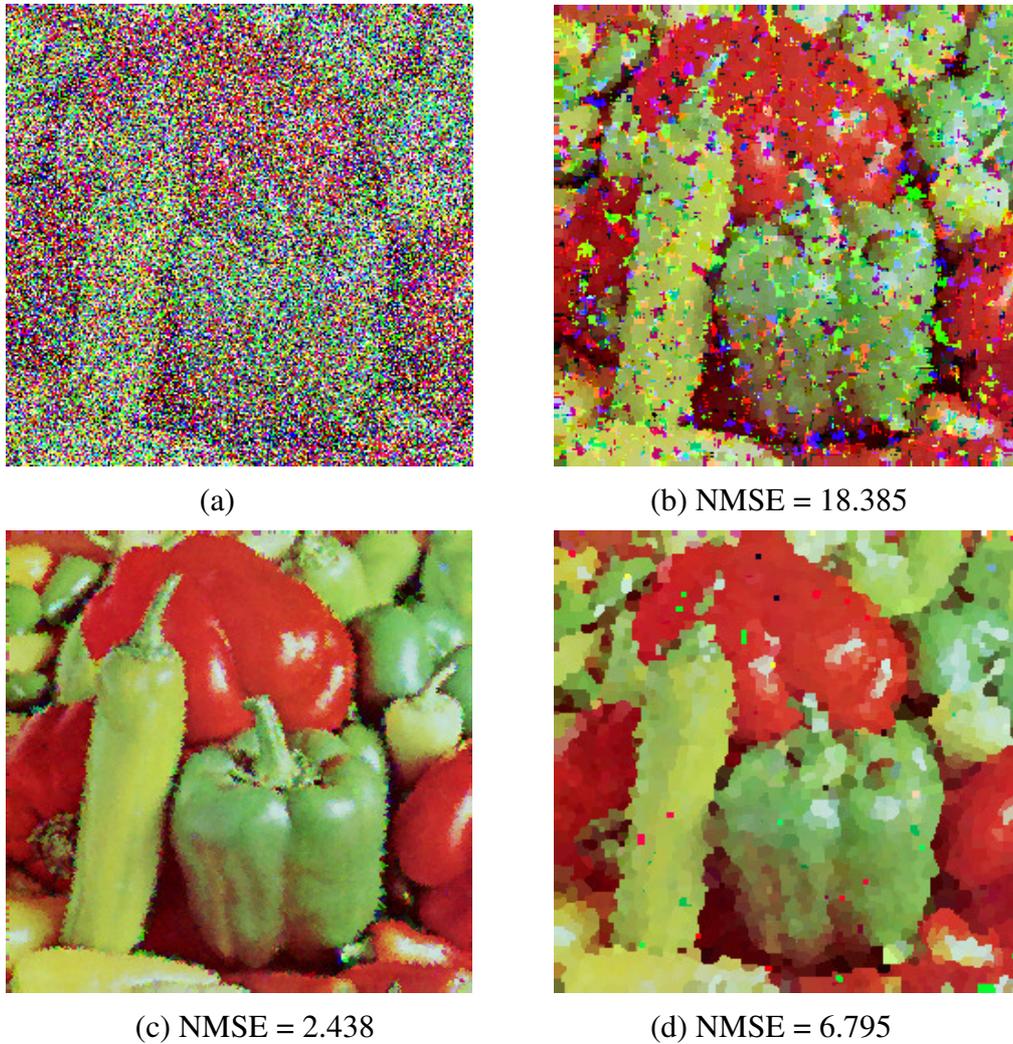
Figure 4.16. Results of noise reduction (a) pepper image with 70% salt and pepper noise added, (b) vector median filter; and conditional toggle mapping by using (c) marginal approach and (d) the proposed HSV ordering.

(a)

(b) NMSE = 97.021

(c) NMSE = 5.352

(d) NMSE = 23.949
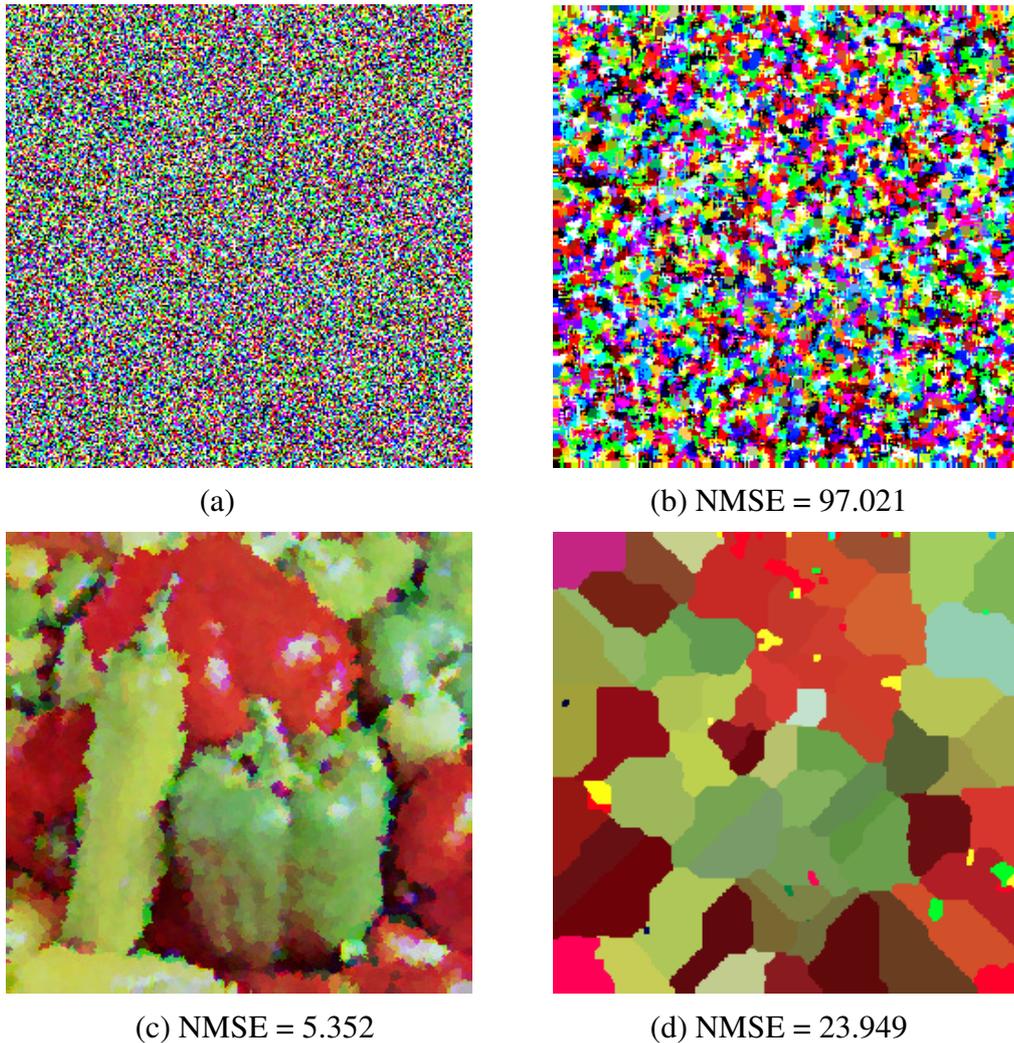
Figure 4.17. Results of noise reduction (a) pepper image with 95% salt and pepper noise added, (b) vector median filter; and conditional toggle mapping by using (c) marginal approach and (d) the proposed HSV ordering.
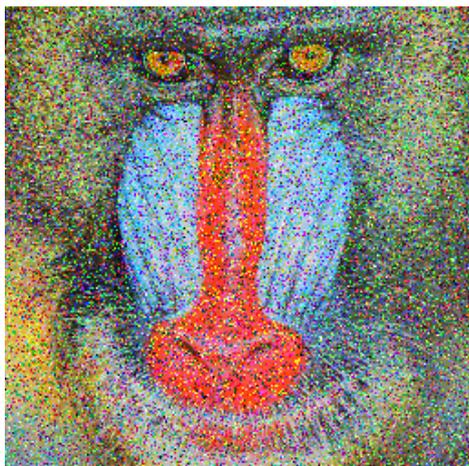
(a)
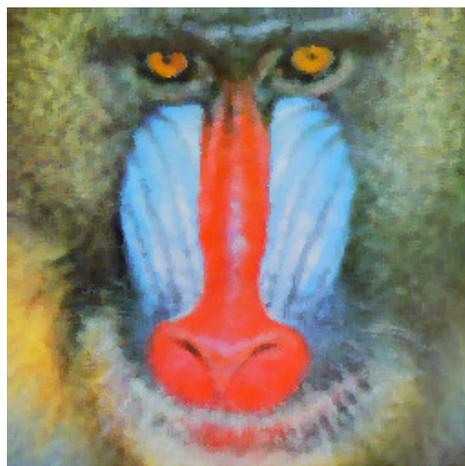
(b) NMSE =2.402
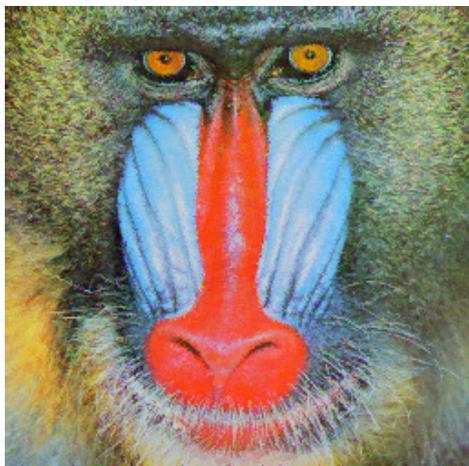
(c) NMSE = 1.376

(d) NMSE = 3.738

Figure 4.18. Results of noise reduction (a) Mandrill image with 20% salt and pepper noise added, (b) vector median filter; and conditional toggle mapping by using (c) marginal approach and (d) the proposed HSV ordering.
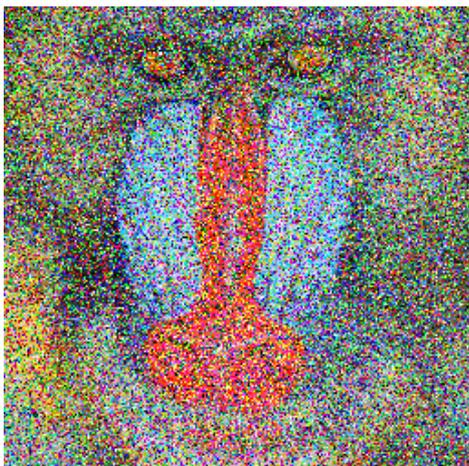
(a)
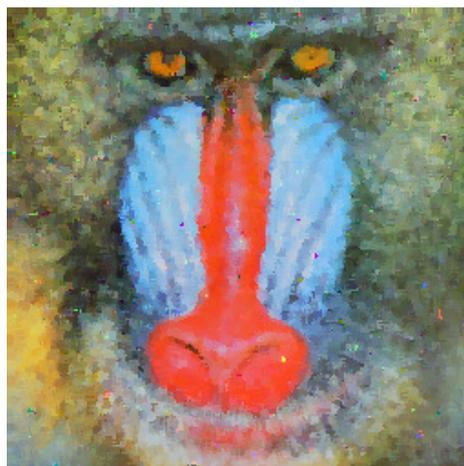
(b) NMSE = 3.365
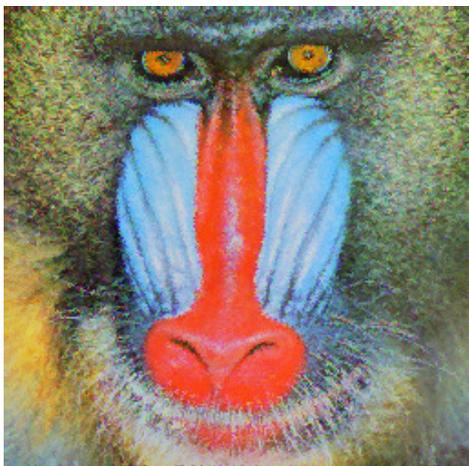
(c) NMSE = 2.297
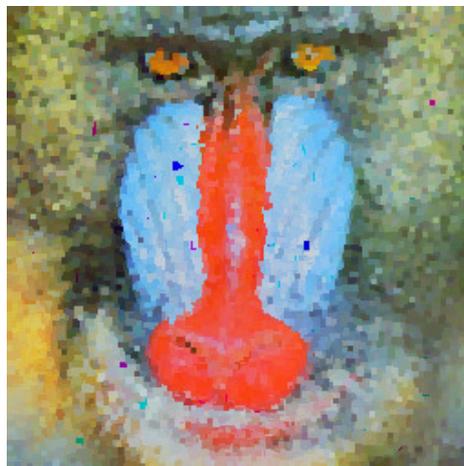
(d) NMSE = 3.89

Figure 4.19. Results of noise reduction (a) Mandrill image with 40% salt and pepper noise added, (b) vector median filter; and conditional toggle mapping by using (c) marginal approach and (d) the proposed HSV ordering.
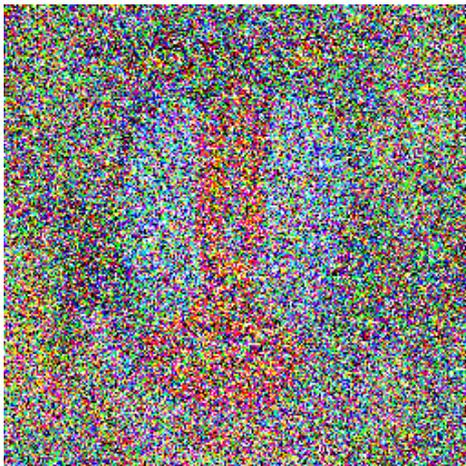
(a)
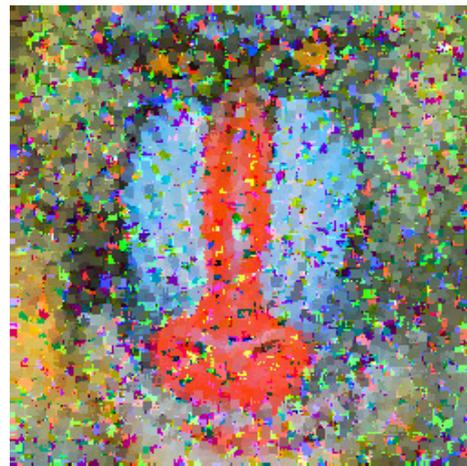
(b) NMSE = 16.437
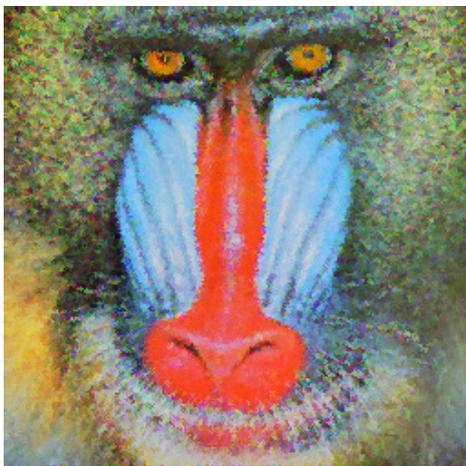
(c) NMSE = 3.233

(d) NMSE = 5.495

Figure 4.20. Results of noise reduction (a) Mandrill image with 70% salt and pepper noise added, (b) vector median filter; and conditional toggle mapping by using (c) marginal approach and (d) the proposed HSV ordering.

(a)

(b) NMSE = 77.299

(c) NMSE = 5.411

(d) NMSE = 16.019
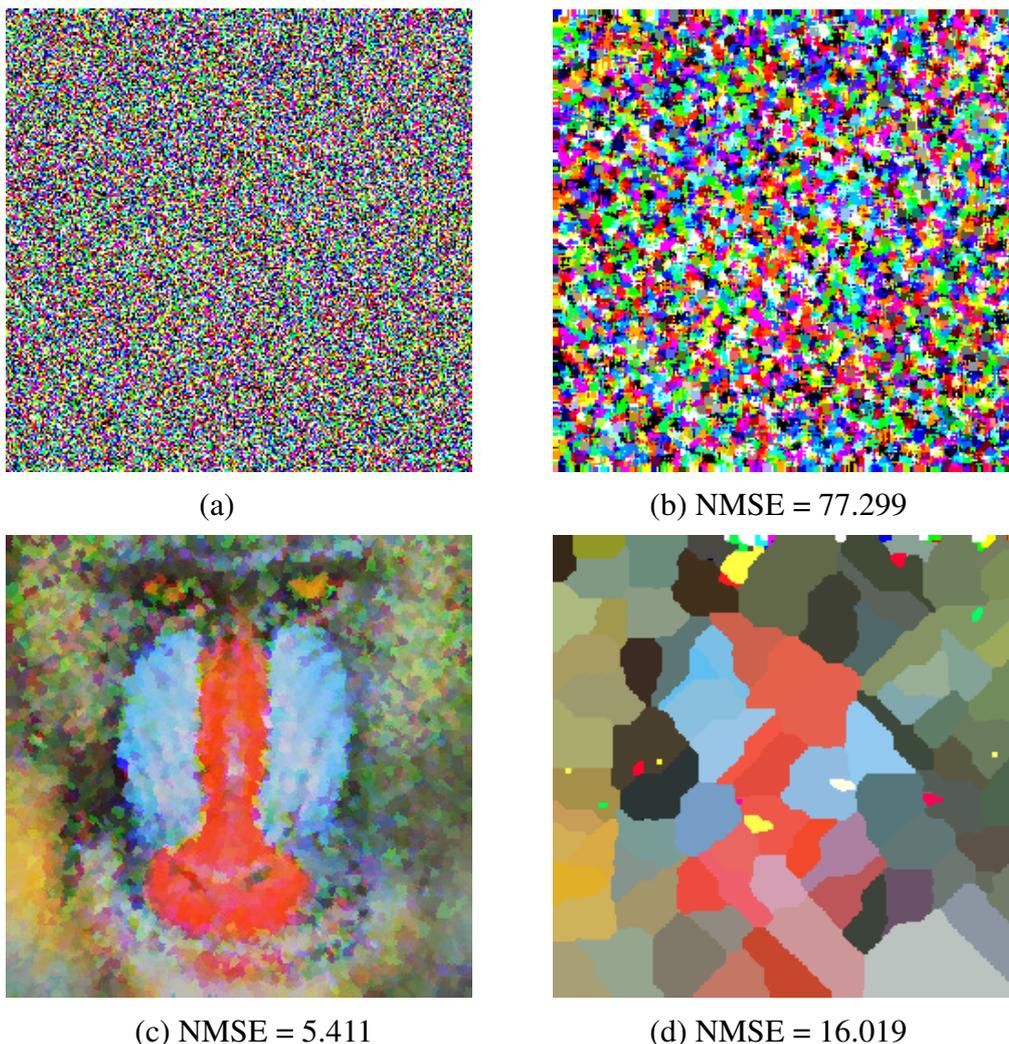
Figure 4.21. Results of noise reduction (a) Mandrill image with 95% salt and pepper noise added, (b) vector median filter; and conditional toggle mapping by using (c) marginal approach and (d) the proposed HSV ordering.

(a)
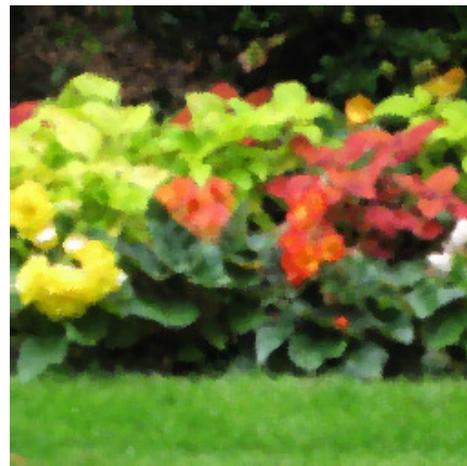
(b) NMSE = 2.193

(c) NMSE = 1.314
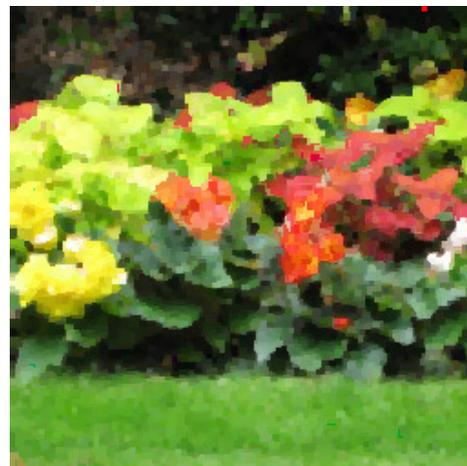
(d) NMSE = 3.211

Figure 4.22. Results of noise reduction (a) Flowers image with 20% salt and pepper noise added, (b) vector median filter; and conditional toggle mapping by using (c) marginal approach and (d) the proposed HSV ordering.

(a)
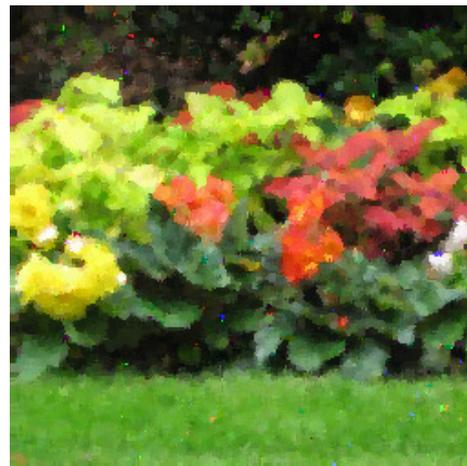
(b) NMSE = 3.775

(c) NMSE = 2.23
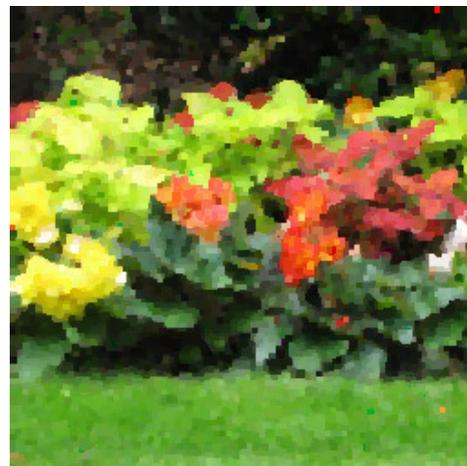
(d) NMSE = 3.751

Figure 4.23. Results of noise reduction (a) Flowers image with 40% salt and pepper noise added, (b) vector median filter; and conditional toggle mapping by using (c) marginal approach and (d) the proposed HSV ordering.
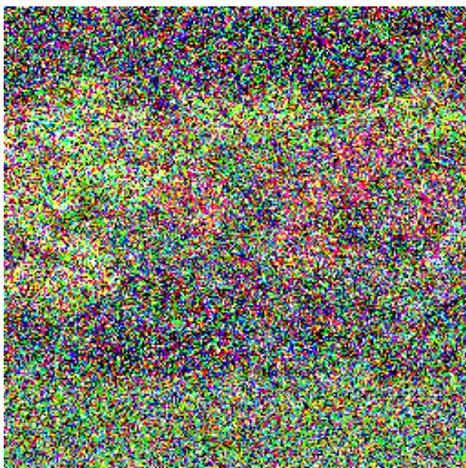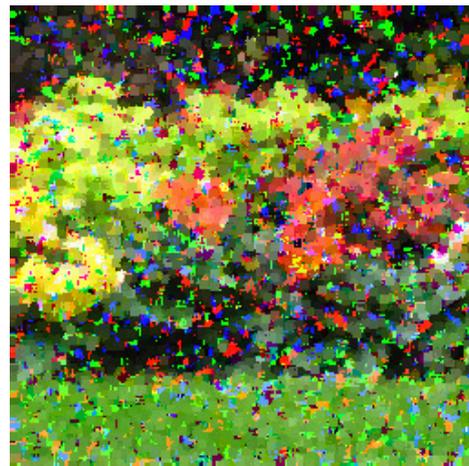
(a)   (b) NMSE = 28.046
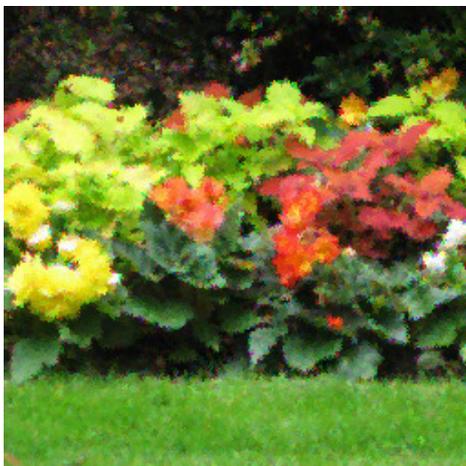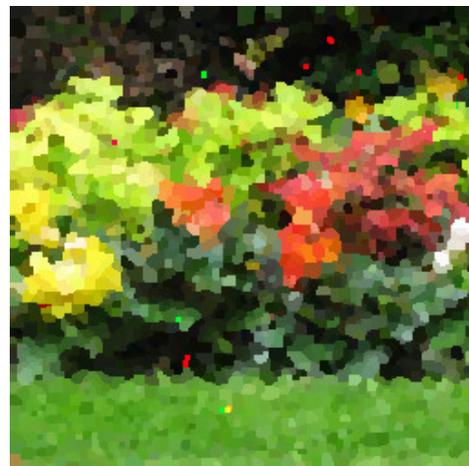
(c) NMSE = 3.21   (d) NMSE = 7.507

Figure 4.24. Results of noise reduction (a) Flowers image with 70% salt and pepper noise added, (b) vector median filter; and conditional toggle mapping by using (c) marginal approach and (d) the proposed HSV ordering.

(a)

(b) NMSE = 136.11

(c) NMSE = 7.604

(d) NMSE = 27.598
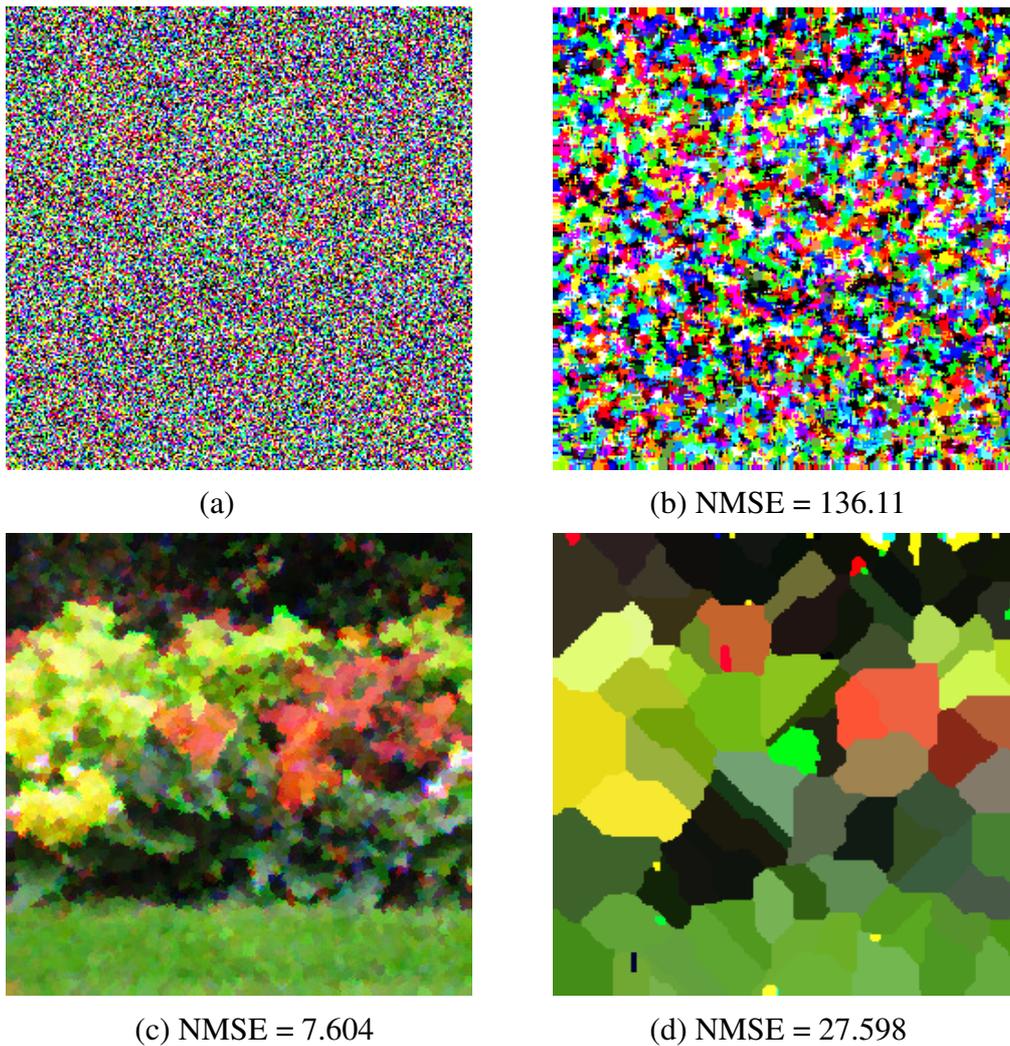
Figure 4.25. Results of noise reduction (a) Flowers image with 95% salt and pepper noise added, (b) vector median filter; and conditional toggle mapping by using (c) marginal approach and (d) the proposed HSV ordering.

4.6.4 Comparison in edge enhancement

The conditional toggle mapping can be also applied with the mask $\mathbf{M}_E$ for edge enhancement by using Eq. (4.27) and Eq. (4.28). To extend this operation to colour, the same ordering schemes as considered in the previous subsection were also adopted for these tests, for consistency. The three natural images, named "Pepper", "Flowers" and "Mandrill", were qualitatively evaluated.

Our proposed ordering schemes each gave similar results for edge enhancement; therefore, we only show one of them in Fig. 4.26, to Fig. 4.28. Fig. 4.26 shows subjective visual results for the "Pepper" image after edge enhancement by conditional toggle mapping using the marginal ordering and our proposed ordering. The marginal ordering method produced artefacts at the boundaries and severely distorted the image, as clearly shown in Fig. 4.26 (e). Similarly, Fig. 4.27 (e) and Fig. 4.28 (e) illustrate the limitations of the marginal ordering for edge enhancement. The proposed orderings produced no false colours, and the edges were enhanced by the conditional toggle mapping as seen in Fig. 4.26 to Fig. 4.28.
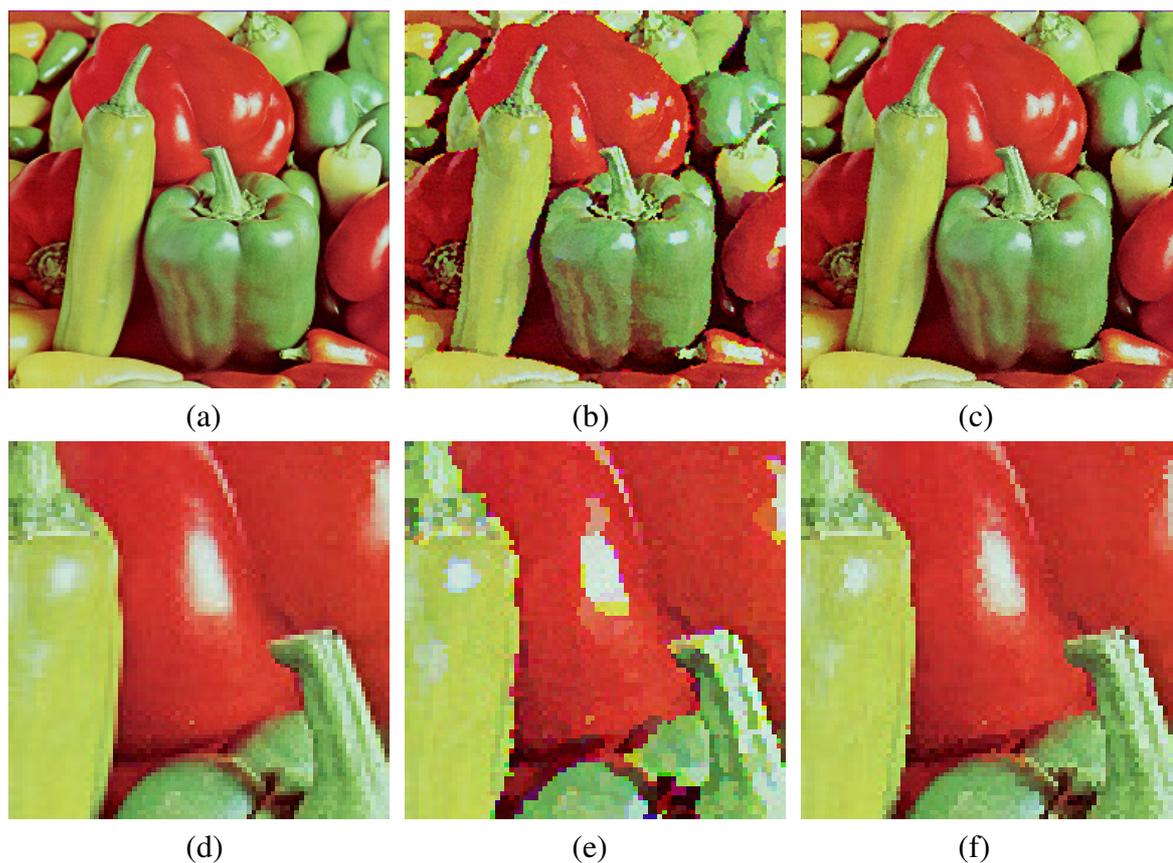
Figure 4.26. "Pepper" image: (a) original image and the result after edge enhancement by the conditional toggle mapping using (b) marginal ordering, (c) the proposed ordering, (d) the enlarged patch of (a), (e) the enlarged patch of (b), and (f) the enlarged patch of (c).
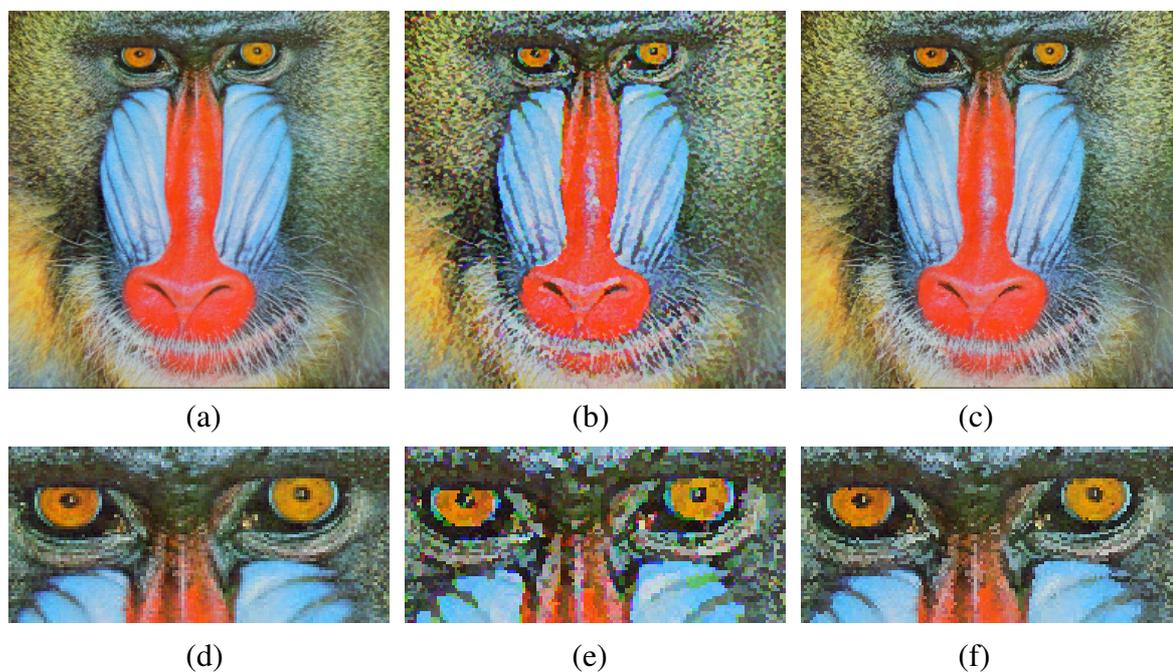

Figure 4.27. "Mandrill" image: (a) original image and the result after edge enhancement by the conditional toggle mapping using (b) marginal ordering, (c) the proposed ordering, (d) the enlarged patch of (a), (e) the enlarged patch of (b), and (f) the enlarged patch of (c).
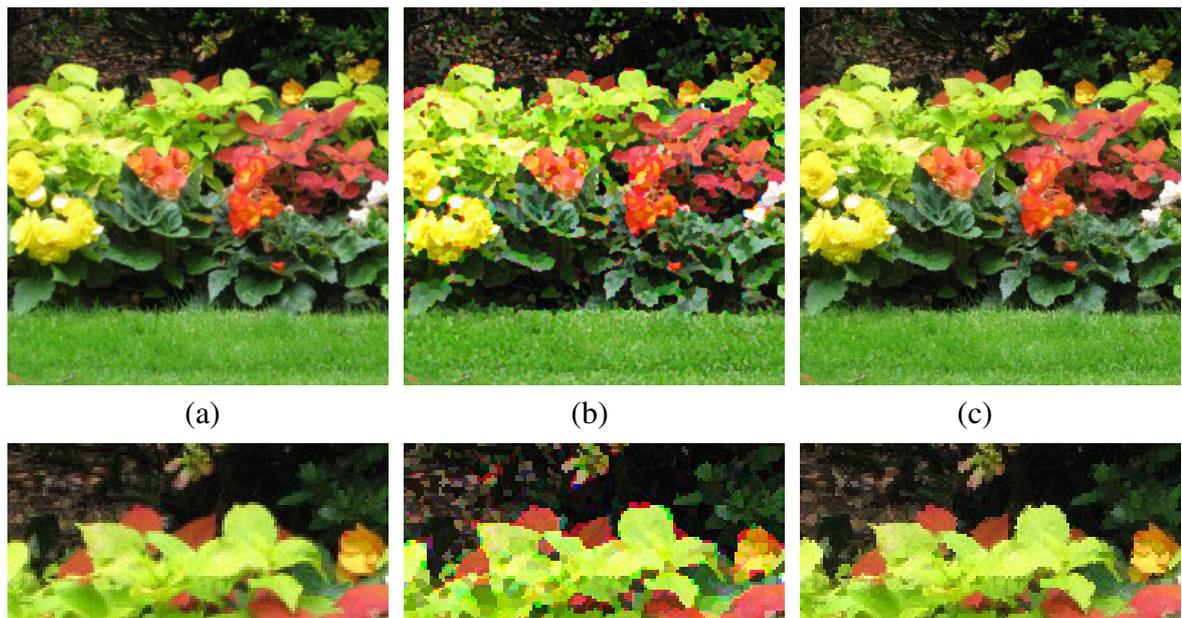
Figure 4.28. "Flowers" image: (a) original image and the result after edge enhancement by the conditional toggle mapping using (b) marginal ordering, (c) the proposed ordering, (d) the enlarged patch of (a), (e) the enlarged patch of (b), and (f) the enlarged patch of (c).

4.6.5 Discussion

In this section, we presented the experimental results and discussed how the different colour ordering schemes influence the performance of basic colour morphological operations and more sophisticated operations of the OC filter and the conditional toggle mapping filter as used for noise reduction and edge enhancement.

4.6.5.1 Basic morphological operations

The proposed ordering scheme produced no artefacts in dilation, erosion, opening and closing for colour images. Conversely, some false colours were introduced using marginal ordering. This is a fundamental property of marginal ordering.

Vector ordering can avoid false colours produced but there is no vector ordering widely accepted for colour morphology. In Cheng's PCA-like ordering the sense of a supremum and an infimum are less well defined for complete lattices. The supremum and the infimum in Cheng's PCA-like ordering are influenced by the neighbourhood; therefore, this method does not meet the requirements for colour mathematical morphology of being increasing, extensive, anti-extensive and idempotent. If an ordering depends on the local values of the neighbourhood as in Cheng's method the implementation of dilation (erosion) cannot commute with the supremum (infimum) and is not distributive. Additionally, Angulo's

ordering needs a reference colour to define the foreground for colour morphology. This suits applications where prior knowledge can be used to identify suitable reference colours. Our proposed orderings overcome this limitation and provide an appropriate response for the basic operations of colour morphology because the sense of a colour extrema is well-defined using Finlayson's model that reflects the behaviour of common image capture devices.

4.6.5.2 OC filter

The proposed ordering scheme performs well in the suppression of impulse noise because the colour extrema adopted are generic and not context related, as in Angulo's ordering. In marginal ordering, conditional ordering and Cheng's PCA-like ordering the sense of an extrema is less well defined.

In the experiments reported here noise was added as maximum values to each colour channel in the RGB colour space, in a manner that reflects the behaviour of common image capture devices and in a manner that is analogous to the colour extrema concept used in the definition of colour mathematical morphology given here. This provides a clear basis for the addition of impulse noise. It is not appropriate to set pepper pixel values to (0, 0, 0) in RGB colour space because this gives greater emphasis to this pepper noise, than the other changes do to colour impulse noise. It is more difficult to formulate a universally appropriate way of adding pepper

impulse noise. We sought only to demonstrate that, the proposed method is beneficial for the suppression of salt impulse noise. Whilst there might be a cause for concern that the evaluation is matched to the method reported it is expected that the improvement would prevail should an alternative colour space be used for noise addition. As shown in Fig. 4.9 and 4.10, the use of colour extrema proposed here is necessary because it is difficult to define a reference colour, and the use of colour difference formula E_{94}^{*} in the L*a*b* colour space is slightly better than that of Euclidean distance in the RGB and HSV colour spaces, respectively, and can be specialised to grey-level and binary morphology.

4.6.5.3 Conditional toggle mapping

The advantage of conditional toggle mapping is that it provides a morphological framework for conditional erosion and dilation to handle different image processing problems, such as image denoising and edge enhancement for grey-level images [VEL13]. Velasco-Forero and Angulo extended conditional toggle mapping to colour using marginal ordering. In the evaluation reported conditional toggle mapping performed the better at noise removal than the other methods reported. This might be because the noise was separately added to each colour channel in the RGB colour space and is analogous to how the definition of the marginal ordering when used in the conditional toggle mapping for R, G and B channels. Whilst there might be a cause for concern that the evaluation is matched to the method reported it is

expected that the improvement would prevail should an alternative colour space be used for

noise addition. However, the marginal ordering of conditional toggle mapping still produced

artefacts around the boundaries as when applied in basic morphological operations and it was

especially severe in edge enhancement. Other compared ordering schemes performed worse

in conditional toggle mapping for denoising because the salt impulse noise is not

well-removed with the Mask $\mathbf{M}_N$ of Eq. (4.29). This resulted in the conditional toggle

mapping not performing well for denoising by using $\mathbf{M}_N$ because the conditional erosion and

conditional dilation in Eq. (4.22) and Eq. (4.23) both work on $\mathbf{M}_N(x) = 0$ where the position

x contains the value of the local minimum (pepper impulse noise) or local maximum (salt

impulse noise). The local maximum $\rho^{\delta}_{\Omega^d_{colour}, S}(\mathbf{I})(x)$ depends on the definition of colour

difference described in Section 4.2 and is greater than zero in the RGB and CIE L*a*b*

colour spaces using Eq. (4.5) and Eq. (4.7) when the x position is a salt impulse noise but not

a local maximum. In the HSV colour space, the defined colour difference of $\rho^{\delta}_{\Omega^d_{colour}, S}(\mathbf{I})(x)$ is

equal to zero when the x position is a salt impulse noise using Eq. (4.6). This means that

whilst in grey-level images salt and pepper noise values are always local maxima and minima,

in colour images this is not always the case.

The proposed ordering scheme performs well in the conditional toggle mapping for both noise

reduction and edge enhancement because the colour extrema adopted are generic and not

context related. The other orderings use local extremas or define a reference colour as the foreground creating context dependence. As a result they demonstrate poor performance in the experiments reported. The design of the mask $\mathbf{M}_N$ and $\mathbf{M}_E$ play an important role in noise removal and edge enhancement, respectively because they are key to locating local extrema. Here, we used Eq. (4.6) as the distance function for image denoising and edge enhancement, respectively and this improved performance.

There is a need for better quantitative measures to judge the performance of colour edge enhancement in the conditional toggle mapping. It would be valuable to develop the understanding of what the problem is with existing measures of edge enhancement and what is needed.

4.7 Summary

A complete ordering for colour morphology has been proposed that combines R-ordering and C-ordering. A definition of colour extrema based on a model of colour image formation has been presented. The presented ordering scheme used the Euclidean distance, E_{94}^{*} colour difference formula and HSV distance in the RGB, L*a*b* and HSV colour spaces, respectively. The performance evaluation considered basic morphologic operations (erosion, dilation, opening and closing), noise removal and edge enhancement. The chief contribution is

a principled method for mathematical morphology that harmonises binary, grey-level and colour morphology. It has been shown that the use of the proposed ordering provides an appropriate response for colour images that improves on some methods for erosion, dilation, opening, closing by eliminating the artefact produced with marginal ordering, and edge enhancement. The proposed ordering was better where noise suppression was concerned, compared to previously reported methods, especially at high noise levels, where noise was added to 40% or more pixels. A novel and effective extension of conditional toggle mapping to colour using a vector method has been presented. Table 4.2 summarises the performance comparison of the proposed difference-based ordering in morphological operations and filters.

Table 4.2 The performance comparison of the proposed difference-based ordering for colour morphology.

Morphologcial Operators in Colour	Performance Comparison
Dilation/Erosion	■ The results of the synthetic image are similar to Angulo's ordering. ■ In the natural image, the proposed orderings demonstrated that the serrated appearance produced after colour erosion. ■ Angulo's ordering demonstrated the smooth results in the qualitative evaluation that is better than ours.
Opening/Closing	■ The proposed orderings still demonstrated that the strong serrated appearance produced after colour opening and closing. ■ Angulo's ordering also demonstrated the smooth results in the qualitative evaluation that is better than ours..
OC filtering	■ The proposed ordering outperforms the other ordering schemes at high levels of added noise (from 30% to 70% of overall impulse noise). ■ Only marginal ordering is slightly better than the proposed ordering at relatively low overall impulse noise levels of 5% to 25%.
Conditional toggle mapping in noise reduction	■ The proposed ordering in the HSV colour space outperformed the other vector ordering schemes, except the marginal ordering method at all levels of added noise. ■ The vector median filter performed significantly worse than the proposed ordering in the HSV colour space at noise levels of 70% to 95%.
Conditional toggle mapping in edge enhancement	■ The marginal ordering produced artefacts at the boundaries and severely distorted the image. ■ The proposed orderings produced no false colours, and the edges were enhanced clearly.

The approach to colour ordering presented meets the formal requirements for complete lattices, a basic requirement for mathematical morphology. This allows the same concept to be applied for morphologic operations in binary, grey-level and colour morphology. There is no reason why this approach to colour morphology cannot be extended to other morphologic operators such as the morphological skeleton and to other forms of multi-channel data.

It has also been shown that care is needed in interpreting how impulse noise should be added to colour and multi-channel images. This is particularly important here because it facilitates the evaluation of colour ordering and colour morphology operations.

There is also a need to extend the difference-based ordering presented in this chapter when the prior knowledge of applications is known, such as hit-or-miss transformation. A new similarity-based ordering will be introduced in the next chapter that takes advantage of the difference-based ordering with prior knowledge. This would help the development of colour template matching for mathematical morphology.

Chapter 5: Similarity-based Colour Morphology

This chapter extends the use of the colour extrema presented in Chapter 4. Two similarity criteria have been defined, one in the RGB and one in the CIE L*a*b* colour space, as a basis for mathematical morphology. This extension is useful when the prior knowledge is known, such as hit-or-miss transformation. To develop morphological operators, a complete lattice structure is needed to define an ordering relationship between colour points. Once an ordering has been established, the morphological operators can be defined in the standard way.

As defined in Chapter 4, the total ordering scheme for similarity-based colour morphology combines an R-ordering and a C-ordering. The R-ordering is based on a colour similarity measure and the C-ordering on a lexicographical cascade by similarity and colour channel. Colour is used in the cascade to resolve any residual ambiguity. The novelty is in relating this ordering to mathematical morphology by considering the closeness of a colour to the values of a structure element. In this approach each pixel of the structure element can be allocated a colour. This would help the development of hit-or-miss transformation in colour as a non-linear template matching method.

5.1 Basic Definitions

A detailed exposition of the principles of colour ordering was given in Section 3.4. Here, the

key issues are summarised and applied to form a similarity based ordering for binary,

grey-level and colour images.

The basic definition of the h-mapping was described in Section 3.4.2. We refer by $\leq_h$ to the

h-ordering given by:

$$r \leq_h r' \Leftrightarrow h(r) \leq h(r'), \quad \forall r, r' \in \mathbb{F} \tag{5.1}$$

Note that $\leq_h$ preserves reflexivity ($r \leq_h r$) and transitivity ($r_1 \leq_h r_2$ and $r_2 \leq_h r_3 \Rightarrow r_1 \leq_h r_3$). Most

importantly, the h-ordering has to be completed in each equivalence class to lead to a

h-injective and a complete total ordering.

5.2 *h*-Similarity Ordering

In the case of an *h*-ordering on similarity the challenge in building complete lattice structures is to define a mapping, h: $\mathbb{F} \rightarrow \mathcal{L}$, where $\mathcal{L}$ can be the lattice of the binary, grey-level and colour images using a pre-ordering $\leq_h$. Two main cases of mappings h for a given $\mathbf{c} \in \mathbb{F}$ can be defined as follows:

■   For binary and grey-level images ($p = 1$) the colour mapping is:

$$h_g^s(c) = \phi_g(t,c) \tag{5.2}$$

where ϕ_g is a similarity measure for binary and grey-level images with a reference value, $t \subseteq \mathbb{R}$. For binary and grey-level images, c is a pixel value also defined in $\mathbb{R}$. The use of *h*-similarity ordering in grey-level images re-defines binary and grey-level morphology for both flat and non-flat structure elements.

- For colour images ($p = 3$):

$$h^s_{colour}(\mathbf{c}) = \phi_{colour}(\mathbf{t}, \mathbf{c}) \tag{5.3}$$

where ϕ_{colour} is a similarity measure for colour images with a reference colour, $\mathbf{t} \subseteq \mathbb{R}^3$. For colour images, $\mathbf{c}$ is also a pixel value defined in $\mathbb{R}^3$. Using *h*-similarity ordering contributes to colour morphology with flat and non-flat structure elements.

The main motivation for defining this similarity-based ordering scheme is to apply mathematical morphology in the lattice $\mathcal{L}$ interpretable with respect to the given structure elements. The foreground colour, C_F, is defined by the grey-levels or colours within a structure element. The background colour, C_B can be naturally defined to be that grey-level or colour with maximum dissimilarity to the reference grey-level or colour within the structure element. Note that $\mathrm{Inf}_{\mathcal{L}}$ and $\mathrm{Sup}_{\mathcal{L}}$ are the smallest and largest elements in the lattice $\mathcal{L}$, respectively. This ordering satisfies the conditions $h(\mathbf{c}) = \mathrm{Sup}_{\mathcal{L}}$ if $\mathbf{c} \in C_F$ and alternatively $h(\mathbf{c}) = \mathrm{Inf}_{\mathcal{L}}$ if $\mathbf{c} \in C_B$. This could be applied in practice when the prior knowledge about the reference colours is known, for instance, a near green has been chosen as the reference colour when the colour morphology was applied for tree canopies counting [LEW14].

5.3 The Definition of Similarity Measures

In this section, we describe similarity measures for binary, grey-level and colour images in the

RGB and CIE L*a*b* colour spaces. Other measures of similarity can be used.

5.3.1 Binary and grey-level similarity

The similarity measure for binary and grey-level images is defined by the grey-level mapping:

$$h_g^s(c) = \phi_g(t,c) = 1 - \frac{|t-c|}{MAX} \tag{5.4}$$

where, *MAX* is 1 and 255 for binary and grey-level images, respectively, and c and t are the

image and reference pixel values, respectively. The similarity measure, ϕ_g, is used to evaluate

the closeness between the image and the reference pixel value. The similarity measure defined

above is normalised over the range [0, 1]. If c is equal to t, $h_g^s(c)$ will be at the maximum

value of 1.

5.3.2 Colour similarity

In Finlayson's model of colour image formation [FIN98] [FIN01], an RGB colour is represented as intensity and chromaticity. Here we formulate colour similarity using a similar representation. Similarity between two colours is defined by the combination of normalised intensity and chromatic similarity:

$$h^s_{colour}(\mathbf{c}) = \phi_{colour}(\mathbf{t},\mathbf{c}) = NI(\mathbf{t},\mathbf{c}) \times Chroma(\mathbf{t},\mathbf{c}) \tag{5.5}$$

To summarise, the definitions of colour extrema presented in Section 4.1, $\mathbf{c}^{MAX}$ and $\mathbf{t}^{MAX}$ are defined as the colour extrema of the image colour $\mathbf{c}$ and the reference colour $\mathbf{t}$, respectively, where:

$$\mathbf{c}^{MAX} = \begin{cases} (\rho^{Max}R, \ \rho^{Max}G, \ \rho^{Max}B), & \text{if } \max(R,G,B) > 0 \\ (255, \ 255, \ 255), & \text{if } \max(R,G,B) = 0 \end{cases} \tag{5.6}$$

Here (R_i, G_i, B_i) is the colour representation of $\mathbf{c}$ and ρ^{Max} is the maximum brightness factor in each chromaticity:

$$\rho^{Max} = \frac{MAX}{\max(R,G,B)} \tag{5.7}$$

where *MAX* is 255 in a colour RGB representation that uses 8-bit integer values for each channel. When the colour is pure black, its extrema is set to white (255, 255, 255).

In the following subsections, we summarise the similarities defined in the RGB and L*a*b* colour spaces. The similarity measures are used instead of the difference function presented in Chapter 4. This is because that the normalised difference function is only defined in the same chromaticity between a colour and its extrema. Hence, the similarities need to be developed that contain the normalised functions of intensity and chromaticity between two different colours. This would be helpful for Hit-or-Miss transformation in colour. The HSV colour space has not been considered here because it lacks of perceptual uniformity and a widely accepted distance measure. This was discussed in Section 3.2.6. These issues make it difficult to define a chromatic similarity between two colours using distance measures.

5.3.2.1 RGB colour space

In the RGB colour space, the normalised intensity and chromatic similarity are defined by:

$$NI_{\mathrm{RGB}}(\mathbf{t},\mathbf{c}) = 1 - \left| \frac{\|\mathbf{c}\|}{\|\mathbf{c}^{MAX}\|} - \frac{\|\mathbf{t}\|}{\|\mathbf{t}^{MAX}\|} \right| \tag{5.8}$$

and

$$Chroma_{\mathrm{RGB}}(\mathbf{t},\mathbf{c}) = 1 - \frac{2}{\pi}\cos^{-1}\frac{\left\langle \mathbf{c}^{MAX}, \mathbf{t}^{MAX} \right\rangle}{\|\mathbf{c}^{MAX}\|\|\mathbf{t}^{MAX}\|} \tag{5.9}$$

where $\|\cdot\|$ is the norm of each vector and $\langle \cdot, \cdot \rangle$ is the scalar product of the colour vectors in the RGB colour space.

NI_{RGB} is the correlation coefficient of the brightness between two colour vectors. Similarly, $Chroma_{\text{RGB}}$ corresponds to the angle between the two colour vectors, i.e., the coefficient of correlation between two RGB chromatic colour vectors. These similarity measures are normalised over the range [0, 1]. If the colours, **c** and **t**, have the same chromaticity, e.g. (255, 125, 0) and (102, 50, 0) in RGB the similarity of chromaticity will be 1. If the colours have exclusive chromaticities, say pure red (255, 0, 0) and pure green (0, 255, 0), in the RGB representation, then the chromatic similarity between them is 0. Additionally, the colour extrema are used to normalise the intensity similarity (*NI*). Together *NI* and chromaticity provide a combined measure of similarity.

5.3.2.2 CIE L*a*b* colour space

In the L*a*b* colour space, the normalised intensity and chromatic similarity are defined by

$$NI_{\text{LAB}}(\mathbf{t},\mathbf{c}) = 1 - \left| \frac{\|\mathbf{c}\|_{E_{94}^*}}{\|\mathbf{c}^{MAX}\|_{E_{94}^*}} - \frac{\|\mathbf{t}\|_{E_{94}^*}}{\|\mathbf{t}^{MAX}\|_{E_{94}^*}} \right| \qquad (5.10)$$

where $\|\cdot\|_{E_{94}^*}$ is the CIE-94 colour difference formula, which was defined in Section 4.2.3, between a colour and its origin (black).

$$Chroma_{\text{LAB}}(\mathbf{t},\mathbf{c}) = 1 - \frac{1}{\pi}\cos^{-1}\frac{\langle \mathbf{c}^{MAX}, \mathbf{t}^{MAX} \rangle}{\|\mathbf{c}^{MAX}\|\|\mathbf{t}^{MAX}\|} \qquad (5.11)$$

where $\|\cdot\|$ is the norm of each vector and $\langle\cdot,\cdot\rangle$ is the scalar product of the colour vectors in

the L*a*b* colour space.

NI_{LAB} is the correlation coefficient of the brightness between two colour vectors. Similarly,

$Chroma_{\text{LAB}}$ corresponds to the angle between the two colour vectors, i.e., the coefficient of

correlation between two chromatic colour vectors. The similarity measures defined above are

normalised over the range [0, 1].

5.4 Similarity-based Mathematical Morphology

The similarity-based morphology proposed here can be used with conceptual consistency in binary, grey-level and colour morphology, and with flat and non-flat structure elements.

Erosion and dilation are increasing operators on a complete lattice $\mathcal{F}(\mathbf{E}, \mathcal{L})$. Commonly, erosion is anti-extensive, i.e., $\varepsilon(\mathbf{I}) \leq_h \mathbf{I}$ and dilation is extensive, i.e., $\mathbf{I} \leq_h \delta(\mathbf{I})$. These properties are defined for the use of flat structure elements.

5.4.1 Binary and grey-level morphology

For a single channel binary or grey-level image $p=1$. Let $S=\{t_i \subseteq \mathbb{R}; i = 1, 2, \ldots, N\}$ represent a structure element of a finite size, N, where $t_1, t_2, \ldots, t_N$ is a set of reference pixel values, in the structure element as defined for each application. Let $\mathbf{I}_x = \{c_i \subseteq \mathbb{R}; I = 1, 2, \ldots, N\}$ represent a set of image pixels within the region of the structure element S, where $c_1, c_2, \ldots, c_N$ is the set of image pixel values in that neighbourhood, centred at position x of an image.

To use a similarity measure in binary and grey-level morphology, a total ordering is required to avoid random decisions in lattice operations. The total ordering Ω_g^s with a lexicographical cascade by similarity and grey value is used to resolve any remaining ambiguity. This is defined as:

$$c_i <_{\Omega_g^s} c_j \Leftrightarrow \begin{cases} \phi_g(t_i, c_i) < \phi_g(t_j, c_j) \text{ or} \\ \phi_g(t_i, c_i) = \phi_g(t_j, c_j) \text{ and } c_i < c_j \end{cases} \tag{5.12}$$

Where ϕ_g represents the grey-level similarity measure of Eq. (5.4). Here it is calculated between c and its corresponding reference pixel value, t. When c_i is close to t_i, then, by definition c_i is close the foreground value. If the reference pixel values are all set to the *MAX* value for binary and grey-level images, similarity-based binary and grey-level morphology under the proposed using ordering, h_g^{total}, is equivalent to the conventional definition of binary and grey-level morphology.

Operators $\wedge_{\Omega_g^s}$ and $\vee_{\Omega_g^s}$ are defined to identify the infimum and supremum pixels of $\mathbf{I}_x$ with the total ordering Ω_g^s, respectively.

Let the matrix of mapping, $\mathbf{I} \in \mathcal{F}(\mathbf{E}, \mathcal{L})$ at position $x \in \mathbf{E}$ by the structure element S. *Binary (Grey-level) erosion* $\varepsilon_{\Omega_g^s, S}$ be given by:

$$\varepsilon_{\Omega_g^s, S} \mathbf{I}(x) = \left\{ \mathbf{I}(y): y = \arg_z \wedge_{\Omega_g^s} [\mathbf{I}(z)], z \in S_x \right\} \tag{5.13}$$

The corresponding *dilation* $\delta_{\Omega_g^s, S}$ is given by:

$$\delta_{\Omega_g^s, S} \mathbf{I}(x) = \left\{ \mathbf{I}(y): y = \arg_z \vee_{\Omega_g^s} [\mathbf{I}(z)], z \in S_x \right\} \tag{5.14}$$

5.4.2 Colour morphology

For a colour image, $p = 3$. Let $\mathbf{S} = \{\mathbf{t}_i \subseteq \mathbb{R}^3; i = 1, 2, \ldots, N\}$ represent a set of reference colour

pixels within a structure element of a finite size, N, where $\mathbf{t}_1, \mathbf{t}_2, \ldots, \mathbf{t}_N$ is a set of reference

colour pixel vectors, specified by users, in a neighbourhood centred at the structure element.

Let $\mathbf{I}_x = \{\mathbf{c}_i \subseteq \mathbb{R}^3; I = 1, 2, \ldots, N\}$ represent a set of image colour pixels within the region of the

structure element $\mathbf{S}$, where $\mathbf{c}_1, \mathbf{c}_2, \ldots, \mathbf{c}_N$ is a set of image colour pixel vectors in a

neighbourhood centred at position x of an image. To extend mathematical morphology to

colour images the pre-ordering h^s_{colour} must be modified to resolve any remaining ambiguity.

The total ordering Ω^s_{colour} with a lexicographical cascade by similarity and RGB colour

channel comparison is defined as:

$$\mathbf{c}_i <_{\Omega^s_{colour}} \mathbf{c}_j \Leftrightarrow \begin{cases} \phi_{colour}(\mathbf{t}_i, \mathbf{c}_i) < \phi_{colour}(\mathbf{t}_j, \mathbf{c}_j) \text{ or} \\ \phi_{colour}(\mathbf{t}_i, \mathbf{c}_i) = \phi_{colour}(\mathbf{t}_j, \mathbf{c}_j) \\ \text{and} \\ \begin{cases} c_i^G < c_j^G \text{ or} \\ c_i^G = c_j^G \text{ and } c_i^R < c_j^R \text{ or} \\ c_i^G = c_j^G \text{ and } c_i^R = c_j^R \text{ and } c_i^B < c_j^B \end{cases} \end{cases} \quad (5.15)$$

where ϕ_{colour} represents the colour similarity measure of Eq. (5.5) and is calculated between $\mathbf{c}$

and its corresponding reference colour vector, $\mathbf{t}$ by using Eq. (5.8) and Eq. (5.9) for RGB

colour space and Eq. (5.10) and Eq. (5.11) for L*a*b* colour space. Here c^R, c^G and c^B are the

red, green and blue channels of $\mathbf{c}$, respectively. For normal human perception the order of

importance for sensitivity of the colour channels is Green, Red and Blue, in order. Note that $\mathbf{t}_i$, represents the foreground colour. Using a flat structure element with a given colour, we have a similarity criterion that is similar to those defined by Angulo [ANG07a].

Operators $\wedge_{\Omega_{colour}^s}$ and $\vee_{\Omega_{colour}^s}$ are defined as the infimum and supremum colour pixel vectors obtained using a total ordering Ω_{colour}^s, respectively.

Let $\mathbf{I} \in \mathcal{F}(\mathbf{E}, \mathcal{L})$ at position $x \in \mathbf{E}$ by the structure element S. *Colour erosion* $\varepsilon_{\Omega_{colour}^s, \mathbf{S}}$ is given by:

$$\varepsilon_{\Omega_{colour}^s, \mathbf{S}} \mathbf{I}(x) = \left\{ \mathbf{I}(y) : y = \arg_z \wedge_{\Omega_{colour}^s} [\mathbf{I}(z)], z \in \mathbf{S}_x \right\} \qquad (5.16)$$

The corresponding *colour dilation* $\delta_{\Omega_{colour}^s, \mathbf{S}}$ is given by:

$$\delta_{\Omega_{colour}^s, \mathbf{S}} \mathbf{I}(x) = \left\{ \mathbf{I}(y) : y = \arg_z \vee_{\Omega_{colour}^s} [\mathbf{I}(z)], z \in \mathbf{S}_x \right\} \qquad (5.17)$$

The total ordering Ω_{colour}^s, is used to represent Ω_{RGB}^s and Ω_{LAB}^s as appropriate when using the RGB and L*a*b* colour spaces, respectively. In this process the output of erosion or dilation is one of the input colour pixel vectors. This avoids the introduction of false colours, and provides a harmonised approach for binary, grey-level and colour morphology.

A similarity-based colour opening is a colour dilation of a colour erosion, i.e.,

$$\gamma_{\Omega^s_{colour},\mathbf{s}}(\mathbf{I})(x) = \delta_{\Omega^s_{colour},\mathbf{s}}(\varepsilon_{\Omega^s_{colour},\mathbf{s}}(\mathbf{I})(x)) \tag{5.18}$$

and a similarity-based colour closing is a colour erosion of a colour dilation, i.e.,

$$\varphi_{\Omega^s_{colour},\mathbf{s}}(\mathbf{I})(x) = \varepsilon_{\Omega^s_{colour},\mathbf{s}}(\delta_{\Omega^s_{colour},\mathbf{s}}(\mathbf{I})(x)) \tag{5.19}$$

The opening (closing) is an anti-extensive (extensive) morphological filter. The opening removes spectral peaks which have a colour vector value close to the foreground and are thinner than the structure element. Conversely, the closing removes spectral peaks which have a colour vector value far from the foreground and are thinner than the structure element.

The residue-based operator defined in Section 2.4.2 is modified for colour by using similarity-based h-measures for colour images, giving the similarity-based morphological gradient:

$$\Delta_{\Omega^s_{colour},\mathbf{s}}(\mathbf{I})(x) = h^s_{colour}\left(\delta_{\Omega^s_{colour},\mathbf{s}}(\mathbf{I})(x)\right) - h^s_{colour}\left(\varepsilon_{\Omega^s_{colour},\mathbf{s}}(\mathbf{I})(x)\right) \tag{5.20}$$

where the function of h^s_{colour} is used to calculate the colour similarity between the image pixel value, $\mathbf{c}_i$, and its reference colour, $\mathbf{t}_i$, by using Eq. (5.5) after applying the morphological operations in colour. Similarly, the white top-hat transform, a positive similarity-based top-hat

transform, is the residue of an opening, i.e.:

$$\rho^{+}_{\Omega^{s}_{colour},\mathbf{S}}(\mathbf{I})(x) = h^{s}_{colour}(\mathbf{I}(x)) - h^{s}_{colour}\left(\gamma_{\Omega^{s}_{colour},\mathbf{S}}(\mathbf{I})(x)\right) \qquad (5.21)$$

The corresponding black top-hat transform, the residue of a closing, is a negative top-hat transform based on similarity, i.e.:

$$\rho^{-}_{\Omega^{s}_{colour},\mathbf{S}}(\mathbf{I})(x) = h^{s}_{colour}\left(\varphi_{\Omega^{s}_{colour},\mathbf{S}}(\mathbf{I})(x)\right) - h^{s}_{colour}(\mathbf{I}(x)) \qquad (5.22)$$

This yields similar results to those for the equivalent a grey-level operator in enhancing the contrasted regions smaller than the structure element, **S**, because the gradually changes grey-level are removed under the *h*-similarity ordering.

5.5 Similarity-based Hit-or-Miss Transform

The hit-or-miss transform (HMT) is a well-known morphological operator for template matching in binary images, but its extension to grey-level and colour images is not straightforward for non-flat structure elements [NAE07] [APT09b] [VEL10] [LED12]. Commonly, template matching is used for a binary HMT of an image. In existing HMT operators extending this approach to colour images commonly requires that major assumptions be made. Some of these assumptions cannot easily be justified. In addition, one method [VEL10] has a high computational complexity.

In Section 2.4.4, we briefly introduced the original definition of the Hit-or-Miss Transform (HMT) in binary images and explained how these definitions can be applied to binary and grey-level images. Here, the extension to colour images based on a complete lattice using similarity, in the similarity-based HMT (SHMT), is developed. Using similarity it is possible to formulate a grey-level and a colour HMT in which grey-level and colour images are treated consistently. The HMT is used to demonstrate the generality of the colour morphology scheme presented.

5.5.1 Hit-or-Miss transform in complete lattices

In the approach described here a binary or grey-level image $\mathbf{I}$ can be transformed to the lattice

$\mathcal{L}$ by the mapping h: $\mathbb{F} \subseteq \mathbb{R} \rightarrow \mathcal{L}$ using grey-level similarity measures leading to the

equivalence $h_g^s(\varepsilon_{\Omega_g^s, S}(I)) = h_g^s(\varepsilon_{\Omega_g^s, S^c}(I^c))$. Therefore, the background structure element, S_2,

can be used on the image $\mathbf{I}$ without complementation, under the h-similarity ordering presented

in Section 5.2. Equation (2.17) can be expressed in terms of h-similarity ordering, giving the

SHMT as:

$$
\begin{aligned}
SHMT\ (\mathbf{I}; S_1, S_2) \\
= \left\{ h_g^s(\varepsilon_{\Omega_g^s, S_1} \mathbf{I}(x)) = h_g^s(\varepsilon_{\Omega_g^s, S_2} \mathbf{I}(x)) = 1,\ x \in \mathbf{E} \right\} \\
= \left\{ h_g^s(\varepsilon_{\Omega_g^s, S} \mathbf{I}(x)) = 1,\ x \in \mathbf{E} \right\}
\end{aligned}
\tag{5.23}
$$

where h_g^s is used to calculate the binary or grey-level similarity between the image pixel

value, c_i, and its reference colour, t_i, by using Eq. (5.4). This is a simple template matching

method expressed using the similarity function. Note that both definitions in Eq. (5.23) are

equivalent because $S = S_1 \cup S_2$ with $S_1 \cap S_2 = \varnothing$. In mathematical morphology a non-flat

structure element is one where the grey-level or colour values in the structure element are not

uniform. The structure element, S, consists of two flat structure elements. A non-flat structure

element S can be reconstructed by n flat structure elements $S_1, S_2, \ldots, S_n$ when it satisfies the

condition $S_1 \cap S_2 \cap \ldots \cap S_n = \varnothing$. It is also shown that the SHMT can be applied in complete

lattices with a non-flat structure element using the *h*-similarity mapping.

From Eq. (5.23), for each structure element, there is an associated set of colour vectors.

Therefore, the SHMT for colour images can be formulated by the mapping *h*: $\mathbb{F} \subseteq \mathbb{R}^3 \rightarrow \mathcal{L}$, so

that :

$$SHMT\ (\mathbf{I};\mathbf{S}) = \left\{ h_{colour}^{s}\ (\varepsilon_{\Omega_{colour}^{s}\ ,\mathbf{S}} \mathbf{I}(x)) = 1,\ x \in \mathbf{E} \right\} \qquad (5.24)$$

where $\mathbf{S}$ is a non-flat structure element and h_{colour}^{s} denotes similarity in the different colour

spaces.

A less noise sensitive and more "robust" version of the SHMT has been defined using a

threshold in a grey-level HMT [APT09b] and for a colour HMT [VEL10] image. This variant

form of HMT (*SHMT-η*) is described in Eq. (5.25) for both grey-level and colour images. The

use of a threshold means that the structure element does not need to exactly match the image

patch. The generalised *SHMT-η* is defined, using *h*-similarity ordering, as:

$$SHMT\ _{\eta}\ (\mathbf{I};\mathbf{S}) = \left\{ h_{similarity}^{s}\ (\varepsilon_{h_{similarity}^{s}\ ,\mathbf{S}} \mathbf{I}(x)) \geq \eta,\ x \in \mathbf{E} \right\} \qquad (5.25)$$

where $h^s_{similarity}$ represents h^s_g and h^s_{colour} for binary/grey-level and colour similarities, respectively. Equation (5.23) and Eq. (5.24) are the particular cases of Eq. (5.25) with $\eta = 1$ in binary and grey-level and colour images that use grey-level and colour similarity measures, respectively. This parameter can be interpreted as the allowed minimum similarity between the image and the reference pixels in the $SHMT_\eta$ operator.

Figure 5.1 shows the impact of SHMT for colour images. The lattice induced by the h-similarity ordering is presented here, using Inf_L and Sup_L for minimum and maximum values in the lattice $\mathcal{L}$, respectively. Figure 5.1 (d) shows the positions of the perfect match between the structure element, *S,* and the Image **I** using Eq. (5.25). The parameter η is set to below one to permit an imperfect match between the structure element and the image. The similarity results of SHMT for Fig. 5.1(b) are shown in Fig. 5.1(c) by using the structure element in Fig. 5.1(a). The results of perfect match are shown in Fig. 5.1(d) when η was set to 1. Additionally, Fig. 5.1(e) shows the result obtained when η was set to 0.5 allowing the white rectangle on the right of the image in Fig. 5.1(b) to be detected although the structure element does not match the image well.
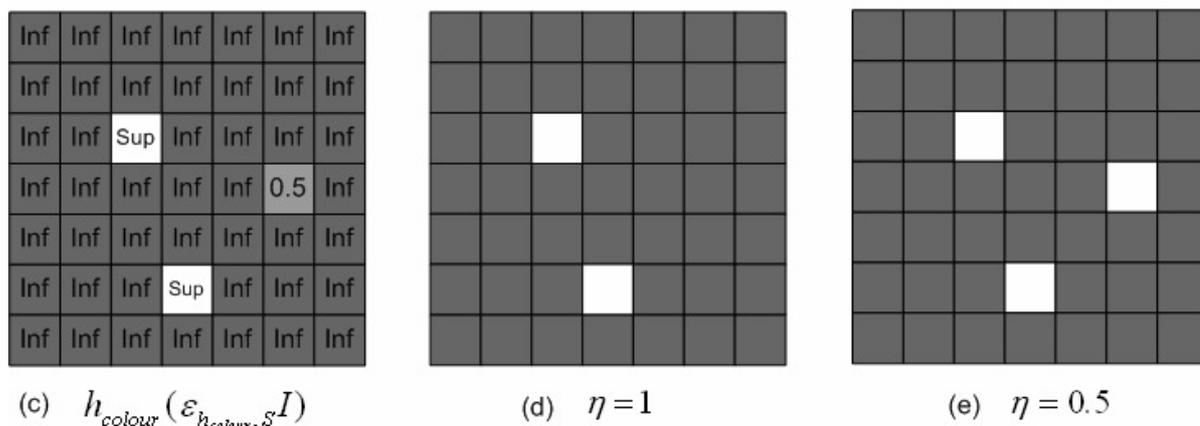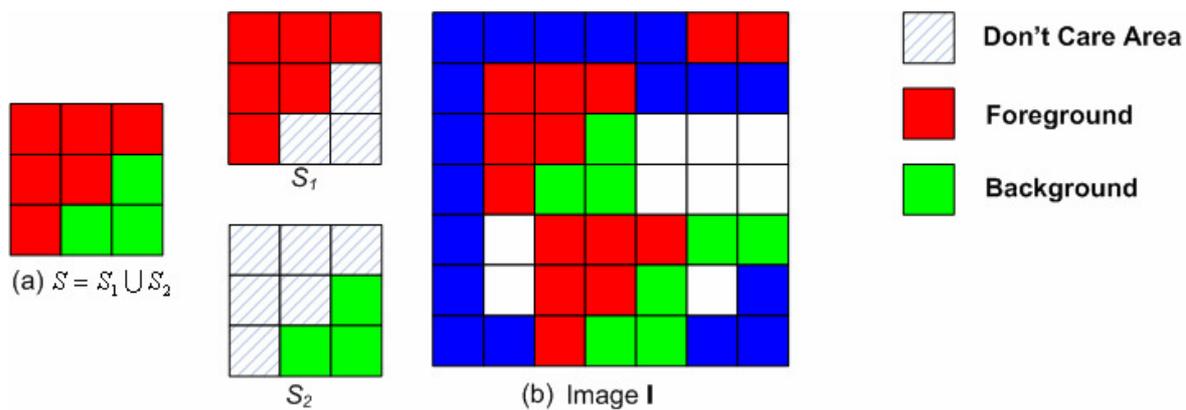
Figure 5.1. Example of Similarity-based HMT for colour images: (a) structure elements S, S_1 and S_2^c, (b) original image, (c) the similarity results of image **I** using SHMT, (d) perfect match results when $\eta = 1$ and (e) imperfect match results when $\eta = 0.5$.

5.5.2 Simplification of structure element

In Fig. 5.2 there is an image, **I,** composed of 5 objects: a synthetic shape with four colours,

the same shape with noisy edges and a small extrusion. Assume that the task is to mark the

location of the clean shape, and form a structure element that is an exact copy of the synthetic

shape. Using the SHMT in image, **I,** with the structure element, **S**, will yield a single marked

point, the centre of the shape, where the structure element fits exactly.
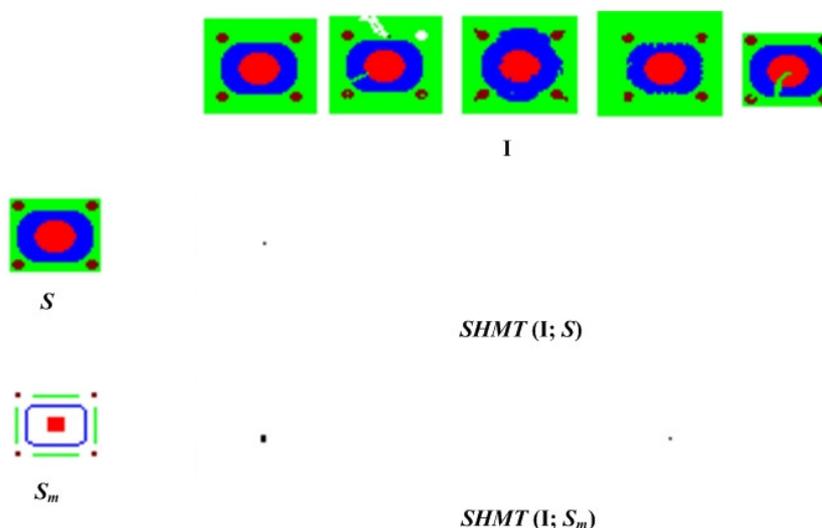
Figure 5.2. Recognition of noisy object using SHMT

When we consider a structure element, S_m, with components representing the major parts of

the Hit-or-Miss mask, and a don't care area, shown in white. Fig.5.2 shows the results after

applying SHMT with the structure element, S_m. This modified structure element identified the

noisy shape and the undistorted shapes on the left and second from the right of Fig. 5.2. The

detected region is not a single point but a small region.

5.6 Experimental Method

In these experiments the performance of basic morphological operations and the hit-or-miss transform are evaluated. The results obtained are discussed.

5.6.1 Design of test images and noise model

Synthetic and natural images were used to evaluate colour erosion, dilation and residue operators using a 3 x 3 structure element. When a transformation from RGB to L*a*b* colour space is performed the maximum, a white reference is used. If the illumination spectrum is not known then the CIE D_{65}, daylight illuminant is assumed [HAN02].

The synthetic test image used in Chapter 4 and shown in Fig. 5.3 (a) is again used here. This set of colours was chosen to observe the behaviour of colour morphological operations when one colour component is the largest or the smallest. The natural test images of Fig. 5.3 (b), Fig. 5.3 (c) and Fig. 5.3 (d) were chosen because they exhibit a wide range of colours. White Gaussian noise at a range of levels was added to the natural test images.
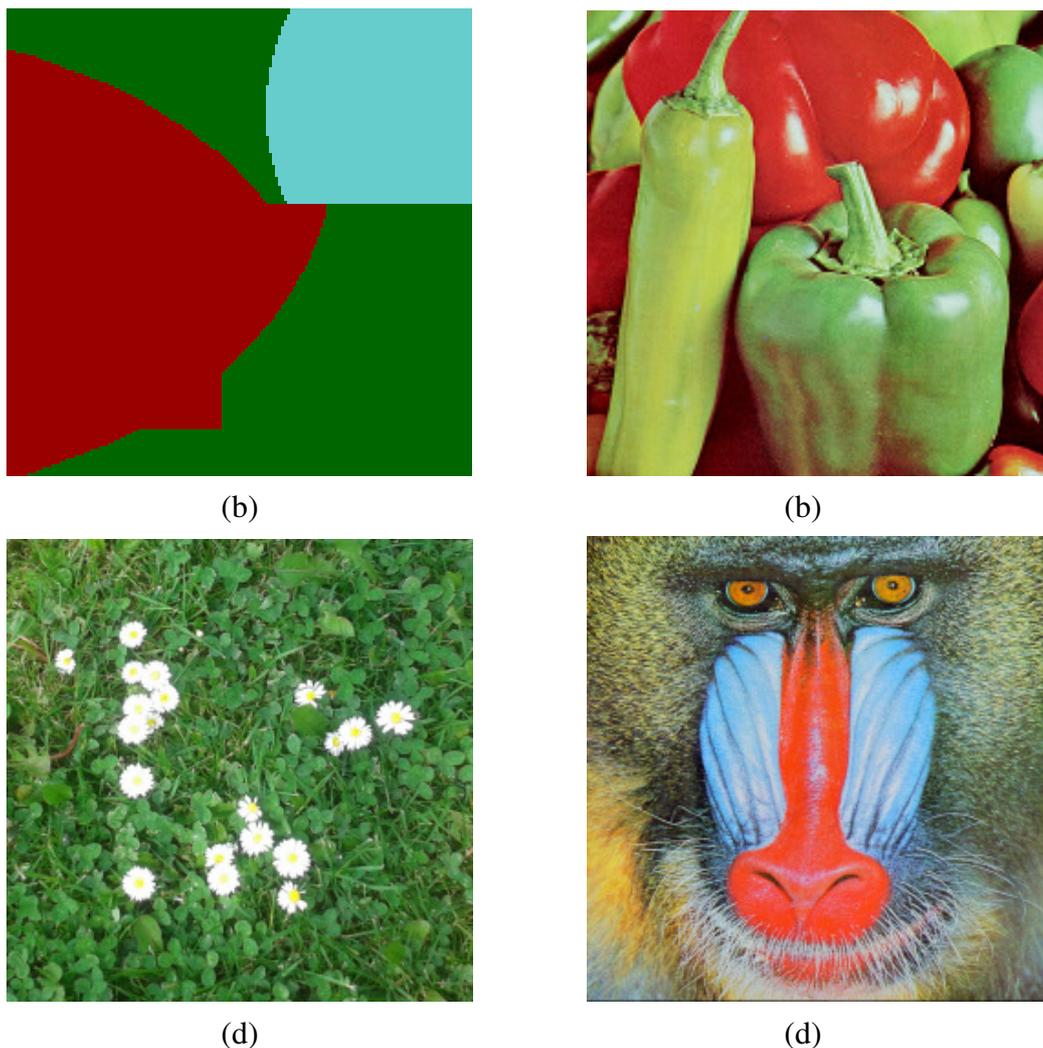
Figure 5.3. Test images: (a) synthetic image, and natural images of (b) peppers, (c) flowers and (d) Mandrill.

5.6.2 Results of basic morphological operations

The results of morphological operations on each image performed in RGB colour space are presented. Fig. 5.4 (b) shows the result of similarity-based dilation, in which the dark green region increases in size because the dark green colour is close to the foreground colour, which is pure green, (0, 255, 0) in the RGB representation.

(a)   (b)   (c)
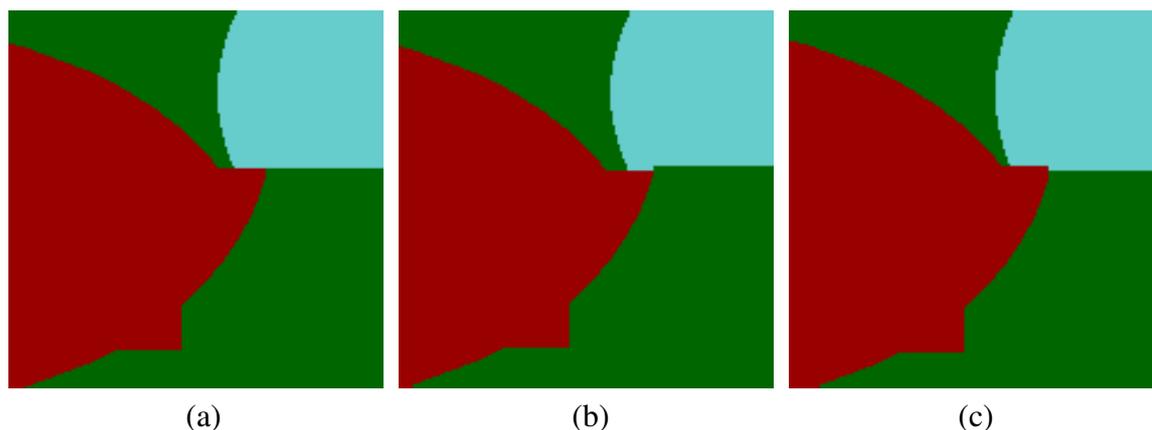
Figure 5.4. Synthetic image: (a) original image and the result after (b) green dilation and (c) green erosion.

This is commonly referred to as green dilation. The chromatic similarity between the dark green and the pure red is 1 using Eq. (5.9), therefore, dark green is more similar to the foreground using Eq. (5.17), than the other colours. Conversely, the green erosion is shown in Fig. 5.4 (c) and the dark green region is decreased in size. Our proposed orderings had similar results to the equivalent basic morphological operations for synthetic and natural images in the RGB and L*a*b* colour spaces; Further results for the L*a*b* colour space and images are shown in Appendix A.3.

The images of Fig. 5.5 show the result of dilation and erosion in enlarged patches of the peppers image, for the similarity-based method. The result of dilation shown in Fig. 5.5 (b) is that the green region is increased in size, compared to the original image whilst the result of erosion, shown in Fig. 5.5 (c) is that the green region is reduced in size and the regions in colours far from green (e.g. red) are enlarged.

Additionally, the results of dilation, erosion, opening, and residue operators where the reference colour is red (255, 0, 0) as shown in Fig. 5.6 and Fig. 5.7. The original results of top-hat transformation were difficult to be observed. Therefore, an equalisation was applied after the two top-hat transforms, as shown in Fig. 5.6 (g), Fig. 5.6 (h), Fig. 5.7 (g) and Fig. 5.7 (h). As can be seen in Fig. 5.6 (f) and Fig. 5.7 (f), only some of the boundaries surrounding the near red region are visible due to the selection of the reference colour red (255, 0, 0).

(a) (b) (c)
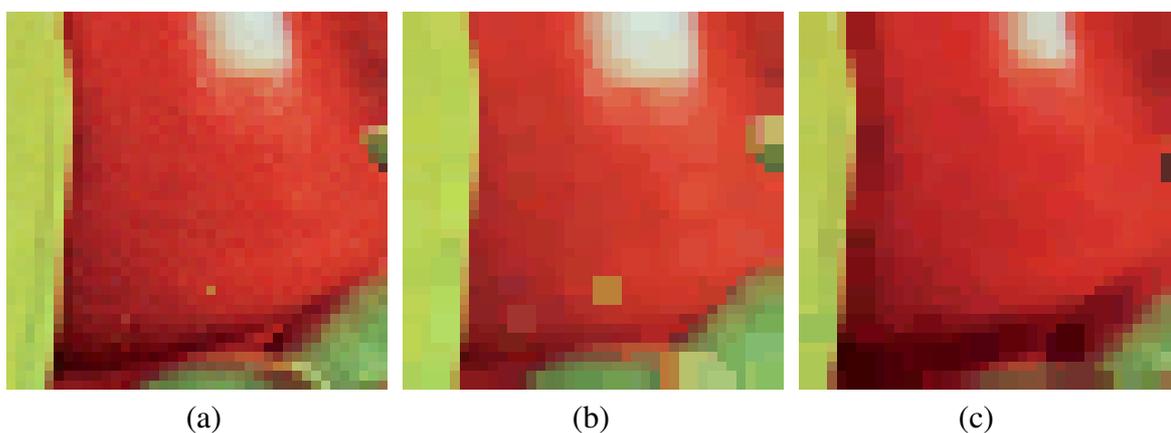
Figure 5.5. The evaluation of similarity based erosion and dilation (a) Enlarged patch from the original image of peppers and the result after (b) dilation and (c) erosion each with respect to green.
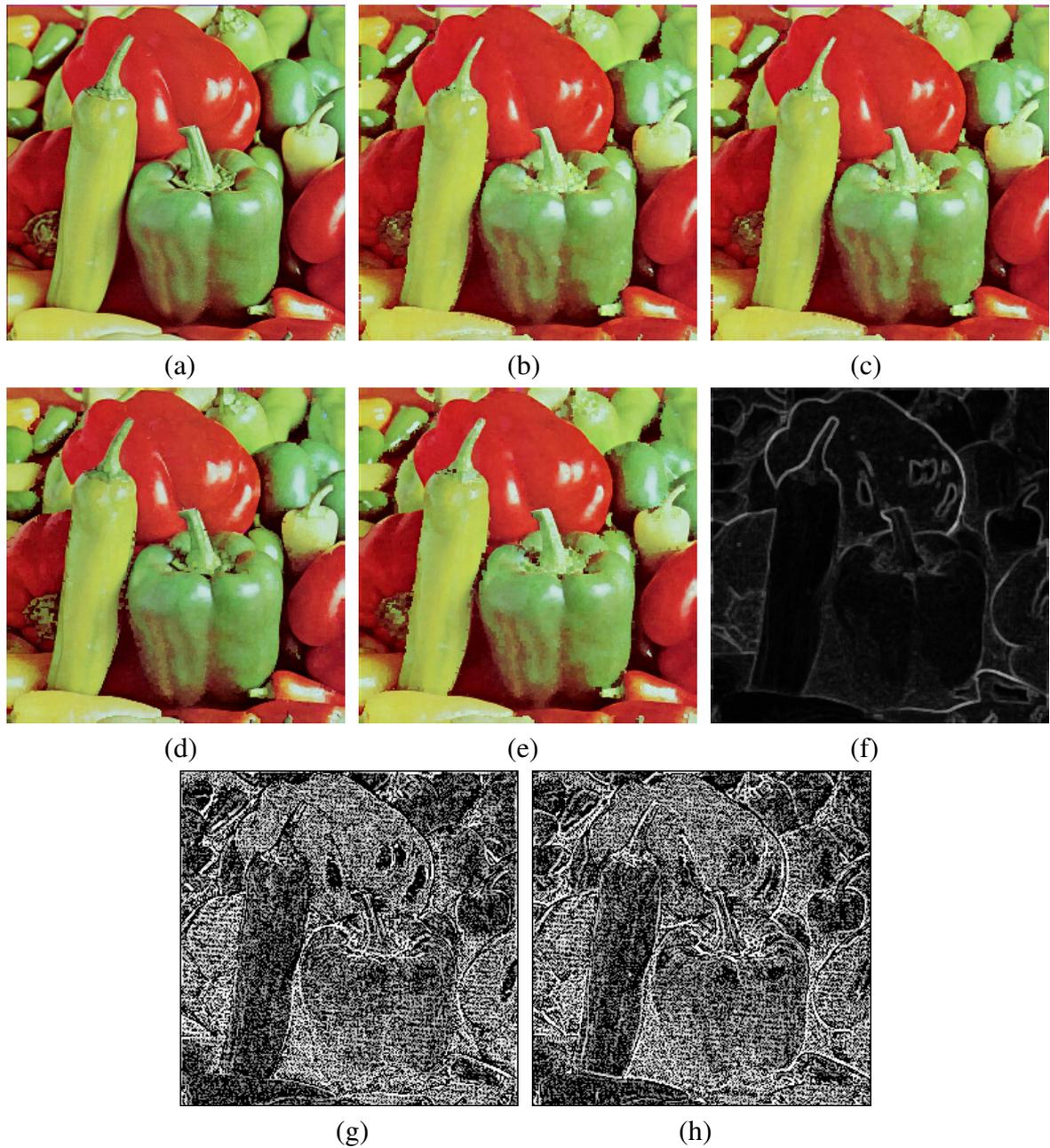
Figure 5.6. Result of applying morphologic operators to a natural image (a) original image of peppers. Result after (b) dilation, (c) erosion, (d) opening, (e) closing, (f) gradient (g) positive top-hat transform after equalisation and (h) negative top-hat transform after equalisation, each with respect to red.
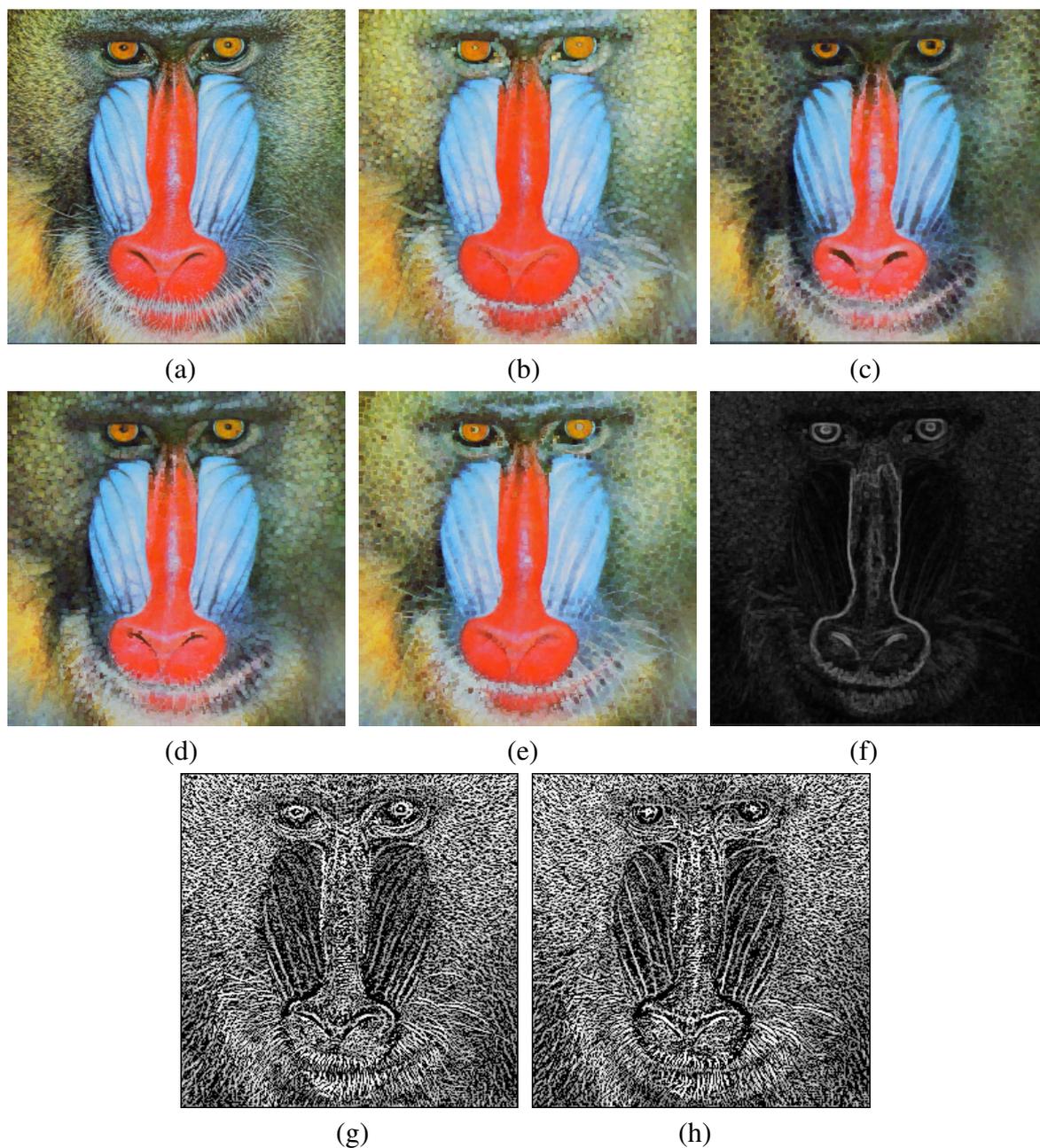
Figure 5.7. Result of applying morphologic operators to a natural image. (a) Original image of a Mandrill. Result after (b) dilation, (c) erosion, (d) opening, (e) closing, (f) gradient (g) positive top-hat transformation after equalisation and (h) negative top-hat transformation after equalisation each with respect to red.

5.6.3 Results of Hit-or-Miss transform

Figure 5.8 shows an image, **I,** composed of two patterns each having zero mean Gaussian

noise with a variance of, $\sigma = 10$ and $\sigma = 30$, respectively, separately added to each colour

channel using the Box-Muller algorithm [BOX58]. Using the "robust" SHMT and $SHMT_\eta$, as

defined in Eq. (5.20), to image **I,** with the structure element, $\mathbf{S}_m$, in the original images and

those corrupted with noise at a range of values for the threshold, η. The use of the structure
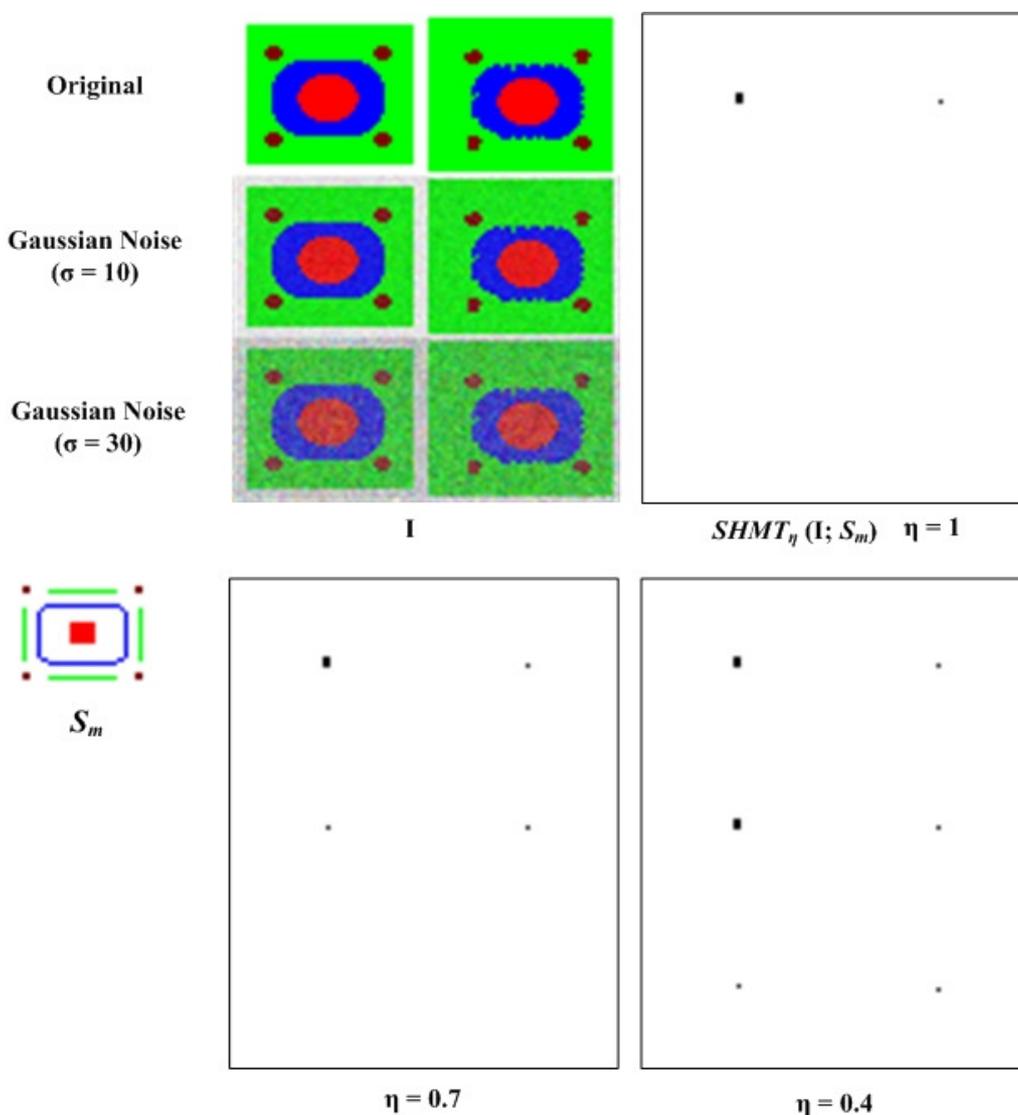
Figure 5.8. Recognition of object with Gaussian noise using $SHMT_\eta$

element, $\mathbf{S}_m$, can detect the presence of the shape when it is distorted by image noise or artefacts, as shown in Fig. 5.8, the target is detected by the $SHMT_\eta$ transform when the matching threshold, η is reduced to 0.4 but not at values of 0.7 and 1.0 depending on the level of Gaussian noise added. In Fig 5.8 the level of noise added is a standard deviation of $\sigma = 30$. The original SHMT ($SHMT_\eta$ with $\eta = 1$) failed to detect objects when the synthetic shapes contains any level of Gaussian noise.

The results for the $SHMT_\eta$ transform when applied to images in the L*a*b* space are similar and shown in the appendix. The $SHMT_\eta$ operator was also evaluated on the natural image of Fig 5.3 (c) with a modified structure element and the results are shown in Fig. 5.9. The modified structure element was generated by manually extracting the medial axis of the structure element. The detected positions are highlighted by the patches in Fig 5.9 (b) and (e) - (h) for values of η of (0.8, 0.7, 0.6, 0.5 and 0.4) respectively. The flowers not detected in Fig. 5.9 (h) when η was decreased to 0.4 are damaged and not representative of the normal appearance of the flower head, as describe by the structure element. The format of the structure element was extracted from another similar image of the same flowers.

(a)   (b)   (c)   (d)

(e)   (f)

(g)   (h)

Figure 5.9. SHMT_η for "Flowers" image: (a) original image, (c) the structure element and (d) the modified structure element, and the results using SHMT_η with (b) $\eta = 0.8$, (e) $\eta = 0.7$, (f) $\eta = 0.6$, (g) $\eta = 0.5$ and (h) $\eta = 0.4$.

5.6.4 Discussion

5.6.4.1 Basic morphological operations

The region that shrinks and grows under erosion or dilation is determined by the reference colour of the structure element as illustrated in Fig. 5.5, Fig. 5.6 and Fig. 5.7. This behaviour follows the same pattern as that described for Fig. 5.4. The gradient response was also strongly influenced by the choice of reference colour, as shown in Fig. 5.6 (f) and Fig. 5.7 (f). The gradient around the region containing the reference colour is clearly shown according to the prior knowledge for similarity-based morphology

5.6.4.2 Hit-or-Miss Transform

The SHMT was designed to operate in a noise free environment, but it can be improved to better handle imprecisely defined or variable shapes by using a skeletal form of structure element, as described elsewhere for binary images [ZHA91]. A "robust" version of the SHMT, $SHMT_\eta$, can be considered to better accommodate images with added Gaussian noise, artefacts and variations of form. A range of the thresholds, η, were used to evaluate the potential "robustness" of the $SHMT_\eta$. The design of the structure element and the selection of the threshold for the $SHMT_\eta$ is not easy for natural images.

5.7 Summary

In this chapter, we have introduced a consistent theoretical basis for binary, grey-level and colour morphology using similarity. This defined a total ordering which causes the similarity-based colour morphological operations being useful when the prior knowledge is well-known. A preliminary performance evaluation was reported for dilation, erosion, opening, closing, residue-based operators and HMT using synthetic and natural images. The similarity-based HMT gives an appropriate, promising, result with non-flat structure elements in complete lattices for the synthetic and flowers images as shown in Fig. 5.8 and Fig. 5.9, respectively. The proposed orderings gave similar results for the basic morphological operators and the SHMT in RGB and L*a*b* colour spaces. There is a need to investigate a way simplifying the design and structure elements for SHMT automatically. There is also a need to further consider how to accommodate approximate matches with structure elements.

Chapter 6: Comparison of Difference-based and Similarity-based Colour Orderings

This chapter evaluated the performance of the morphological operations under the proposed difference-based ordering and the similarity-based ordering. The aim is to observe the behaviours of these two different orderings, including context-independent method and context-dependent method with different reference colours.

6.1 Noise Model and Image Design

Natural images were used to evaluate colour erosion, dilation, residue operators and other filters using a 3 x 3 structure element. When a transformation from RGB to L*a*b* colour space was performed the maximum, a white reference was used.

The test images used in Chapters 4 and 5 are shown in Fig. 6.1. The images were chosen for
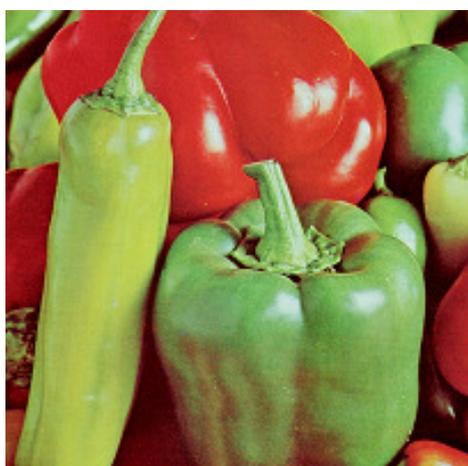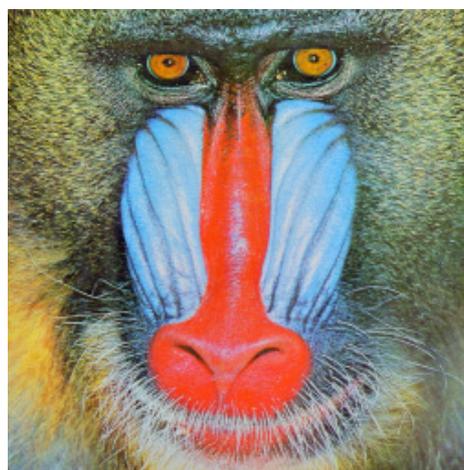
(a)   (b)

Figure 6.1. Test images: natural images of (a) peppers and (b) Mandrill.

consistency. A range of salt-and-pepper impulse noise levels ranging from 0 to 60% of pixels were used. Following the rules in Section 4.6.1, salt-and-pepper impulse noise was similarly added to the natural test images

6.2 Comparison of Basic Morphological Operations

Fig. 6.2 and Fig. 6.3 show the different results of dilation for natural images. The results for dilation in Fig. 6.2 (a) show that the red region increased in size compared to the original image whilst Fig. 6.2 (b) show that green regions are enlarged in size. In particular, the white highlight surrounded by the red region is increased in size and the green region surrounding a white highlight both shrank after dilation. However, the results for dilation in Fig. 6.3 (a) show that the red region increased in size compared to the original image whilst Fig. 6.3 (b) show that the white regions were enlarged in size. In particular, the green highlight between the eye and nose is increased in size in both Figs. 6.3 (a) and (b).

A closer inspection of the pepper images of Fig. 6.4 reveals that after erosion the edges of the long yellow pepper take on a serrated appearance in Fig 6.4 (a) and smooth in Fig. 6.4 (b). The results for erosion in Fig. 6.5 (a) show that the red regions decreased in size compared to the original image whilst Fig. 6.5 (b) show that red regions are enlarged in size.

(a)

(b)

(c)

(d)
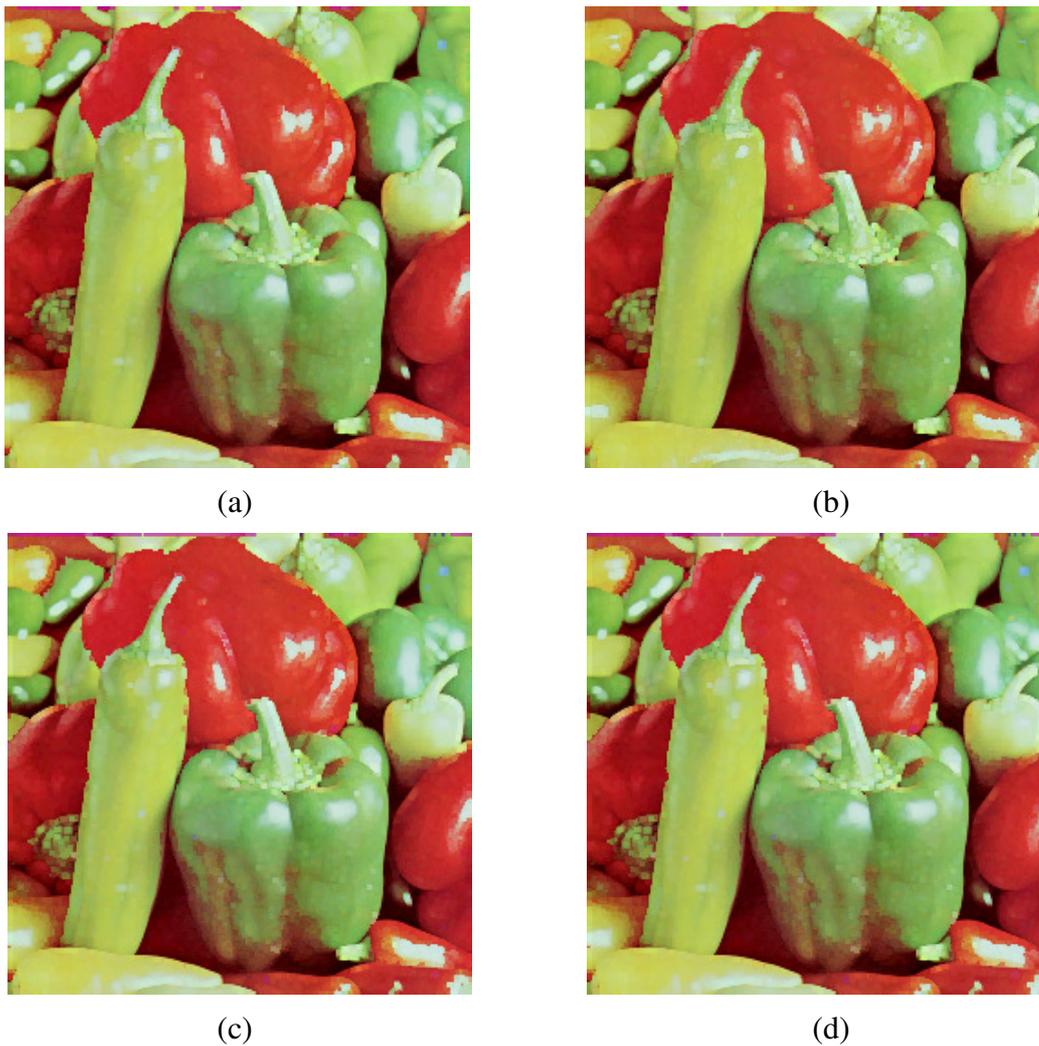
Figure 6.2. Colour dilation for "Pepper" image using (a) the difference-based ordering in L*a*b* colour space and the similarity-based ordering with a reference colour, (b) pure green for (0, 255, 0), (c) pure red for (255, 0, 0) and (d) pure blue for (0, 0, 255) in RGB colour space.
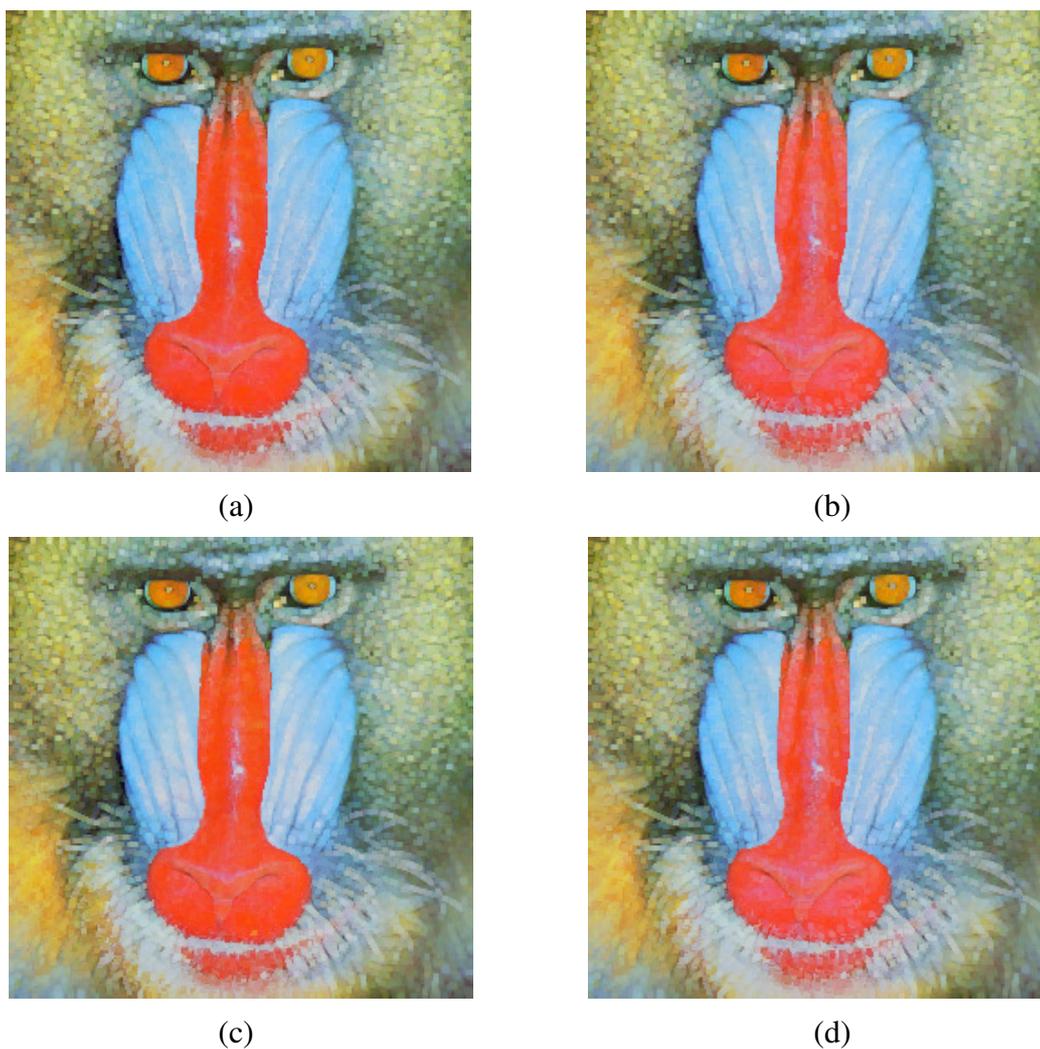
Figure 6.3. Colour dilation for "Mandrill" image using (a) the difference-based ordering in L*a*b* colour space and the similarity-based ordering with a reference colour, (b) pure green for (0, 255, 0), (c) pure red for (255, 0, 0) and (d) pure blue for (0, 0, 255) in RGB colour space.

(a)

(b)

(c)

(d)
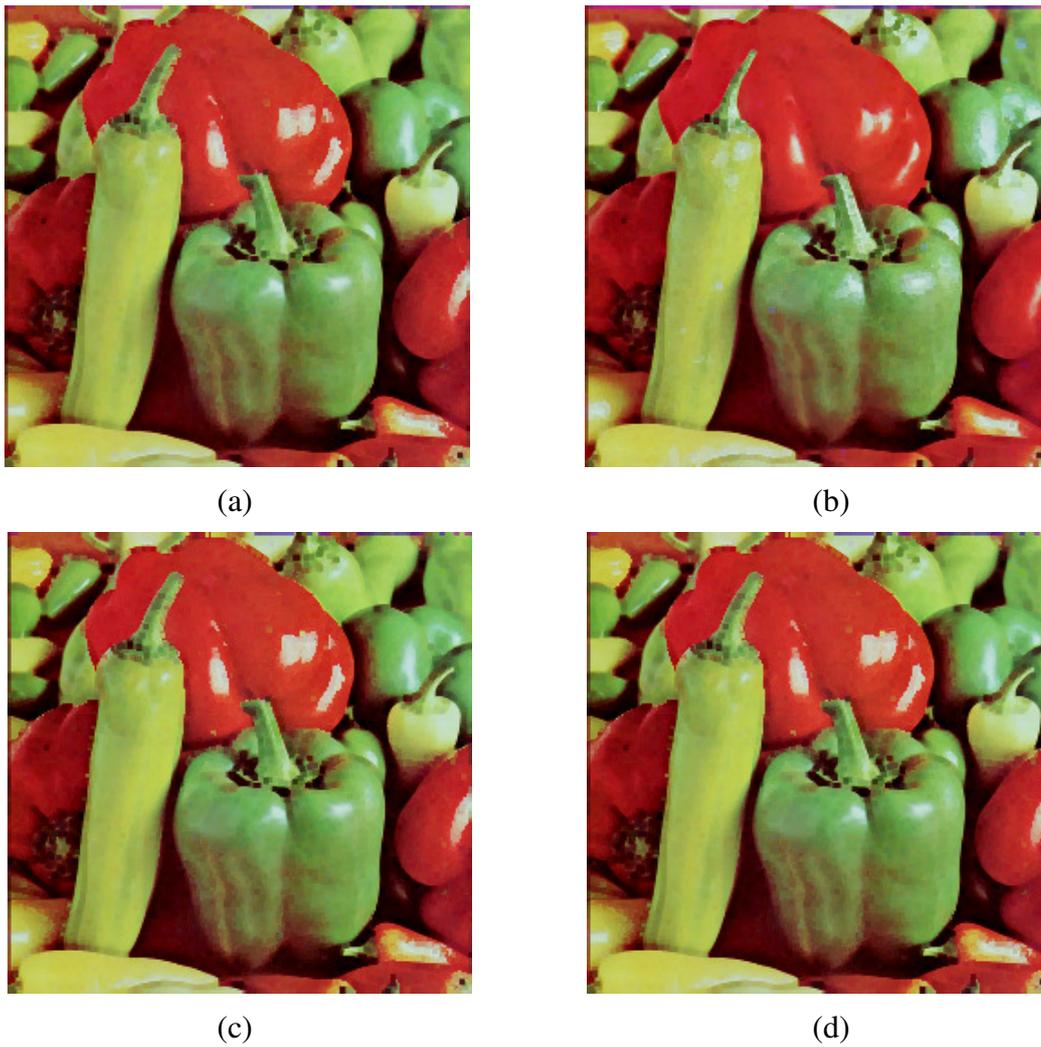
Figure 6.4. Colour erosion for "Pepper" image using (a) the difference-based ordering in L*a*b* colour space and the similarity-based ordering with a reference colour, (b) pure green for (0, 255, 0), (c) pure red for (255, 0, 0) and (d) pure blue for (0, 0, 255) in RGB colour space.

(a)

(b)

(c)

(d)
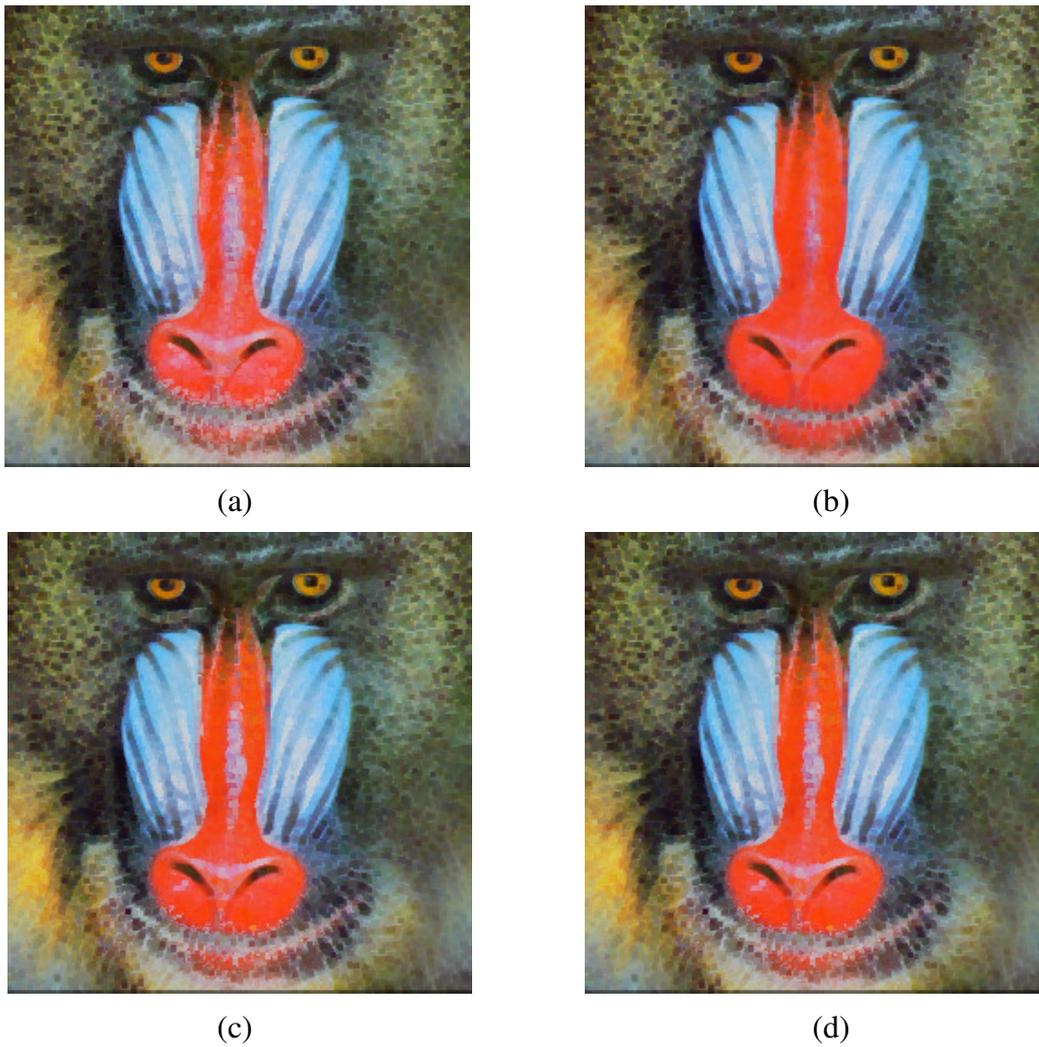
Figure 6.5. Colour erosion for "Mandrill" image using (a) the difference-based ordering in L*a*b* colour space and the similarity-based ordering with a reference colour, (b) pure green for (0, 255, 0), (c) pure red for (255, 0, 0) and (d) pure blue for (0, 0, 255) in RGB colour space.

6.3 Comparison in Salt and Pepper Noise Reduction

Following Section 4.6.3 we used the normalised mean squared error (NMSE) as a measure of residual noise. To compare the proposed orderings for salt and pepper noise removal in colour, the opening followed by closing (OC) filter was considered in this experiment. The similarity-based ordering is similar to Angulo's method when doing OC filter because they both need reference colours. The complete comparison of Angulo's method has been done in Chapter 4 by using multiple images. Hence, only a single image was used to evaluate the performance of the two different orderings proposed. This might be enough to show the behaviours of them.

In Fig. 6.6 a lower NMSE value represents better noise removal. The difference-based ordering in CIE L*a*b* colour spaces outperforms the similarity-based orderings in the RGB colour space with reference colours in red, green and blue, at all levels of added noise (from 5% to 60% of overall impulse noise). Additionally, for noise suppression the result obtained using the similarity-based ordering with reference blue is slightly and significantly better than that that obtained with reference red and reference green, respectively. With reference blue, the performance of the similarity-based ordering is close to that of the difference-based ordering at relatively low overall impulse noise levels of 5% to 20% and high 60%.

Fig. 6.7 shows a natural image with 40% of overall impulse noise and the result after opening followed by closing (OC) under the difference-based ordering and similarity-based orderings. With similarity-based ordering large areas of image corruption remain and the impact of the added noise is extended, especially with reference red and reference green. The difference-based ordering performs significant better. The difference-based ordering here reduces the number of corrupted pixels and is more effective at limiting the spatial spread of this corruption.
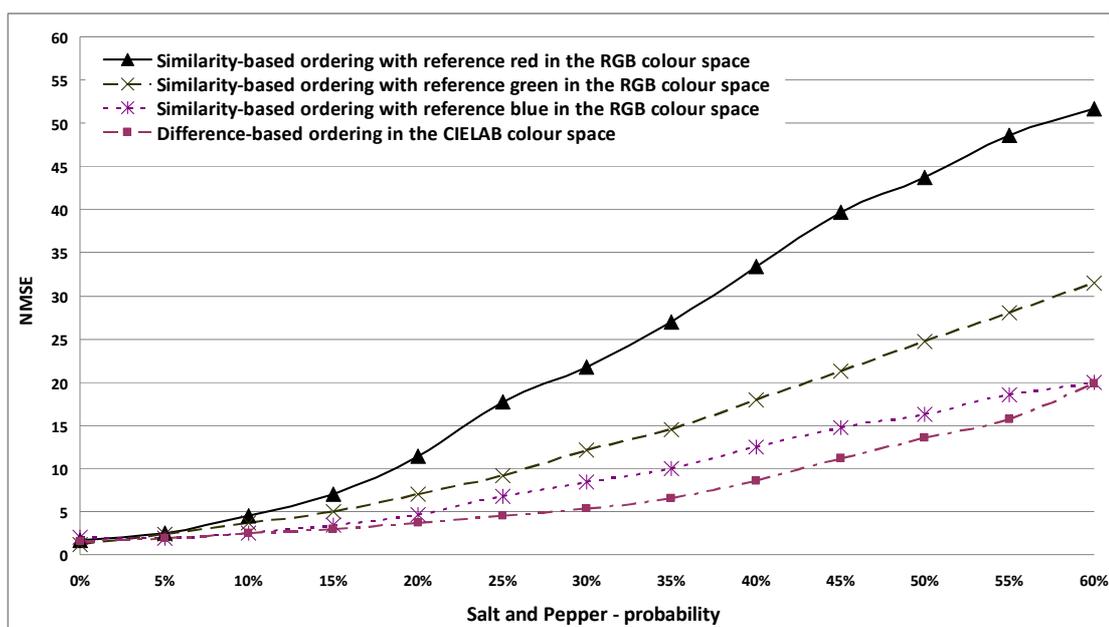
Figure 6.6. Impulse noise reduction using OC filter and the proposed ordering schemes.
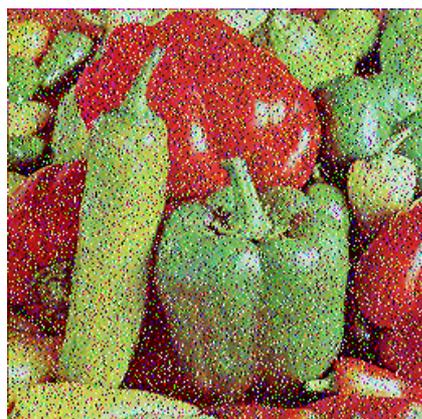
(a) Noisy image
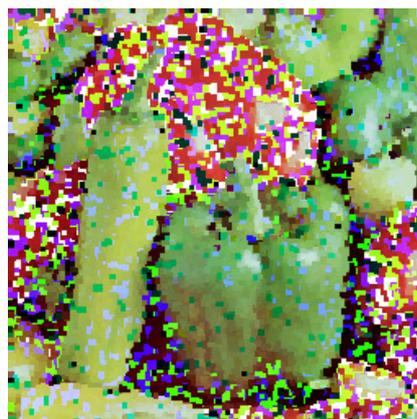
(b) NMSE = 33.418

(c) NMSE = 17.92

(d) NMSE = 12.474

(e) NMSE = 8.581

Figure 6.7. (a) Original image with 40% salt and pepper noise added. The result of noise reduction using, an OC filter with (b) similarity-based ordering (reference red), (c) similarity-based ordering (reference green), (d) similarity-based ordering (reference blue), (e) the difference-based ordering in L*a*b* colour space.

6.4 Discussion

In this section, we presented the experimental results and discussed how the proposed colour

ordering schemes influence the performance of basic colour morphological operations and

more sophisticated operations of the OC filter as used for noise reduction.

The difference-based and similarity-based ordering schemes both produced no artefacts in

dilation or erosion for colour images. The similarity-based ordering scheme needs a reference

colour to define the foreground for colour morphology. This suits applications where prior

knowledge can be used to identify suitable reference colours, and it is valuable for hit-or-miss

transform in colour as discussed in Chapter 5.

The difference-based ordering scheme performs well in the suppression of impulse noise

because the colour extrema adopted are generic and not context related. But in the

similarity-based orderings, prior knowledge is needed to select a suitable reference colour for

salt and pepper noise removal, as shown in Fig. 6.7. The performance with reference red is the

worst because there are many pure red regions in the original pepper image. This caused the

noiseless red regions to be removed by opening because they were regarded as part of impulse

noise with high similarity scores. As can be seen, with a reference colour of blue the similarity

method performed better than the other reference colours because there are few blue regions

in the original image. Hence, the added impulse noise gave higher similarity scores than the

noiseless parts, and they were removed using opening followed by closing.

Chapter 7: Conclusions and Future Work

7.1 Conclusion

We have studied colour orderings and their relationship with mathematical morphology for the analysis of colour images for noise reduction, edge enhancement and non-linear template matching. The contribution of this thesis is to define colour extrema and to demonstrate the importance of this for mathematical morphology. The concept of colour extrema has been used to develop the mathematical morphology operators based on colour difference and similarity in RGB, HSV and L*a*b* colour spaces. These two principled methods harmonise the definition of binary, grey-level and colour mathematical morphology.

The definition of colour extrema is inspired by the colour correction model [HEO11]. The main contributions of this work include:

- The generalisation of classical morphological operators to colour with a novel use of the concept of colour extrema.

- A colour version of conditional toggle mapping has been developed and evaluated for the removal of salt-and-pepper noise and edge enhancement.

- Several colour orderings from the literature were compared with those proposed in this

Thesis to demonstrate the benefits of the colour orderings proposed here for mathematical morphology.

■ A similarity-based hit-or-miss transform (SHMT) for colour images, that supports non-linear template matching is presented and shown to be promising as a method for identifying objects in natural colour images.

7.2 Suggestions for Future Work

The outstanding issue regarding the SHMT is how to automatically select the best comparison threshold, η, and how to design the structure element as a flexible template by using colour skeletonisation or adopting a statistical definition of the structure element. Further evaluation of the proposed method using practical applications and alternative ways of defining the structure elements is needed.

Finally, there is a need in investigating the extension of the proposed methods of mathematical morphology to multi-dimensional images that are encountered in remote sensing and medical imaging. The challenge is to define extrema in a higher dimensional space and a consideration of how the physical characteristics of the multi-dimension data capture device might influence the definition of extrema.

It would also be valuable to study the extension of colour morphology to skeletonisation and watershed segmentation in colour. The applications of tree canopies counting and image segmentation can be further evaluated through the development of the colour hit-or-miss transform, colour skeletonisation and colour watershed algorithms. At present, Lewis [LEW14] reported to count tree canopies in grey-level and colour images and adopted a part of our proposed works in colour. His report shows the potential for counting tree canopies by using mathematical morphology. However, the evaluation was not sufficient extensive to show that the method is significantly better than other reported methods or manual counting.

More work is needed. This would require fundamental questions regarding the nature of colour skeletonisation and the watershed algorithms will need to be addressed in any further studies. There are also special issues to be considered for high dimensionality, multi-spectral images or data sets. The existing ambiguities in the definition of skeletonisation for binary and grey-level images shows that there are many issues to be addressed in extending skeletonisation to colour images. The key issue is to determine what a colour skeleton should be and how it differs from a colour thinning or a colour medial axis. These terms of skeletonisation, thinning and medial axis were used in an ambiguous manner in the literature. The medial axis is the set of points and the maximal disks at that point need to reconstruct a region. A thinning is a set of points that characterizes the shape of an object without retaining

the connectivity of the object. A skeleton is a minimal set of points that preserves the

connectivity of the object. Therefore, more work is needed to investigate them in colour.

References

[AL003]   H. Al-Otum, "Morphological operators for color image processing based on Mahalanobis distance measure", *SPIE Optical Eng*, 42(9):2595-2606, 2003.

[ANG05]   J. Angulo, "Unified morphological color processing framework in a lum/sat/hue representation", *In Proc. of the International Symposium on Mathematical Morphology 2005,* 387-396, 2005.

[ANG07a] J. Angulo, "Morphological colour operators in totally ordered lattices based on distances: application to image filtering, enhancement and analysis", *Computer Vision and Image Understanding*, 107: 56-73, 2007.

[ANG07b] J. Angulo and J. Serra, "Modelling and segmentation of colour images in polar representation", *Im. Vis. Comp*, 25:475-495, 2007.

[APT07]   E. Aptoula, and S. Lefevre, "A comparative study on multivatiate mathematical morphology", *Pat. Recogn*, 40:2914-2929, 2007.

[APT08]   E. Aptoula, and S. Lefevre, "On lexicographical ordering in multivariate mathematical morphology", *Pat. Recogn. Lett.*, 29:109-118, 2008.

[APT09a] E. Aptoula, S. Lefevre, "On the morphological processing of hue", *Im. Vis. Comp*, 27(9):1394-1401, 2009.

[APT09b] E. Aptoula, S. Lefevre and C. Ronse, "A Hit-or-Miss transform for multivariate images", *Patt. Recog. Lett.*, 30:760-764, 2009.

[BAR76]   V. Barnett, "The ordering of multivariate data", *J. Stat. Soc. A*, 139:318-355, 1976.

[BON00]   C. Boncelet, "Image noise models", *Handbook of Image and Video Processing*, Academic Press, New York, 325-335, 2000.

[BOX58]   G. E. P. Box and M. E. Muller, "A note on the generation of random normal deviates", *Annals of Mathematical Statistics*, 29:610-611, 1958.

[BUR13]   B. Burgeth and A. Kleefeld, "Morphology for color images via Lowener order for matrix fields", *Lecture Notes in Computer Science*, 7883:243-254, 2013.

[CAL13]   A. Caliman, M. Ivanovici, N. Richard and G. Toacse, "A multivariate mathematical morphology based on orthogonal transformation, probabilistic extrema estimation and distance optimization", *Lecture Notes in Computer Science*, 7883:255-266, 2013.

[CHE03]   S. C. Cheng and S. C. Hsia, "Fast algorithm for color image processing by principal component analysis", *J. Visual Comm. & Im. Rep*, 14:184-203, 2003.

[COM99]   M. Comer and E. Delp, "Morphological operations for color image processing", *J. Elec. Imag*, 8(3):279-289, 1999.

[FIN01]   G. D. Finlayson, S. D. Hordley and P. M. Hubel, "Color by correlation: a simple, unifying framework for color constancy", *IEEE Trans. on Pattern Analysis and Machine Intelligence*, 23:1209-1221, 2001.

[FIN03]   G. D. Finlayson and R. Xu, "Illuminant and gamma comprehensive normalisation in Log RGB space", *Patt. Recog. Lett.*, 24:1679-1690, 2003.

[FIN98]   G. D. Finlayson, B. Schiele and J. L. Crowley, "Comprehensive colour image normalization", *Lecture Notes in Computer Science*, 1406:475-490, 1998.

[GAR09]   A. Garcia and C. Vachier, "Simplification of color images using semi-flat morphological operators and statistical metrics", *In Proc. of the International Conference on Image Processing 2009*, 469-472, 2009.

[GIB03]   S. Gibson, R. Harvey and J. A. Bangham, "Evaluating colour morphological scale-spaces", *In Proc. of the 14th British Machine Vision Conference*, 799-808, 2003.

[GOU95]   J. Goutsias, H. Heijmans and K. Sivakumar, "Morphological operators for image sequences", *Computer Vision and Image Understanding*, 62:326-346, 1995.

[GRU07]   M. Grundland and N. A. Dodgson, "Decolorize: Fast, contrast enhancing, color to greyscale conversion", *Pat. Recogn.*, 40:2891-2896, 2007.

[HAN01a] A. G. Hanbury and J. Serra, "Mathematical morphology in the HLS colour space", *In Proc. of the 12th British Machine Vision Conference*, 451-460, 2001.

[HAN01b] A. G. Hanbury and J. Serra, "Morphological operators on the unit circle", *IEEE Trans. on Image Processing*, 10:1842-1850, 2001.

[HAN02] A. Hanbury and J. Serra, "Mathematical morphology in the CIELAB Space", *Image Anal. Stereology*, 21:201-206, 2002.

[HEI90] H. J. A. M. Heijmans and C. Ronse, "The algebraic basis of mathematical morphology. i. dilations and erosion", *Computer Vision, Graphics, and Image Processing*, 50:245-295, 1990.

[HEI91] H. Heijmans, "Theoretical aspects of gray-level morphology", *IEEE Trans. on Pattern Analysis and Machine Intelligence*, 13:568-582, 1991.

[HEI95] H. J. A. M. Heijmans, "Mathematical morphology: A modern approach in image processing based on algebra and geometry", *Society for Industrial and Applied Mathematics Review*, 37(1):1-36, 1995.

[HEO11] Y. S. Heo, K. M. Lee and S. U. Lee, "Robust stereo matching using adaptive normalized cross-correlation", *IEEE Trans. on Pattern Analysis and Machine Intelligence*, 33(4):807-821, 2011.

[JOC97] T. Jochems, "Morphologie mathematique appliqué au controle industriel de pieces coulees", *PhD Thesis*, Ecole National Superieure des Mines de Paris, 1997.

[KRA75] H. P. Kramer and J. B. Bruckner, "Iterations of a non-linear transformation for enhancement of digital images", *Pat. Recogn.*, 7:53-58, 1975.

[LED12] A. Ledoux, N. Richard and A. S. Capelle-Laize, "Color Hit-or-Miss transform", *In Proc. 20th European Sig. Proc. Conf.*, 2248-2252, 2012.

[LEW14] C. Lewis, "Mathematical morphology and computer vision for the quantification of tree canopies", *MEng Final Year Project*, University of Birmingham, Birmingham, 2014.

[LEZ07]   O. Lezoray, A. Elmoataz and C. Meurie, "Mathematical morphology in any color space", *In Proc. of the 14th International Conference of Image Analysis and Processing*, 183-187, 2007.

[LEZ09]   O. Lezoray, C. Charrier and A. Elmoataz, "Learning complete lattices for manifold mathematical morphology", *In Proc. of the International Symposium on Mathematical Morphology 2009*, 1-4, 2009.

[LI04]   J. Li and Y. Li, "Multivariate mathematical morphology based on principal component analysis: initial results in building extraction", *International Archives for Photogrammetry, Remote Sensing and Spatial Information Sciences*, 35:1168-1173, 2004.

[LOU02]   G. Louverdis, M. I. Vardavoulia, I. Andreadis and P. Tsalides, "A new approach to morphological color image processing", *Pat. Recogn*, 35:1733-1741, 2002.

[MAT75]   G. Matheron, *Random Sets and Integral Geometry*, John Wiley & Sons, New York, 1975.

[MEY89]   F. Meyer and J. Serra "Contrasts and activity lattice", *Sig Proc*, 16:303-317, 1989.

[NAE07]   B. Naegel and N. Passat, "Grey-level hit-or-miss transforms – part 1: unified theory", *Patt. Recog.*, 40(2):635-647, 2007.

[NAJ10]   L. Najman and H. Talbot, *Mathematical Morphology*, ISTE Ltd, London, 2010.

[NAJ14]   L. Najman and J. Cousty, "A graph-based mathematical morphology reader", *Patt. Recog. Lett.*, 47:3-17, 2014.

[PET97]   R. A. Peters, "Mathematical morphology for angle-value images", *In Proc. of Nonlinear Image Processing SPIE*, 3026:84-94, 1997.

[PLA04]   A. Plaza, P. Martinez, R. Perez and J. Plaza, "A new approach to mixed pixel classification of hyperspectral imagery based on extended morphological profiles", *Pat. Recogn*, 37(6):1097-1116, 2004.

[RIV93]   J. F. Rivest, P. Soille and S. Beucher, "Morphological gradients", *J. Elec. Imag*,

2(4):326-336, 1993.

[ROM08]   R. Roman, *Lattices and Ordered Sets*, Springer, Heidelberg, 2008.

[RON06]   C. Ronse, "Flat morphology on power lattices", *J. Math. Imaging Vis.*, 26:185-216, 2006.

[RON90]   C. Ronse, "Why mathematical morphology needs complete lattices", *Signal Processing*, 10:129-154, 1990.

[SAL95]   P. Salembier and J. Serra, "Flat zones filtering, connected operators and filters by reconstruction", *IEEE Trans. on Image Processing*, 4:1153-1160, 1995.

[SAL98]   P. Salembier, A. Oliveras and L. Garrido, "Antiextensive connected operators for image and sequence processing", *IEEE Trans. on Image Processing*, 7(4):555-570, 1998.

[SAR01]   L. J. Sartor and A. R. Weeks, "Morphological operations on color images", *J. Elec. Imag*, 10:548-559, 2001.

[SCH00]   J. Schavemaker, M. J. T. Reinders, J. J. Gerbrands and E. Backer, "Image sharpening by morphological filtering", *Pat. Recogn.*, 33(6):997-1012, 2000.

[SER09]   J. Serra, "The "false colour" problem", *In Proc. of the International Symposium on Mathematical Morphology 2009*, 13-23, 2009.

[SER82]   J. Serra, *Image Analysis and Mathematical Morphology*, Vol. 1, Academic Press, London, 1982.

[SER88]   J. Serra, *Image Analysis and Mathematical Morphology*, Vol. 2, Academic Press, London, 1988.

[SER92]   J. Serra and L. Vincent "An overview of morphological filtering", *Circuits, System and Signal Processing*, 11(1):47-108, 1989.

[SHA03]   G. Sharma, *Digital Color Imaging Handbook*, CRC Press, New York, 2003.

[SOI02]   P. Soille and M. Pesaresi, "Advances in mathematical morphology applied to geoscience and remote sensing", *IEEE Trans. on Geoscience and Remote Sensing*, 40(9):2042-2055, 2002.

[SOI03]   P. Soille, *Morphological Image Analysis*, Speinger-Verlag, Heidelberg, 2003.

[STE87]   R. L. Stevenson and G. R. Arce. "Morphological filters: statistics and further syntactic", *IEEE Trans. on Circuits Systems*, 34:1292-1305, 1987.

[UMB10]   S. E. Umbaugh, *Digital Image Processing and Analysis: Human and Computer Vision Applications with CVIPtools*, Vol. 2, CRC Press, New York, 2010.

[VAN89]   L. Van-Vliet, I. Young and G. Beckers, "A nonlinear Laplace operator as edge detector in noisy images", *Computer Vision, Graphics, and Image Processing*, 45(2):167-195, 1989.

[VAR02]   I. A. M. I. Vardavoulia and P. Tsalides, "Vector ordering and morphological operations for colour image processing: fundamentals and applications", *Pattern Analysis and Applications*, 5:271-287, 2002.

[VEL10]   S. Velasco-Forero and J. Angulo, "Hit-or-miss transform in multivariate Images", *Lecture Notes in Computer Science*, 6474:452-463, 2010.

[VEL11]   S. Velasco-Forero, and J. Angulo, "Supervised ordering in R^p: application to morphological processing of hyperspectral images", *IEEE Trans. on Image Processing*, 20:3301-3308, 2011.

[VEL12]   S. Velasco-Forero and J. Angulo, "Random projection depth for multivariate mathematical morphology", *Journal of Selected Topics in Signal Processing*, 6(7):753-763, 2012.

[VEL14]   S. Velasco-Forero, J. Angulo and P. Soille, "Conditional toggle mapping: principles and applications", *J. Math. Imaging Vis.*, 48:544-565, 2014.

[ZHA91]   D. Zhao and D. G. Daut, "Morphological Hit-or-Miss transformation for shape recognition", *J. Vis. Comm. & Image Rep.*, 2(3):230-243, 1991.

[ZHO08]   H. Zhou and K. Z. Mao, "An impulsive noise color image filter using learning-based color morphological operations", *Dig Sig Proc*, 18:406-421, 2008.

Appendix

A.1 Comparison of basic morphological operations

This Section shows the results of dilation, erosion, opening and closing for a synthetic image and the natural images of the Flowers and the Mandrill using the orderings which were introduced in Section 4.
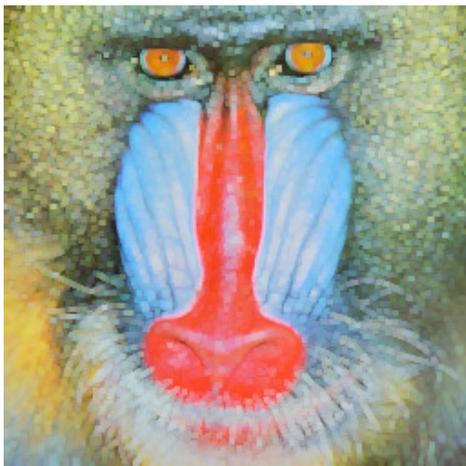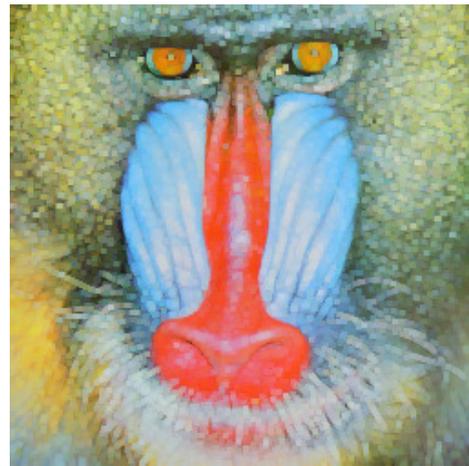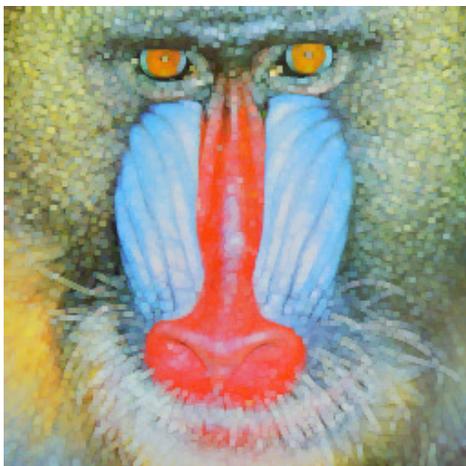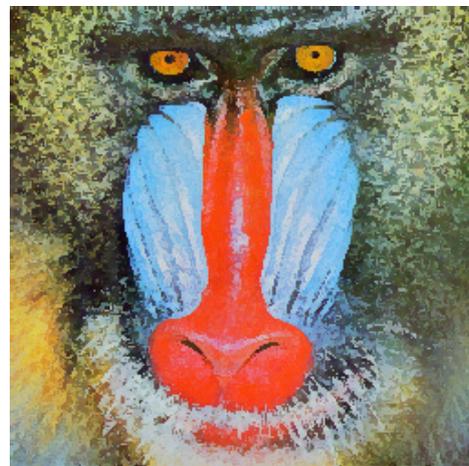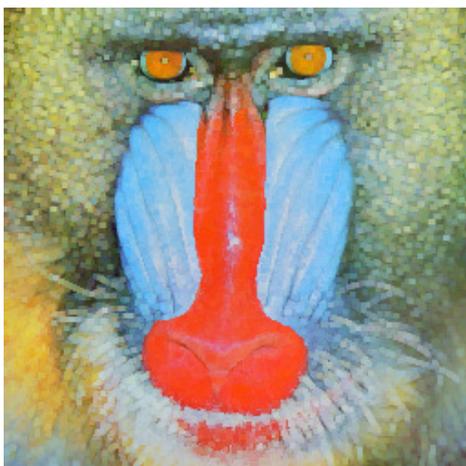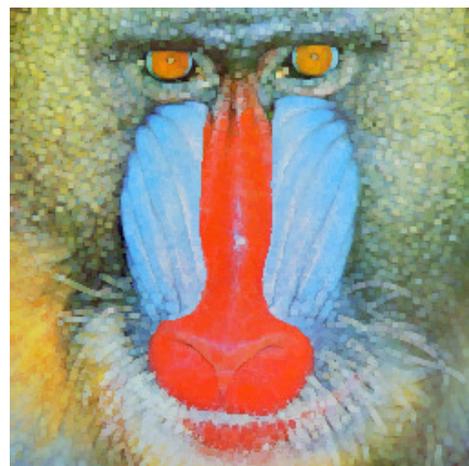
Figure. A.1. Colour dilation of "Mandrill" image using (a) marginal ordering, (b) conditional ordering, (c) Angulo's ordering, (d) Cheng's PCA-like ordering and the proposed ordering in (e) HSV and (f) L*a*b* colour spaces.
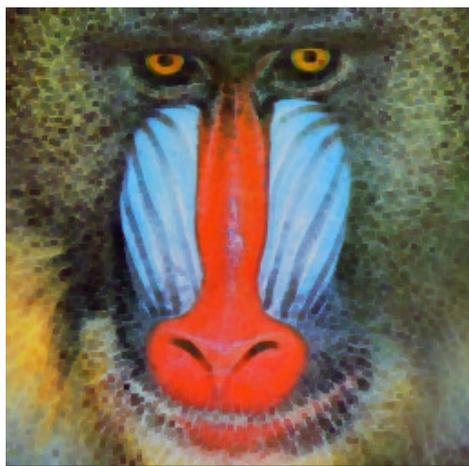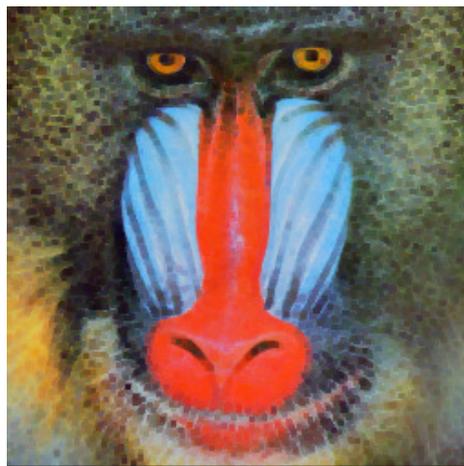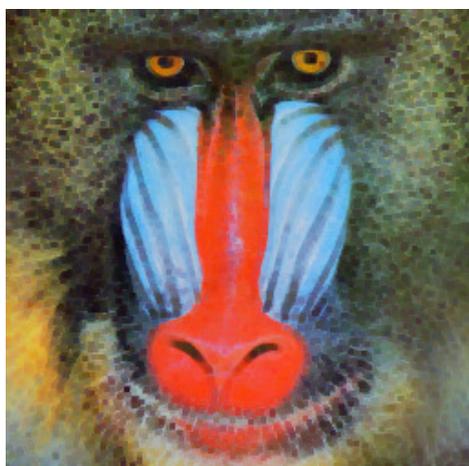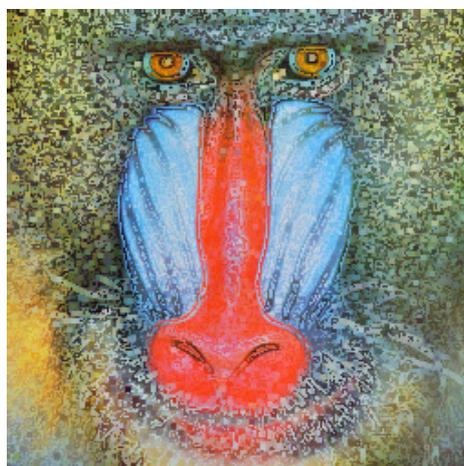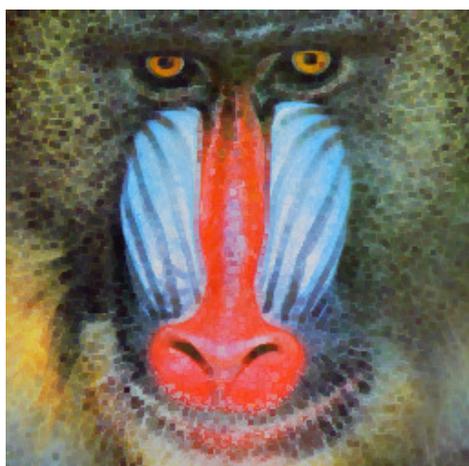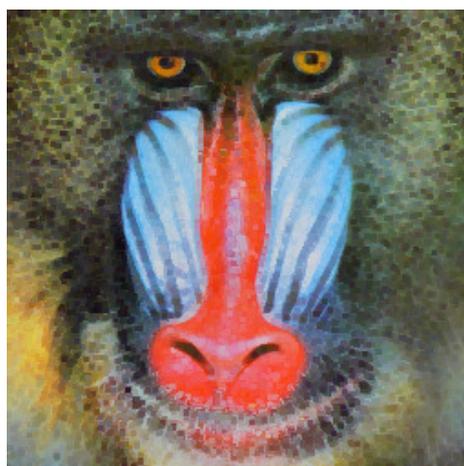
Figure. A.2. Colour erosion of "Mandrill" image using (a) marginal ordering, (b) conditional ordering, (c) Angulo's ordering, (d) Cheng's PCA-like ordering and the proposed ordering in (e) HSV and (f) L*a*b* colour spaces.
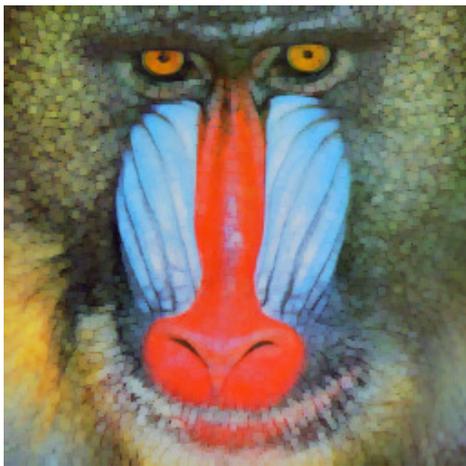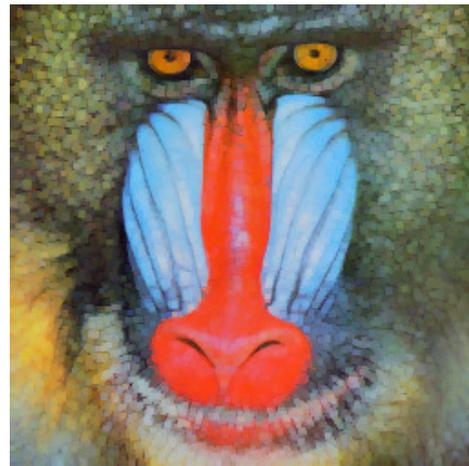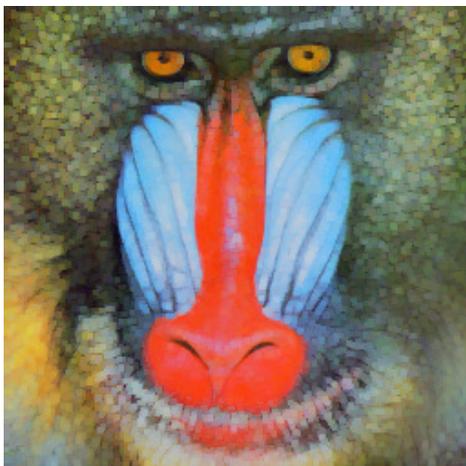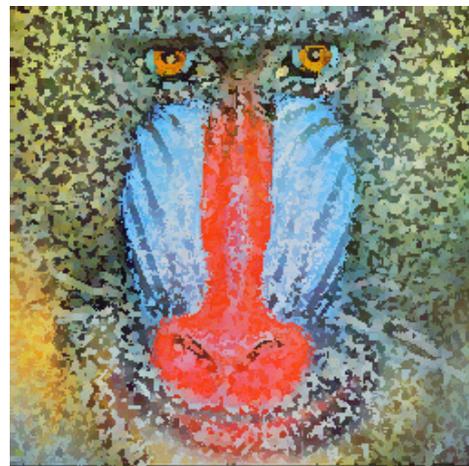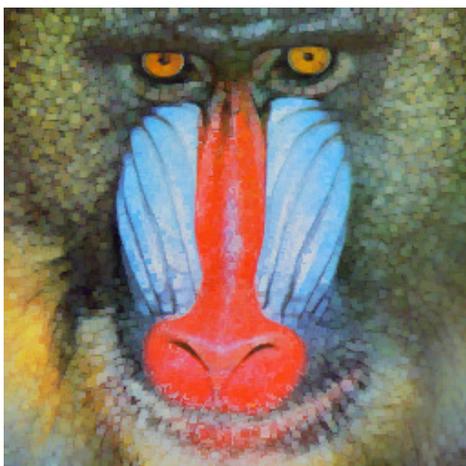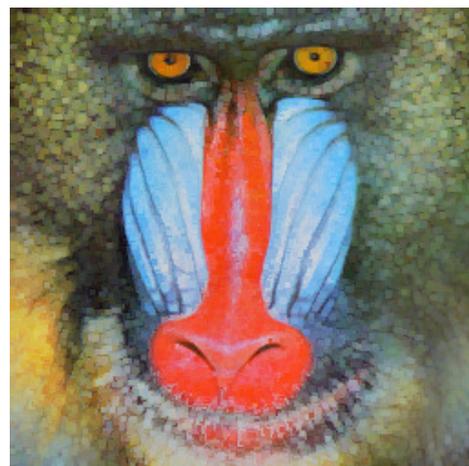
Figure. A.3. Colour opening of "Mandrill" image using (a) marginal ordering, (b) conditional ordering, (c) Angulo's ordering, (d) Cheng's PCA-like ordering and the proposed ordering in (e) HSV and (f) L*a*b* colour spaces.
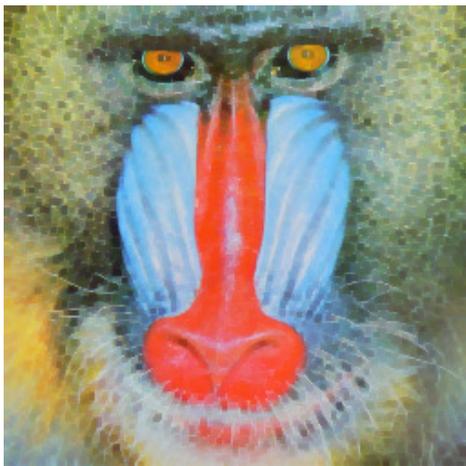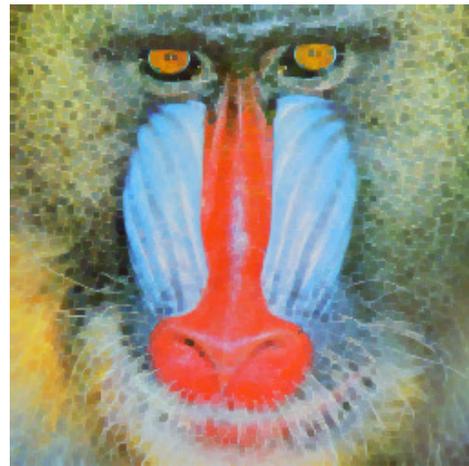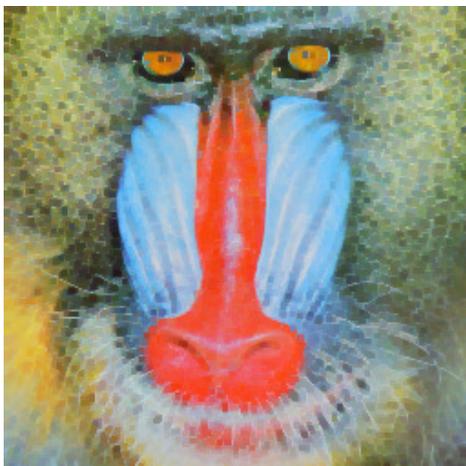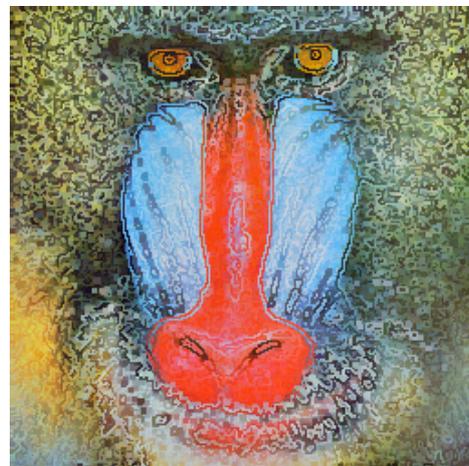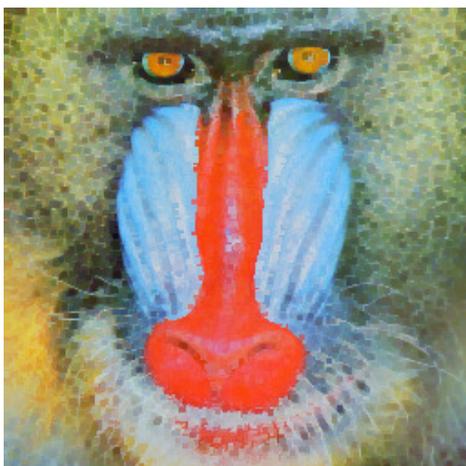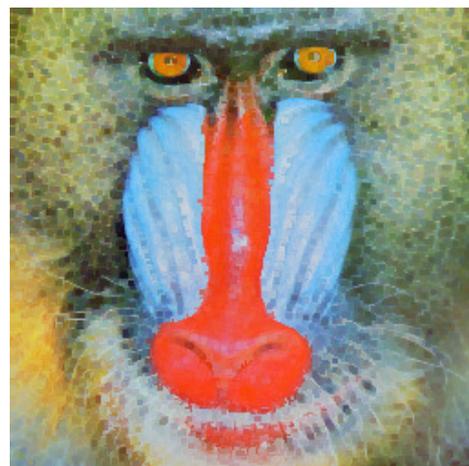
Figure. A.4. Colour closing of "Mandrill" image using (a) marginal ordering, (b) conditional ordering, (c) Angulo's ordering, (d) Cheng's PCA-like ordering and the proposed ordering in (e) HSV and (f) L*a*b* colour spaces.
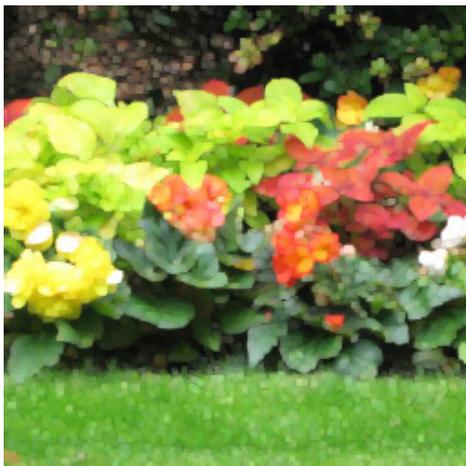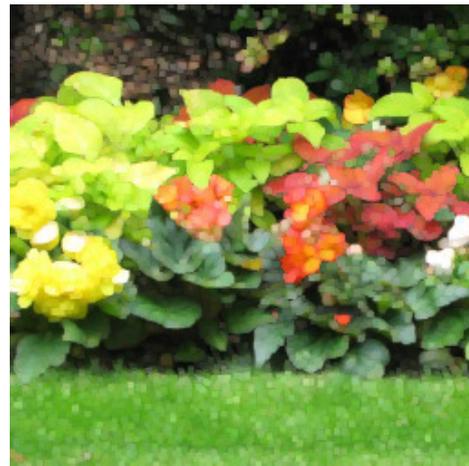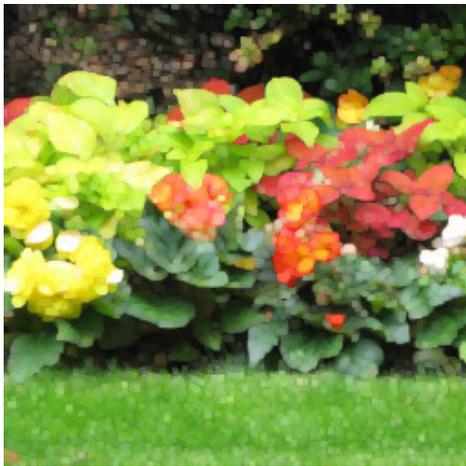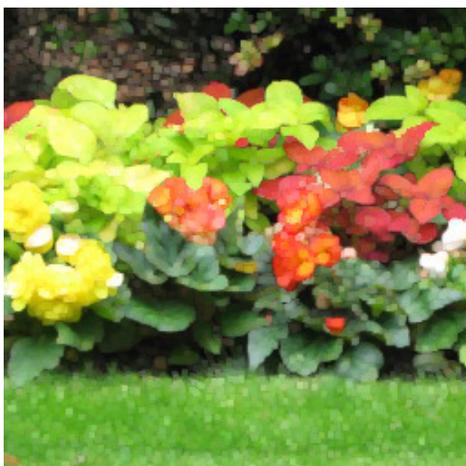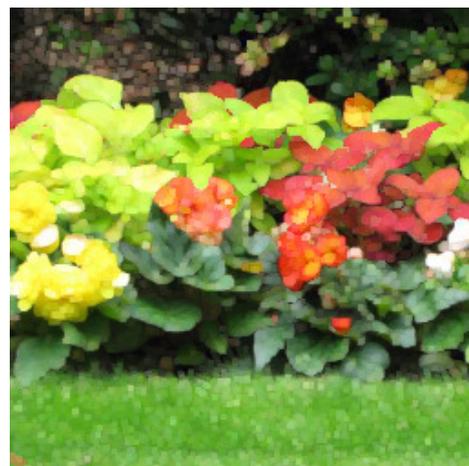
Figure. A.5. Colour dilation of "Flowers" image using (a) marginal ordering, (b) conditional ordering, (c) Angulo's ordering, (d) Cheng's PCA-like ordering and the proposed ordering in (e) HSV and (f) L*a*b* colour spaces.
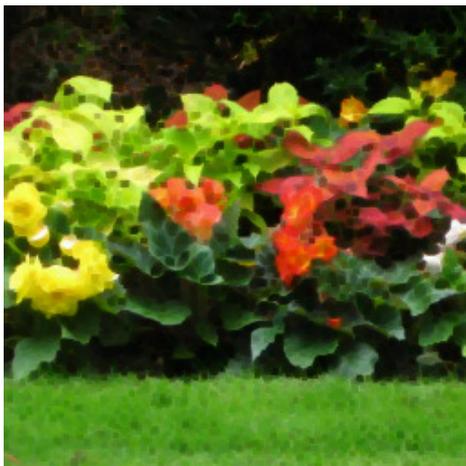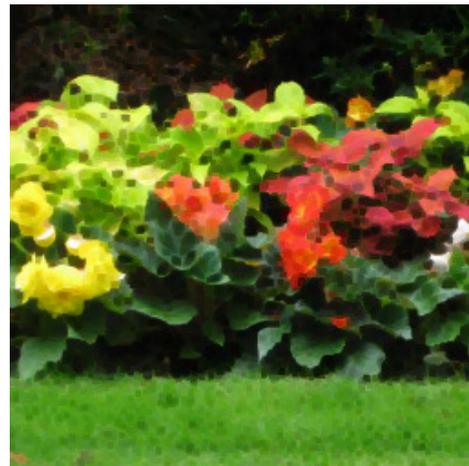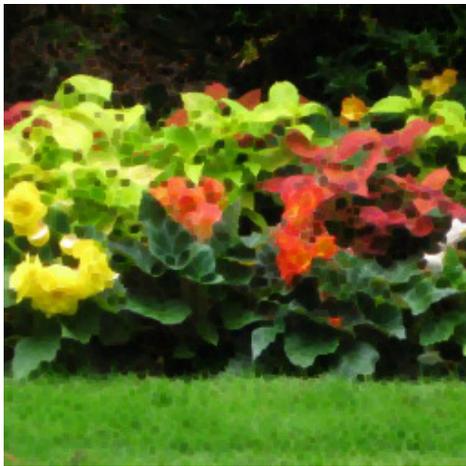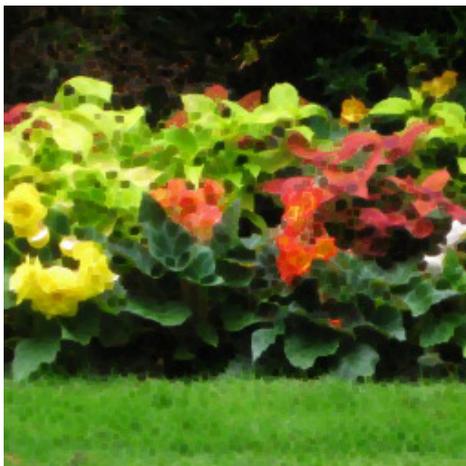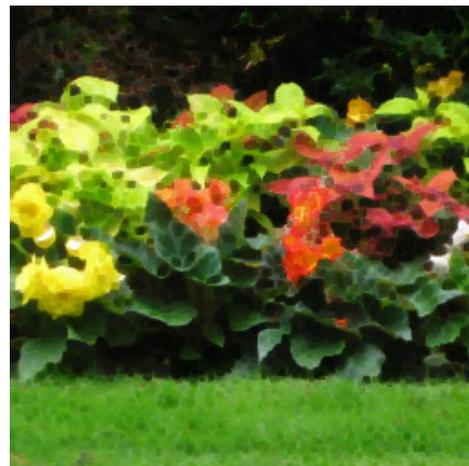
Figure. A.6. Colour erosion of "Flowers" image using (a) marginal ordering, (b) conditional ordering, (c) Angulo's ordering, (d) Cheng's PCA-like ordering and the proposed ordering in (e) HSV and (f) L*a*b* colour spaces.
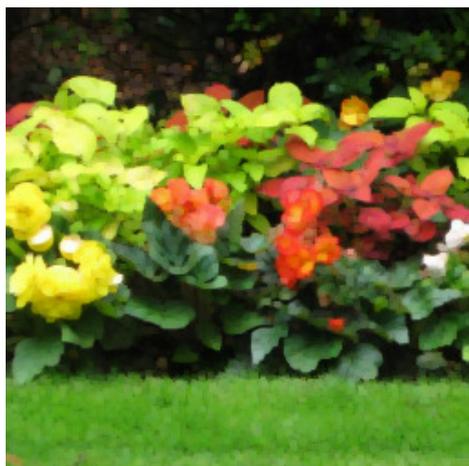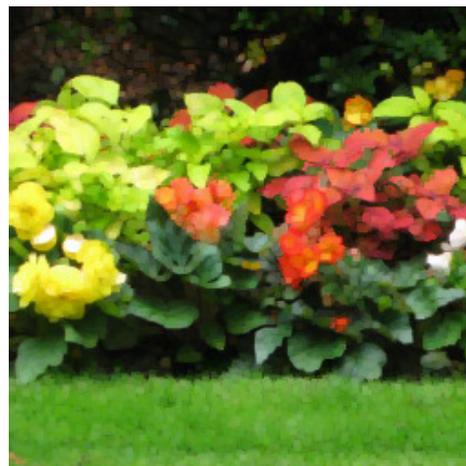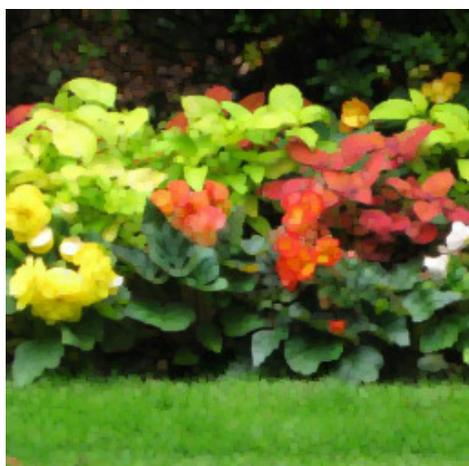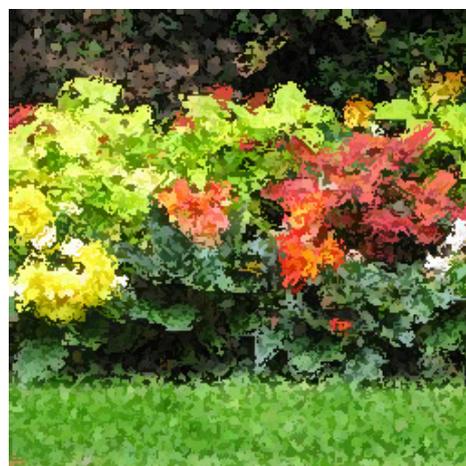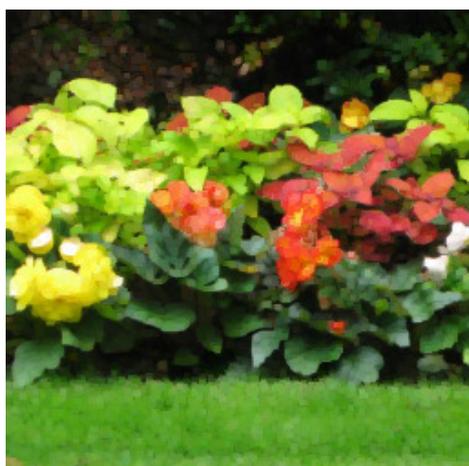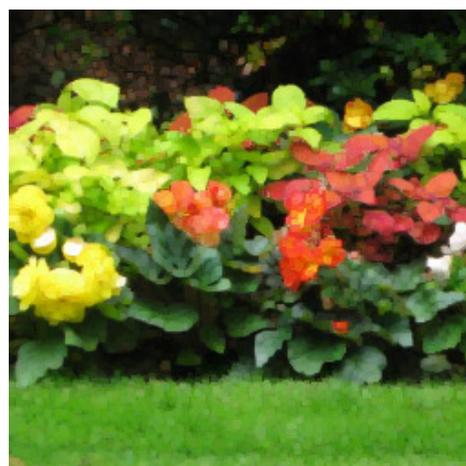
Figure. A.7. Colour opening of "Flowers" image using (a) marginal ordering, (b) conditional ordering, (c) Angulo's ordering, (d) Cheng's PCA-like ordering and the proposed ordering in (e) HSV and (f) L*a*b* colour spaces.
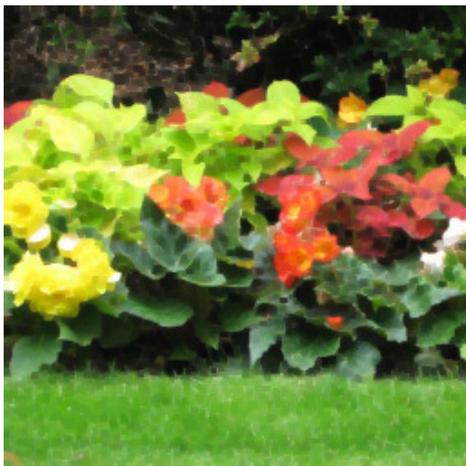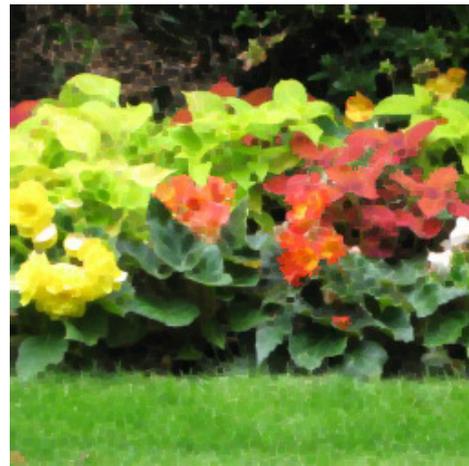
(a)   (b)
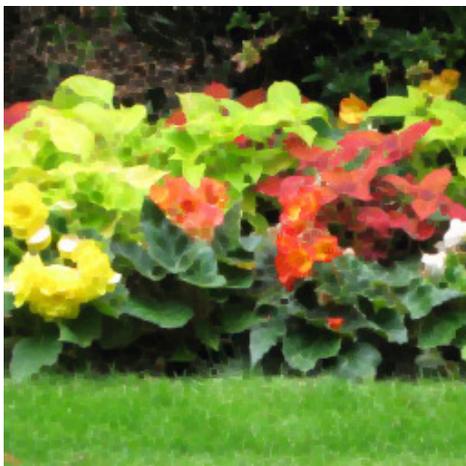
(k)   (d)
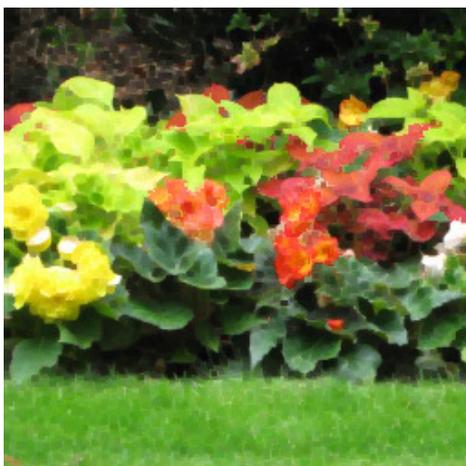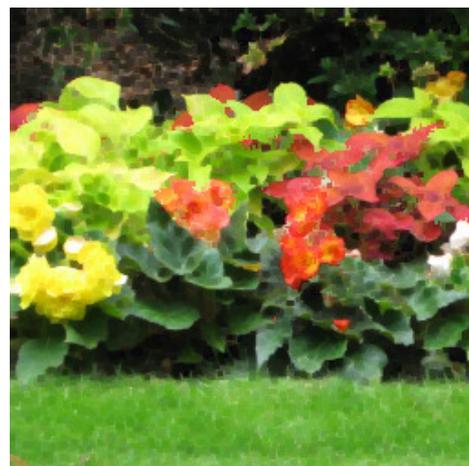
(e)   (f)

Figure. A.8. Colour closing of "Flowers" image using (a) marginal ordering, (b) conditional ordering, (c) Angulo's ordering, (d) Cheng's PCA-like ordering and the proposed ordering in (e) HSV and (f) L*a*b* colour spaces.

A.2 OC filter

This Section shows the results of salt and pepper noise removal using the orderings which were introduced in Section 4.6.
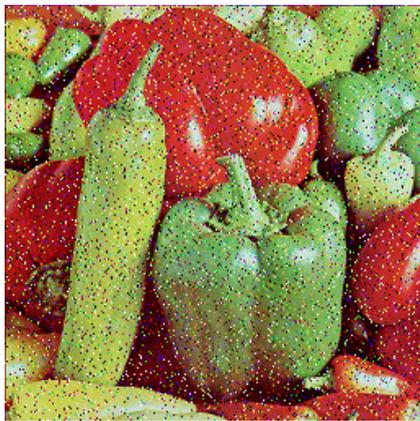
(a) Noisy image

(b) NMSE = 2.15

(c) NMSE = 6.182

(d) NMSE = 4.631

(e) NMSE = 3.524

(f) NMSE = 3.638

Figure. A.9. Image in (a) with 20% salt and pepper noise and the result of noise reduction using, an OC filter with (b) marginal ordering, (c) conditional ordering, (d) Angulo's ordering, (e) the proposed ordering in RGB and (f) the proposed ordering in L*a*b* colour space.
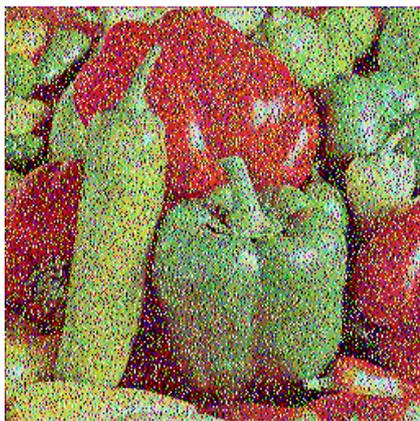
(a) Noisy image
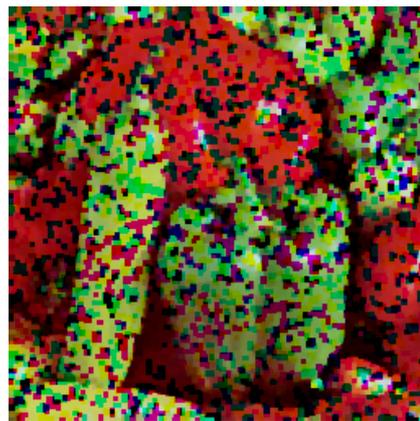
(b) NMSE = 31.675
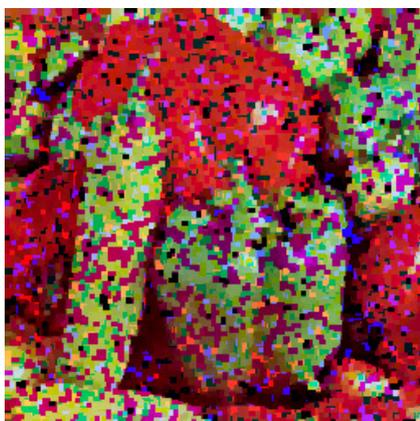
(c) NMSE = 27.724
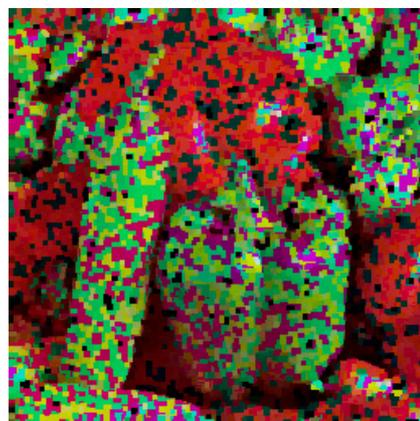
(d) NMSE = 33.705
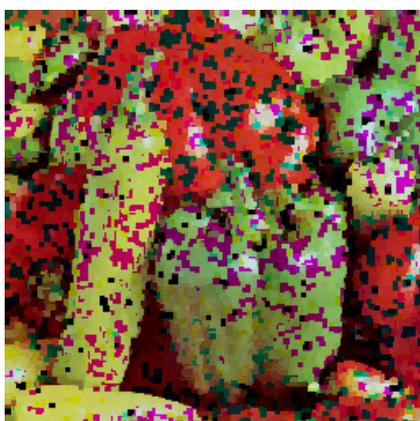
(e) NMSE = 20.361
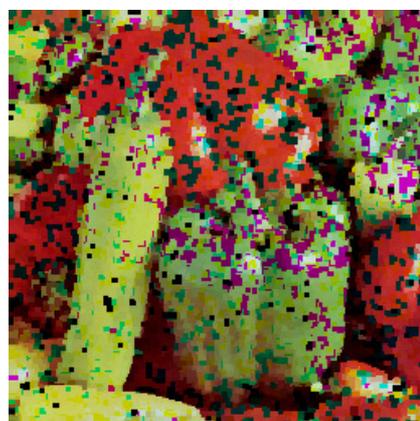
(f) NMSE = 19.832

Figure. A.10. Image in (a) with 60% salt and pepper noise and the result of noise reduction using, an OC filter with (b) marginal ordering, (c) conditional ordering, (d) Angulo's ordering, (e) the proposed ordering in RGB and (f) the proposed ordering in L*a*b* colour space.

A.3 Similarity-based colour morphology in the CIE L*a*b* colour space

This Section shows the results of dilation, erosion, opening, closing, gradient positive top-hat transform, negative top-hat transform and Hit-or-Miss transform using the similarity-based ordering in the L*a*b* colour space which was introduced in Section 5.4.
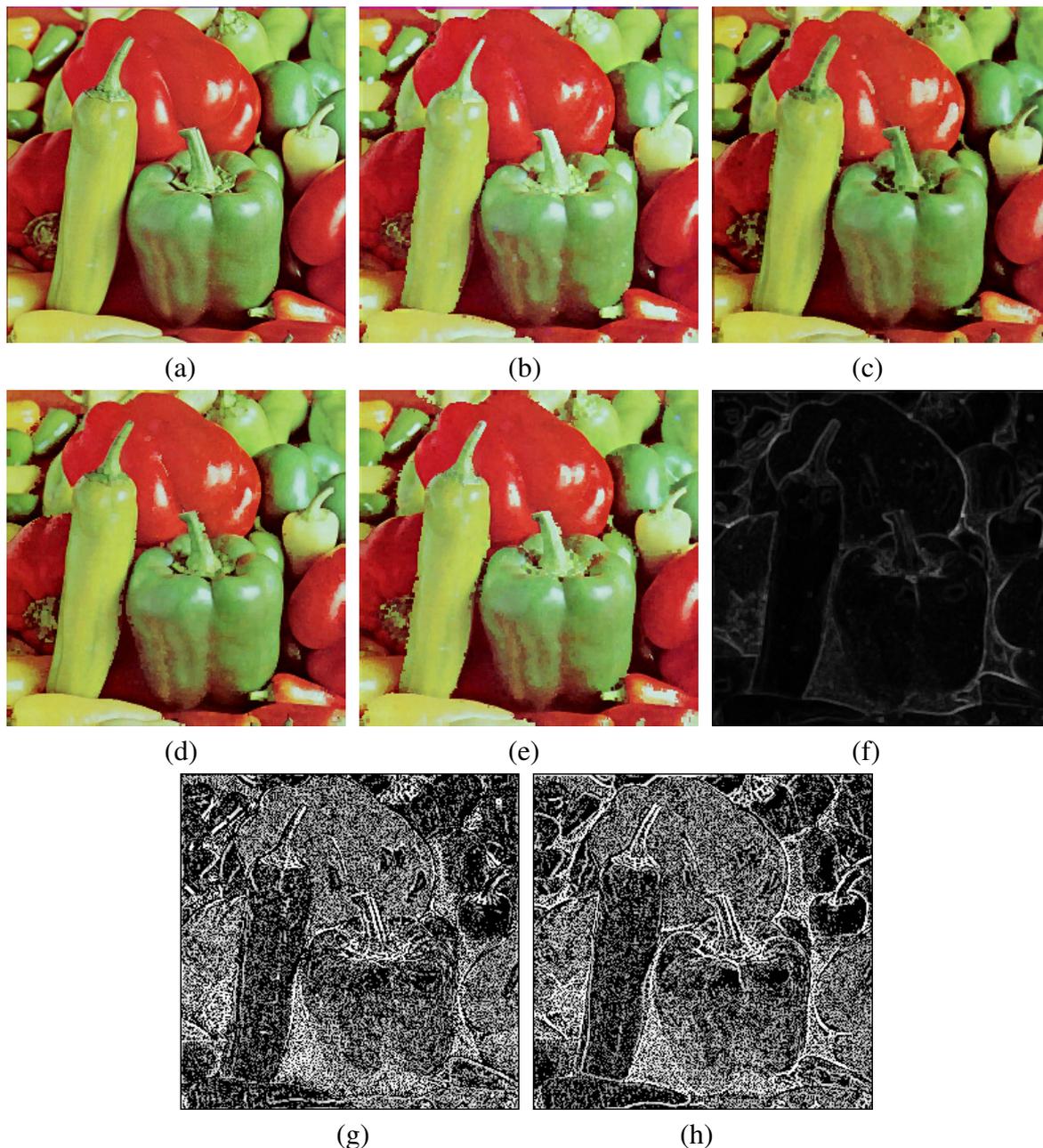

Figure. A.11. Result of applying morphologic operators to a natural image (a) original image of peppers. Result after (b) dilation, (c) erosion, (d) opening, (e) closing, (f) gradient (g) positive top-hat transform after equalisation and (h) negative top-hat transform after equalisation, each with respect to red.
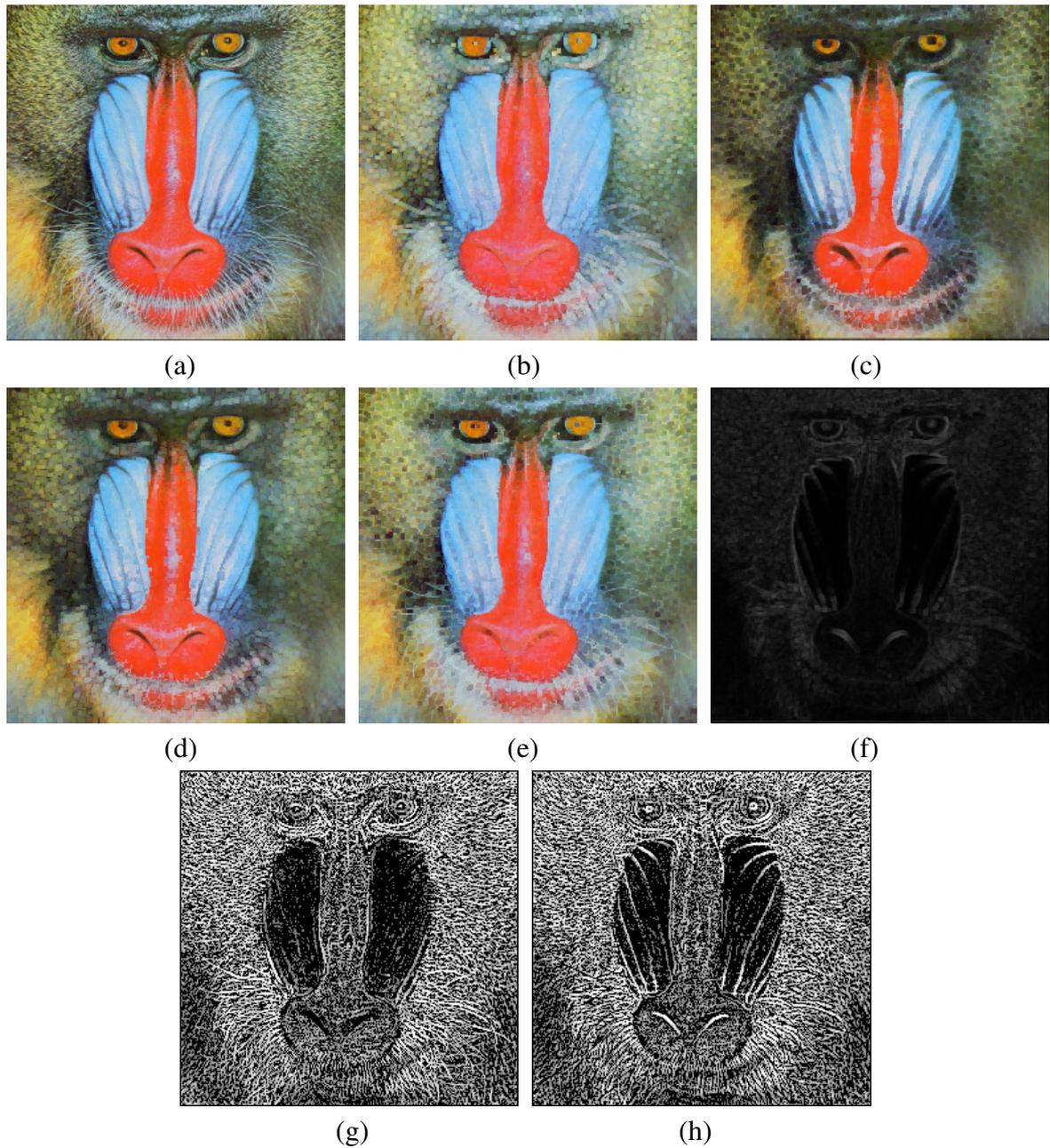
Figure. A.12. Result of applying morphologic operators to a natural image. (a) Original image of a Mandrill. Result after (b) dilation, (c) erosion, (d) opening, (e) closing, (f) gradient (g) positive top-hat transformation after equalisation and (h) negative top-hat transformation after equalisation each with respect to red.

(a)   (b)   (c)   (d)

(e)   (f)

(g)

Figure. A.13. SHMTη for "Flowers" image: (a) original image, (c) the structure element and   (d) the modified structure element, and the results using SHMTη with (b) η = 0.9, (e) η = 0.8, (f) η = 0.7 and (g) η = 0.6.